Local Translation in Sustained Autophagy

Yunping Xue

Thesis submitted to the University of Ottawa

in partial Fulfillment of the requirements for the

Doctorate in Philosophy degree

Department of Cellular and Molecular Medicine

Faculty of Medicine

University of Ottawa

© Yunping Xue, Ottawa, Canada, 2025

TABLE OF CONTENTS

TABLE OF CONTENTS ..... *ii*

LIST OF FIGURES ..... *viii*

LIST OF TABLES ..... *x*

LIST OF ABBREVIATIONS ..... *xi*

ABSTRACTS ..... *xviii*

RÉSUMÉ ..... *xix*

ACKNOWLEDGEMENTS ..... *xx*

PREFACE ..... *xxii*

COPYRIGHTED CONTENTS ..... *xxiii*

Chapter 1. General Introduction *1*

1.1 Autophagy **1**

1.1.1 Definition of Autophagy 1

1.1.2 Autophagosome Formation 2

1.1.3 Regulation of Autophagy by mTORC1 and AMPK Kinases 9

1.1.4 Translation During Autophagy 11

1.1.5 Autophagy of Stress Granules and Mitochondria 13

1.1.6 Autophagy and Disease 16

1.2 General and Local Translation 17

1.2.1 General mRNA Translation 17

1.2.2 mRNA Localization and Local Translation 20

1.2.3 The Localization of ATG mRNAs to the ER 22

1.3 The Roles of RACK1 and eIF5A in mRNA Translation and Autophagy 24

1.3.1 The Role of RACK1 in mRNA Translation and Autophagy 24

1.3.2 The Role of eIF5A in mRNA Translation and Autophagy 26

1.4 Hypotheses and Objectives 27

1.4.1 Hypotheses 27

1.4.2 Objectives 27

Chapter 2. Materials and Methods 30

2.1 Materials and Reagents 30

Table 2. Reagents and equipment 30

Table 3. Primer sequences 39

2.2 Cell Culture 41

2.3 Plasmid Transfection Using Polyethylenimines (PEIs) 42

2.4 siRNA Knockdown with Lipofectamine 42

2.5 Western Blotting 43

2.6 In Vitro APEX2 Proximity Labeling 43

2.7 Streptavidin Purification of Biotinylated RNAs 44

2.8 RT-qPCR on Biotinylated RNAs 45

2.9 Immunofluorescence Analysis 45

2.10 Polysome Profiling Fractionation 46

2.11 Streptavidin-based Purification of Biotinylated RNAs from Distinct Ribosome Fractions 47

2.12 FISH Staining 47

2.13 Nascent Protein Labeling with Click-iT® AHA (L-Azidohomoalanine) 48

2.14 Stable Isotope Labeling by Amino Acids in Cell Culture (SILAC) in APEX2-Expressing Cells 48

2.15 SILAC-Labeled Biotinylated Protein Pulldown and Sample Preparation for Mass Spectrometry 49

2.16 Live-Cell Imaging 50

2.17 Colocalization Spots Analysis with Imaris Software 50

2.18 Immunoprecipitation 51

2.19 RNA Immuno-Blot Assay 51

2.20 Proximity Ligation Assay (PLA) 52

2.21 Lentiviral Vector Production and Transduction 53

2.22 Seahorse XF Cell Mito Stress Test 53

2.23 Mitochondrial Morphology Analysis 54

2.24 Nascent Protein Labeling with 6-FAM-dc-Puromycin..... 55

2.25 Streptavidin Purification of APEX2-Biotinylated Nascent Proteins..... 55

2.26 APEX2-sequencing 56

2.27 Statistics 56

Chapter 3. Nascent Translation During Sustained Autophagy.....57

3.1 Background 57

3.2 Results 57

3.2.1 Overall cellular translation was inhibited during autophagy. 57

3.2.2 Specificity of APEX2-based proximity labeling..... 60

3.2.3 Translation is required to maintain the levels of several Atg proteins during sustained autophagy 65

3.2.4 Translation is required for synthesis of autophagosome/ autophagolysosome during sustained autophagy..... 68

3.3 Discussion..... 70

Chapter 4. Atg mRNAs were Localized to Phagophores for Local Translation ..73

4.1 Background 73

4.2 Results 74

4.2.1 Atg mRNAs localize in proximity to phagophores and autophagosomes. 74

4.2.2 Atg mRNAs are specifically recruited to DFCP1 and LC3B to a greater extent than NPM1, cyto-V5, and perilipin. 77

4.2.3 Atg mRNAs are specifically recruited to phagophores and autophagosomes 80

4.2.4 Nascent protein synthesis in proximity to phagophores 83

4.2.5 Nascent translation near forming autophagosomes is not affected by ribophagy. 85

4.2.6 mRNAs encoding proteins essential for autophagy are translated near phagophores. 87

4.3 Discussion 90

Chapter 5. Roles of RACK1 and eIF5A in Localization and Local Translation of Atg mRNA Near Forming Autophagosomes 94

5.1 Background 94

5.2 Results 95

5.2.1 Translating ribosomes are essential for localizing Atg mRNAs to phagophores and autophagosomes 95

5.2.2 RACK1 co-localizes with phagophores and autophagosomes and associates with Atg mRNAs 97

5.2.3 RACK1 associates with key Atg mRNAs 98

5.2.4 RACK1 regulates localization of Atg mRNAs to phagophores 99

5.2.5 RACK1 regulates local translation of Atg mRNAs near phagophores 103

5.2.6 RACK1 mediated localization of Atg mRNAs to phagophores for *in situ* translation is essential to sustained autophagy 105

5.2.7 eIF5A regulates localization of Atg mRNAs to phagophores 108

5.2.8 eIF5A regulates local translation of Atg mRNAs near phagophores 111

5.3 Discussion..... 114

Chapter 6. Roles of RACK1 and eIF5A in Autophagy of Stress Granules and Mitochondria..... 116

6.1 Background 116

6.2 Results 117

6.2.1 CHX and knockdown of RACK1 or eIF5A prevent stress granule degradation 117

6.2.2 CHX and knockdown of RACK1 or eIF5A affect mitochondrial respiratory function 120

6.2.3 CHX and knockdown RACK1 or eIF5A inhibit mitophagy 123

6.3 Discussion..... 126

Chapter 7. General Discussion and Conclusion..... 128

APPENDICES..... 135

1. Appendix A 135

2. Appendix B 136

3. Appendix C 137

4. Appendix D 139

5. Appendix E 140

6. Appendix F 141

BIBLIOGRAPHY.....*142*

LIST OF FIGURES

Figure.1-1 Overview of the autophagy process and core autophagy-related proteins involved. 4

Figure.1-2 The conjugation of PE to LC3-I to form LC3-II is catalyzed by two main ubiquitin-like covalent conjugation systems: the ATG8 and ATG12 systems. 6

Figure.1-3 Regulation of autophagy by mTORC1 and AMPK Kinases. 11

Figure.1-4 Mitochondria dynamics. 16

Figure.3-1 Cellular translation was inhibited during autophagy. 60

Figure.3-2 Model of APEX2-based proximity biotinylation. 61

Figure.3-3 Specificity of APEX2-based proximity labeling. 64

Figure.3-4 Translation is required to maintain the levels of several Atg proteins during sustained autophagy. 68

Figure.3-5 Translation is required for the formation of autophagosomes and autophagolysosomes during sustained autophagy. 70

Figure.4-1 mRNAs encoding proteins required for autophagy localize in proximity to phagophores and autophagosomes. 77

Figure.4-2 mRNAs encoding proteins required for autophagy specifically localize in proximity to phagophores and autophagosomes to a greater extent than CytoV5, Perilipin or NPM1. .. 80

Figure.4-3 Atg mRNAs are specifically recruited to DFCP1/ LC3B under autophagy. 83

Figure.4-4 Nascent translation occurs in proximity to forming autophagosomes. 85

Figure.4-5 Nascent translation in proximity to forming autophagosomes is not affected by ribophagy. 87

Figure.4-6 mRNAs encoding proteins required for autophagy are translated in proximity to forming autophagosomes. 90

Figure.5-1 Translating ribosomes are essential for localizing Atg mRNAs to phagophores and autophagosomes. 96

Figure.5-2 RACK1 co-localizes with phagophores and autophagosomes. 98

Figure.5-3 RACK1 associates with key Atg mRNAs. 99

Figure.5-4 RACK1 regulates localization of core Atg mRNAs to phagophores. 102

Figure.5-5 RACK1 regulates translation of several Atg proteins in proximity to phagophores. 104

Figure.5-6 RACK1 regulates translation of several Atg proteins in proximity to phagophores. 108

Figure.5-7 eIF5A regulates localization of Atg mRNAs to phagophores. 111

Figure.5-8 eIF5A regulates local translation of Atg mRNAs near phagophores. 114

Figure.6-1 CHX and knockdown of RACK1 or eIF5A inhibit stress granule clearance. 120

Figure.6-2 CHX, RACK1 siRNAs and eIF5A siRNAs affect mitochondrial respiratory function. 123

Figure.6-3 Mitophagy is affected by CHX and knockdown of RACK1 or eIF5A. 126

LIST OF TABLES

Table 1. Autophagy-related proteins, formed complexes and conjugation systems 7

Table 2. Reagents and equipment 30

Table 3. Primer sequences 39

LIST OF ABBREVIATIONS

Atg/ATG (autophagy related**)**

HSPA8/HSC70 (heat shock protein family A member 8/ Heat shock cognate 70 kDa)

LAMP2A (lysosome-associated membrane protein type 2A)

ER (endoplasmic reticulum)

ULK1 (Unc-51-Like Kinase 1)

FIP200 (RB1-inducible coiled-coil protein/ focal adhesion kinase family-interacting protein of 200 kDa)

PI3KC3 (class III PI3K)

VPS34 (Vacuolar Protein Sorting 34)

AMBRA1 (activating molecule in Beclin 1-regulated autophagy protein 1)

PtdIns/ PI (phosphatidylinositol)

PI3P (phosphatidylinositol 3-phosphate)

DFCP1 (double FYVE-containing protein 1)

WIPIs (WD-repeat domain phosphoinositide-interacting proteins)

GABARAPs (γ-aminobutyric acid receptor-associated proteins)

MAP1LC3/LC3 (microtubule-associated protein light chain 3)

PE (phosphatidylethanolamine)

UVRAG (UV-radiation resistance-associated gene protein)

HOPS (Homotypic Fusion and Protein Sorting)

SNARE (Soluble N-ethylmaleimide-sensitive factor Attachment Protein Receptor)

SQSTM1 (sequestosome1)

NBR1 (Neighbor of BRCA1)

NDP52/CALCOCO2 (Nuclear Dot Protein 52 kDa/ Calcium Binding and Coiled-Coil Domain 2)

OPTN (Optineurin)

UBA (ubiquitin-associated domain)

LIRs (LC3-interacting regions)

GIR (GABARAP-Interacting Region)

mTORC1 (mechanistic target of rapamycin complex 1)

AMPK (AMP-activated protein kinase)

DEPTOR (DEP-domain-containing mTOR-interacting protein),

Raptor (regulatory-associated protein of mTOR)

PRAS40 (the 40 kDa proline-rich Akt substrate)

mLST8 (mammalian lethal with SEC13 protein 8)

mSIN1 (mammalian stress-activated protein kinase-interacting protein 1)

Rictor (rapamycin-insensitive companion of mTOR)

Protor /PRR5 (Proline-rich protein 5)

mRNAs (messenger RNAs)

eIF4F (eukaryotic Initiation Factor 4F)

eIF4A (eukaryotic initiation factor 4A)

eIF4E (eukaryotic initiation factor 4E)

eIF4G (eukaryotic initiation factor 4G)

4E-BPs (eIF4E-binding proteins)

EM (electron microscopy)

NUFIP1 (Nuclear fragile X mental retardation-interacting protein 1)

ZNHIT3 (zinc finger HIT domain-containing protein 3)

mRNP (messenger ribonucleoprotein)

RBPs (RNA-binding proteins)

G3BP1 (Ras-GTPase-activating protein (GAP)-binding protein 1)

ZFAND1 (Zinc Finger AN1-type Containing 1)

ROS (reactive oxygen species)

PINK1 (PTEN-induced kinase 1)

SLE (systemic lupus erythematosus),

mRNP (messenger ribonucleoprotein particle)

SRP (signal-recognition particle)

MERFISH (multiplexed error-robust fluorescence in situ hybridization)

APEX (engineered ascorbate peroxidase)

IRES (internal ribosome entry site)

5' UTRs (5′ untranslated regions)

HCV (Hepatitis C virus)

c-Myc (Cellular Myelocytomatosis Oncogene)

uORFs (upstream open reading frames)

ATF4 (activating transcription factor 4)

eIF2α (eukaryotic initiation factor 2 subunit alpha)

3' UTR (3' untranslated regions)

ZBP1 (zipcode binding protein)

ASPM (Abnormal Spindle-like Microcephaly-associated Protein)

ERK (extracellular signal-regulated kinase)

S1R (Sigma-1 Receptor)

RACK1 (receptor for activated C-kinase 1)

GNB2L1 (guanine nucleotide-binding protein subunit beta-2-like 1)

PKCβII (Protein Kinase C-βII)

Bcl-xL (B-cell lymphoma-extra large)

Kcnj10 (Potassium Inwardly Rectifying Channel Subfamily J Member 10)

eIF5A (Eukaryotic translation initiation factor 5A)

TFEB (transcription factor EB)

FISH (Fluorescence *In Situ* Hybridization)

SILAC (Stable Isotope Labeling by Amino acids in Cell culture)

AHA (L-azidohomoalanine)

siRNAs (small interfering RNAs)

RT-qPCR (Reverse Transcription Quantitative Polymerase Chain Reaction)

DMEM (Dulbecco's Modified Eagle's Medium)

G3BP2 (Ras-GTPase-activating protein-binding protein 2)

eGFP (enhanced Green Fluorescent Protein)

PBS (Phosphate-Buffered Saline)

FBS (Fetal Bovine Serum)

PEI (polyethylenimine)

RIPA (Radio-Immunoprecipitation Assay)

BCA (bicinchoninic acid)

SDS–PAGE (Sodium Dodecyl Sulfate–Polyacrylamide Gel Electrophoresis)

PDVF (Polyvinylidene Difluoride)

TBST (Tris-Buffered Saline with Tween-20)

HRP (Horseradish Peroxidase)

BP (Biotin-Phenol/ biotin-tyramide)

RT (room temperature)

DPBS (Dulbecco's Phosphate-Buffered Saline)

EDTA (Ethylenediaminetetraacetic acid)

DEPC (Diethyl pyrocarbonate)

cDNA (complementary DNA)

CHX (cycloheximide)

DTT (Dithiothreitol)

OD260 (Optical Density at 260 nanometers)

HEPES (4-(2-hydroxyethyl)-1-piperazineethanesulfonic acid)

WT (wild type)

PLA (Proximity Ligation Assay)

OCR (oxygen consumption rate)

FCCP (carbonyl cyanide 4 (trifluoromethoxy) phenylhydrazone)

ANOVA (Analysis of Variance)

BAF (Bafilomycin A1)

EGFR (Epidermal Growth Factor Receptor)

eIF3D (Eukaryotic Translation Initiation Factor 3 Subunit D)

INSR (Insulin Receptor)

IGF1R (Insulin-like Growth Factor 1 Receptor)

MCC (Manders' colocalization coefficient)

SCs (Stress granules)

G3BP (Ras GTPase-activating protein SH3 domain-binding protein)

TDP-43 (TAR DNA-binding protein 43)

ABSTRACTS

Autophagy is an evolutionarily conserved catabolic process. It involves a cascade of over 35 autophagy-related genes. During this process, a cupped phagophore membrane expands to surround cytoplasmic material, and eventually seals itself to form an autophagosome, which then fuses with lysosomes. Large numbers of autophagosomes form during stress responses, while simultaneously cells drastically reduce translation to conserve energy. Here, using proximity-labeling and Fluorescence *in situ* Hybridization we demonstrate that multiple mRNAs encoding proteins required for autophagy preferentially localize in proximity to forming autophagosomes. Polysome fractionation and proteomics of nascent proteins in proximity to forming autophagosomes further reveal that these mRNAs are preferentially actively translated there.

The ribosome-binding protein RACK1 and eIF5A were essential to the localization of these autophagy-related mRNAs to forming autophagosomes and their local translation. Depletion of RACK1 or eIF5A disrupts the synthesis of essential autophagy proteins, leading to a reduction in autophagosome formation. This suggests that local translation provides an energy-efficient mechanism for rapidly supplying autophagy-related proteins, ensuring cells to massively induce autophagy while conserving energy during cell stress. Our findings highlight the critical role of local translation in autophagy regulation and demonstrate that inhibiting this process compromises cellular homeostasis, potentially exacerbating defects in autophagy and contributing to cellular dysfunction.

RÉSUMÉ

L'autophagie est un processus catabolique conservé au cours de l'évolution. Il implique une cascade de plus de 35 gènes liés à l'autophagie. Au cours de ce processus, une membrane en forme de coupe appelée phagophore s'étend pour entourer le matériel cytoplasmique, puis se referme pour former un autophagosome, qui fusionne ensuite avec les lysosomes. Un grand nombre d'autophagosomes se forment lors des réponses au stress, tandis que les cellules réduisent considérablement la traduction pour conserver de l'énergie. Dans cette étude, en utilisant le marquage de proximité et l'hybridation *in situ* par fluorescence, nous montrons que plusieurs ARNm codant des protéines nécessaires à l'autophagie se localisent préférentiellement à proximité des autophagosomes en formation. La fractionnement des polysomes et la protéomique des protéines naissantes proches des autophagosomes en formation révèlent que ces ARNm sont préférentiellement traduits activement à cet endroit.

La protéine de liaison aux ribosomes RACK1 et eIF5A étaient essentielles pour la localisation de ces ARNm liés à l'autophagie vers les autophagosomes en formation et leur traduction locale. La déplétion de RACK1 ou d'eIF5A perturbe la synthèse des protéines essentielles à l'autophagie, entraînant une réduction de la formation des autophagosomes. Cela suggère que la traduction locale fournit un mécanisme économe en énergie pour approvisionner rapidement les protéines liées à l'autophagie, permettant aux cellules de déclencher massivement l'autophagie tout en conservant de l'énergie pendant le stress cellulaire. Nos résultats soulignent le rôle crucial de la traduction locale dans la régulation de l'autophagie et montrent que l'inhibition de ce processus compromet l'homéostasie cellulaire, ce qui peut aggraver les défauts d'autophagie et contribuer à des dysfonctionnements cellulaires.

ACKNOWLEDGEMENTS

First and foremost, I would like to express my sincere gratitude to my supervisor Dr. Derrick Gibbings for all his invaluable supervision and support throughout my PhD journey. His expertise, encouragement, and constant belief in my potential have been essential to my growth as a researcher. I am also deeply thankful to all my TAC examiners: Dr. Marceline Côté, Dr. Marc-André Langlois, and Dr. John Copeland for their technical support and constructive feedback on my study. Their feedback has played a key role in shaping the direction of my research and improving the quality of my work.

I would like to express my gratitude to my parents, Changhe Xue and Tongnian Wang, and my husband Qing Ma. Without their tremendous understanding, support, and encouragement over the past few years, it would be impossible for me to complete my studies.

I am also grateful to all my lab mates: Annie (Huishan) Guo, Dr. Alexandre Savard, Adnie Etienne, Dr. Anantharam Devrajan, Ben Milley, Charlotte Manser, Carmen Daniela Miranda Sosa, Jenna McCann, Dr. James Taylor, Kaela O'Connor, Dr. Kallol Dutta, Kusal Bellana, Dr. Kiran Jagdish Todkar, Kristoferson Tandoc, Dr. Maisa Alkailani, Nicholas Valentino, Dr. Olanta Negeri, and Dr. Ryan Reshke for the cherished time spent together in the lab, and for their assistance at every stage of the research project. I would like to extend my sincere thanks to Annie for her great help with lab skill training and for always being ready to assist whenever I needed her. I would like to thank Olanta and Kallol for their kindness and support, especially during difficult times. I am also very grateful to Maisa for being warm and supportive, and for

her positive attitude, which has had a big impact on me. I am also thankful to James for his kind help with cloning and mutant creation in plasmids.

Last but not least, I am deeply grateful for the assistance of Dr. Liyuan Wang and Dr. Chloë Van Oostende-Triplet from the Cell Biology and Image Acquisition Core Facility (CIBA) for their help with microscope imaging. I also greatly appreciate the help of Dr. Stephen Baird from the High Throughput Screening Lab in analyzing the RNA-seq and mass spectrometry data using the IPA platform. Additionally, I am thankful to Dr. Zhibin Ning from the Proteomics Resource Center for performing the mass spectrometry.

PREFACE

The manuscript titled “Translation in Proximity to Forming Autophagosomes During Sustained Autophagy” authored by Yunping Xue, Nicholas Valentino, Kaela O’Connor, Karsten Nalbach, Alexandre Savard, Karen E. King, Ryan C Russell, Christian Behrends, and Derrick Gibbings, has been submitted to *Nature Communications*. It is currently under second-round revision, and it contains contributions from our collaborators.

Yunping Xue performed the bulk of experiments, helped design experiments, and drafted the manuscript. Nicholas Valentino generated the stable APEX2-expressing cells and prepared samples for mass spectrometry. Kaela O’Connor performed and analyzed part Western blot experiments. Alexandre Savard performed FISH staining. Karsten Nalbach established the APEX2-DFCP1 vectors and cells, contributing to their validation. Karen E. King generated FIP200 knockout cells and validated FIP200 knockouts using Sanger sequencing, as shown in Appendix C, which confirms the mutations in both alleles of FIP200. Ryan C Russell provided LC3B-mCherry-GFP expressing cell lines and contributed to interpreting results related to FIP200 knockout experiments. Christian Behrends contributed to design of APEX2 proximity labeling-related experiments and manuscript editing. Derrick Gibbings conceived the project, designed experiments, and wrote the manuscript. All authors reviewed and approved the manuscript.

This project was funded by the Canadian Institute for Health Research Project Grant (to Derrick Gibbings) and China Council Scholarship Council (to Yunping Xue), which made this work possible.

COPYRIGHTED CONTENTS

The text, figures, and tables in this thesis were created independently and originally, unless stated otherwise. Any sources or references to previously published works will be clearly indicated.

Copyright licenses (5981640018161) were obtained from Springer Nature to reproduce parts of published figures, as indicated in Figure.1-1 of this thesis. Copies of the mentioned above licenses are attached to Appendix F.

Chapter 1. General Introduction

1.1 Autophagy

1.1.1 Definition of Autophagy

In 1993, Prof. Yoshinori Ohsumi discovered autophagy-related genes in yeast (Tsukada and Ohsumi, 1993) and was awarded a Nobel Prize in Physiology or Medicine for discovering the mechanisms of autophagy in 2016. Autophagy is an evolutionarily conserved process that eukaryotes use to degrade intracellular components under stress. There are three main types of autophagy: macroautophagy, microautophagy, and chaperone-mediated autophagy (Xie et al., 2015b). Macroautophagy (hereafter referred to as autophagy) is the most studied and characterized type (Klionsky, 2007). Macroautophagy is characterized by formation of double-membrane autophagosomes, which later fuse with lysosomes to form autolysosomes. The acidic hydrolases in lysosomes will degrade and recycle autophagic cargoes (Yang and Klionsky, 2010). Microautophagy is a direct lysosomal uptake and degradative process and can be categorized into three types: Type 1 (lysosomal protrusion): In this type, an arm-like lysosomal protrusion extends from the lysosomal/vacuolar membrane to engulf cytoplasmic cargo. Type 2 (lysosomal invagination): In this type, the lysosome membrane invaginates to internalize cytoplasmic cargo. Type 3 (endosomal invagination): In this process, the endosomal membrane invaginates to generate intraluminal vesicles, forming the multivesicular body that subsequently fuses with lysosomes for degradation (Oku and Sakai, 2018). Chaperone-mediated autophagy: Chaperone protein, heat shock protein family A member 8/ Heat shock cognate 70 kDa (HSPA8/HSC70), mediates the translocation of cytosolic target proteins with the KFERQ

sequence to lysosomes for degradation by binding to the exposed KFERQ motifs and lysosome-associated membrane protein type 2A (LAMP2A) receptors on the lysosome membrane (Tekirdag and Cuervo, 2018). Unlike microautophagy and chaperone-mediated autophagy, macroautophagy poses a distinct challenge for the cell, as it requires the de novo biosynthesis of the autophagosomes.

1.1.2 Autophagosome Formation

It was commonly believed that membrane protrudes from the Endoplasmic Reticulum (ER) to form omegasomes (Chang et al., 2021; Melia et al., 2020), which further expand by collecting surrounding lipids to be double-membraned, cup-like phagophores and engulf cytoplasmic substrates. The phagophore membrane seals to form a double-membrane autophagosome, approximately 500 nm in diameter, effectively sequestering its substrates from the cytoplasm. The autophagosome eventually fuses with lysosomes, where its contents are degraded (Noda et al., 2009).

During the formation process of autophagosomes and autophagolysosomes, a variety of Atg proteins and their complexes are involved in a sequential way (Kitada and Koya, 2021). The Unc-51-Like Kinase 1 (ULK1) complexes, which contain ULK1, Focal Adhesion Kinase Family-Interacting Protein of 200 kDa (FIP200), ATG13, and ATG101, are formed and translocated to ER-membrane contact sites under stress conditions, such as starvation (Karanasios et al., 2016). The activated ULK1 complex triggers phagophore nucleation by phosphorylating the Phosphatidylinositol-3-Kinase Class III (PI3KC3) complex I, which includes Vacuolar Protein Sorting 34 (VPS34), Beclin1/BECN1, ATG14, Activating Molecule in Beclin 1-regulated Autophagy 1 (AMBRA1), and the vesicular transport factor p115. This

phosphorylated PI3KC3 complex I relocates to the ER membrane, where it contribute to the conversion of phosphatidylinositol (PI) into phosphatidylinositol 3-phosphate (PI3P) on ER-derived omegasomes (Biazik et al., 2015), which are named for their shape resembling the Greek letter omega (Ω). PI3P on omegasomes recruits its effectors, Double FYVE-Containing Protein 1 (DFCP1) and WD-Repeat Domain Phosphoinositide-Interacting Proteins (WIPIs, WIPI1/2), to omegasomes by interacting with their PI3P-binding domains (Axe et al., 2008; Lamb et al., 2013). WIPIs facilitate the recruitment of ATG12~ATG5–ATG16L1 complex ("~" represents the covalent bond between ATG12 and ATG5, while "–" represents the non-covalent interaction between ATG5 and ATG16) to the phagophore membrane by binding to ATG16L1 through interaction with its WD40 domains at the C-terminus. The ATG12~ATG5–ATG16L1 complex then enhances the lipidation of LC3 and its subfamily members, the Gamma-Aminobutyric Acid Receptor-Associated Proteins (GABARAPs, including GABARAP, GABARAPL1, and GABARAPL2/GATE-16), which along with the ATG9 containing vesicles-mediated delivery of lipid bilayer membranes from various cellular organelles, such as Golgi, and mitochondria contribute to phagophore membrane formation and extension (Xie et al., 2015b; Zhang et al., 2022) (Figure.1-1).

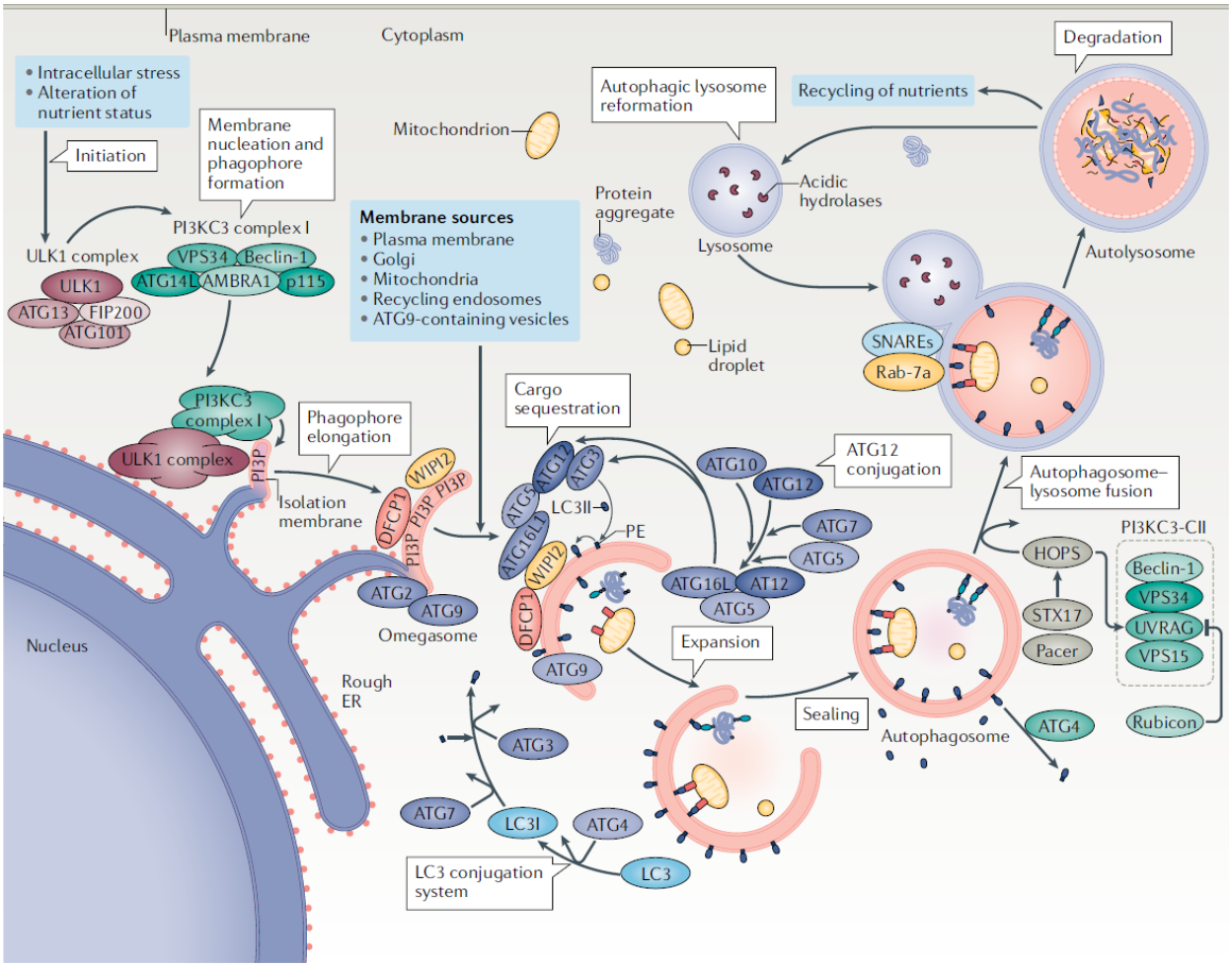

Figure.1-1 Overview of the autophagy process and core autophagy-related proteins involved.

This figure is presented with permission from (Kitada and Koya, 2021). Copyright Springer Nature.

Microtubule-Associated Protein 1 Light Chain 3 (MAP1LC3/LC3), a member of ATG8 family, consists of three homologous isoforms (LC3A, LC3B, LC3C) and is cleaved by the cysteine protease ATG4, exposing its carboxy (C)--terminal glycine residue required for lipidation. This results in the formation of LC3-I (the soluble form), which is then covalently conjugated with

phosphatidylethanolamine (PE) to form LC3-II, a lipidated form. This process is catalyzed by two main ubiquitin-like covalent conjugation systems: the ATG8 and ATG12 systems (Zhang et al., 2022). The ubiquitylation-like system refers to the processes in which ubiquitin-like proteins are activated, transferred, and conjugated to target proteins through a series of enzymatic steps involving E1 (activating enzyme), E2 (conjugating enzyme), and, sometimes E3 (ligase enzyme) (Ohsumi, 2001). In the ATG8 system, the C-terminal glycine residue of ubiquitin-like protein ATG8 is cleaved by cysteine protease ATG4, forming LC3-I, then it is activated by the E1-like enzyme ATG7 in an ATP-dependent manner, and transferred to the E2-like enzyme ATG3, which facilitates the covalent conjugation of LC3-I to PE. In the ATG12 system, the ubiquitin-like protein ATG12 is activated by forming a thioester bond between its C-terminal glycine and a cysteine residue of ATG7, which is then transferred to the cysteine of the E2-like enzyme ATG10. ATG10 facilitates the conjugation of ATG12 to the lysine residue of ATG5 via an isopeptide bond. Two ATG12–ATG5 conjugates then form a heterohexameric complex with the ATG16L dimer through noncovalent association, which functions as an E3-like enzyme to facilitate the conjugation of LC3-I to PE on the phagophore membrane (Figure.1-2). LC3-II is located on both sides of the phagophore membrane, aiding in membrane expansion and elongation, and contributing to the formation of double-layered autophagosomes that subsequently fuse with lysosomes. After autophagosomes fuse with the lysosomes, LC3-II on the outer autophagosome membrane is deconjugated from PE by ATG4 and returns to the cytosol, while LC3-II on the inner autophagosome membrane is degraded (Mizushima and Yoshimori, 2007; Mizushima et al., 2010). LC3-II levels typically reflect the steady-state quantity of autophagosomes (Kabeya et al., 2000).

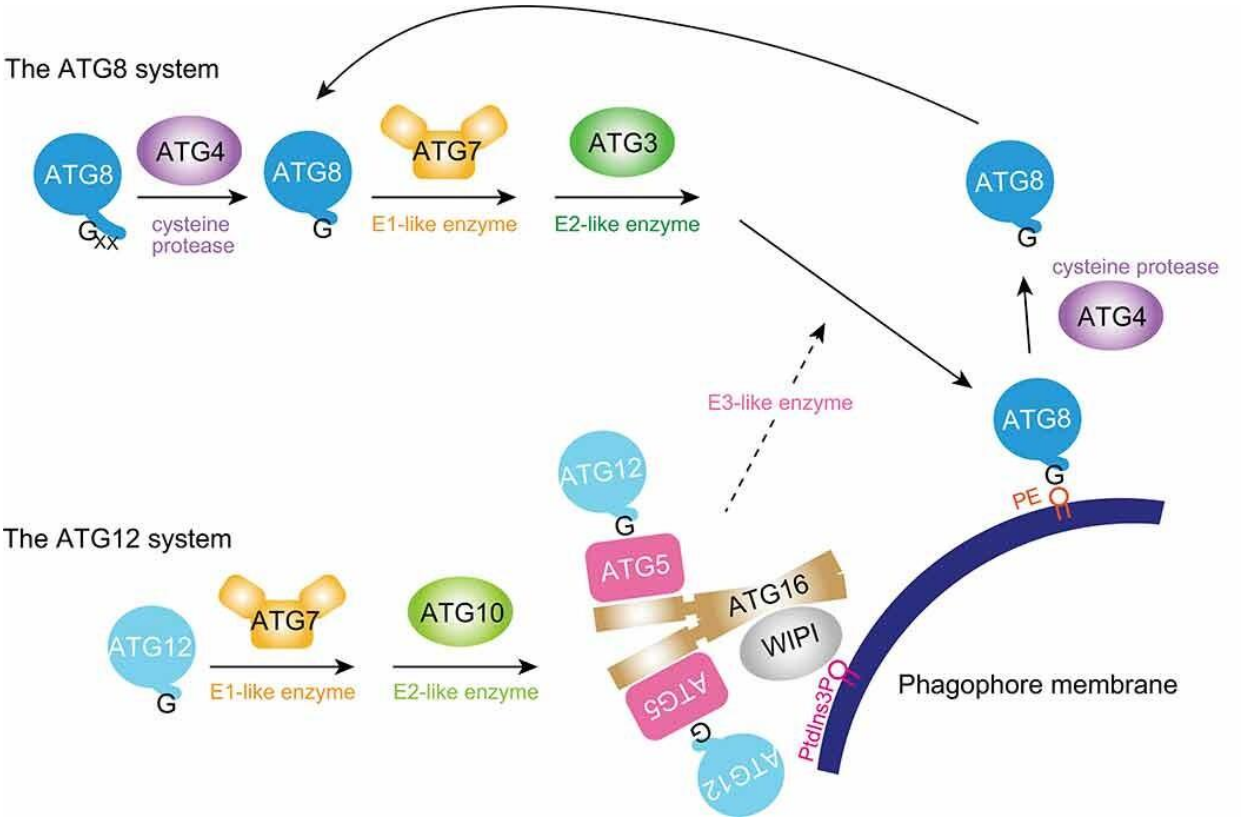

Figure.1-2 The conjugation of PE to LC3-I to form LC3-II is catalyzed by two main ubiquitin-like covalent conjugation systems: the ATG8 and ATG12 systems.

This figure is from (Zhang et al., 2022) with free access.

During the process of autophagosomes fusion with the lysosomes, the outer autophagosome membrane fuses with the single lysosomal membrane, while the inner autophagosome membrane and its contents, including autophagic cargo, are degraded by acidic hydrolases in the lysosome, facilitating the recycling of nutrients (Mauvezin et al., 2015; Yu et al., 2018). This fusion process is stimulated by the interaction between PI3KC3-Complex II (PI3KC3-CII), which consists of VPS34, VPS15, Beclin-1, ATG14, and UVRAG (UV-radiation resistance-associated gene protein), and the HOPS (Homotypic Fusion and Protein Sorting) complex, including such as VPS39, VPS41, and VPS33 (Kitada and Koya, 2021). SNARE (Soluble N-ethylmaleimide-

sensitive factor Attachment Protein Receptor) proteins, Rab GTPases, motor proteins (dynein and kinesin), and cytoskeleton components (microtubules and actin filaments) also play an important role in the fusion of lysosomes with autophagosomes (Yu et al., 2018) (Figure.1-1). The core autophagy-related proteins involved in this formation process of autophagosomes, and their main functions are summarized in the following Table 1.

Table 1. Autophagy-related proteins, formed complexes and conjugation systems

The table is made by referring the following publications (Dikic and Elazar, 2018; Kitada and Koya, 2021; Klionsky et al., 2011).

Autophagy complex or conjugation system	ATG protein	Function
ULK1 complex	ULK1	• serine/threonine kinase • initiates autophagy by phosphorylating multiple downstream targets, including Beclin1 and PI3KC3 complex I, to promote phagophore nucleation.
	FIP200	• scaffold protein • interacts with ULK1, ATG13, and ATG101 to mediate autophagy initiation
	ATG13	• dephosphorylated under starvation • binds to FIP200 and ATG101
	ATG101	• stabilizes the ULK1 complex
PI3KC3 Complex I	VPS34	• phosphoinositide kinase that generates PI3P
	Beclin1	• regulatory subunit
	ATG14	• targets the PI3KC3 complex I to autophagic membranes
	AMBRA1	• activates Beclin1 • promotes the formation of the PI3KC3 complex

		• recruits the complex to the autophagic membranes
	p115	• assists in the fusion of PI3KC3 complex I with the autophagic membrane for vesicle formation
Ubiquitin-Like Conjugation System	ATG8 (LC3s/GABARAPs)	• ubiquitin-like protein and conjugated to PE • decides autophagosome size • aids in cargo recruitment • autophagosome marker
	ATG4	• cysteine protease • process ATG8 to expose its glycine for conjugation to PE • deconjugate PE from ATG8
	ATG7	• E1 (ubiquitin-activating) like enzyme • activates ATG8 and ATG12
	ATG3	• E2 (ubiquitin-conjugating) like enzyme • conjugates ATG8 to PE
	ATG12	• ubiquitin-like protein that forms the ATG12~ATG5 conjugate covalently
	ATG5	• covalently conjugated to ATG12
	ATG16L (ATG16L1/2)	• component of the Atg12–Atg5 complex
	ATG10	• E2 (ubiquitin-conjugating) like enzyme • conjugates ATG12 to ATG5
Other core ATG proteins	ATG9	• transmembrane protein that serves as a lipid carrier for phagophore expansion • localizes to small vesicles, trans-Golgi network, and endosomes
	WIPI1/2	• binds PI3P and ATG9 • recruits the Atg12~Atg5–Atg16 complex to phagophore membrane
	DFCP1	• binds PI3P and localizes on phagophores

Autophagy can be either selective or nonselective. Nonselective autophagy handles bulk and random cytoplasmic turnover under stress, while selective autophagy was reported to degrade specific targets, such as damaged or excess organelles (Vargas et al., 2023). Stress granules (Chitiprolu et al., 2018), mitochondria (Deffieu et al., 2009; Youle and Narendra, 2011), and ribosomes (Wyant et al., 2018) have been reported to be selectively degraded under nutrient-rich conditions. Selective autophagy is mediated by selective receptors, such as Sequestosome1 (p62/SQSTM1), Neighbor of BRCA1 (NBR1), Nuclear Dot Protein 52 kDa/Calcium Binding and Coiled-Coil Domain 2 (NDP52/CALCOCO2), and Optineurin (OPTN). These receptors typically contain a Ubiquitin-Associated (UBA) domain and an LC3-Interacting Region (LIR)/ GABARAP-Interacting Region (GIR). These autophagy receptors bind ubiquitinated cargos via its UBA and LC3/ GABARAP via a LIR/GIRs simultaneously, facilitating the recruitment of cargos to autophagosomes for degradation during selective autophagy (Pankiv et al., 2007; Rogov et al., 2014; Xie et al., 2015a). After autophagosome fusion with lysosomes, these autophagy receptors and LC3/ GABARAP will also be degraded by lysosomal hydrolases together with engulfed cargoes, which is consistent with the relatively short half-lives of several autophagy-related proteins (Bjorkoy et al., 2005). Therefore, under sustained autophagy, rapid, and continuous turnover of LC3, autophagy receptors, and other proteins required for autophagy risks exhausting essential autophagy-related proteins without a continuously renewed supply.

1.1.3 Regulation of Autophagy by mTORC1 and AMPK Kinases

The intensity of autophagy activity is known to be tightly regulated by the opposing effect of Mammalian Target of Rapamycin Complex 1 (mTORC1) and AMP-Activated Protein Kinase (AMPK). mTOR is a serine/threonine kinase that dimerizes to form the catalytic subunit of two

distinct multiprotein complexes, mTORC1 and mTORC2 (Gaubitz et al., 2016; Xie et al., 2018). The mTORC1 is a composite of DEPTOR (DEP-domain-containing mTOR-interacting protein), Raptor (regulatory-associated protein of mTOR), PRAS40 (the 40 kDa proline-rich Akt substrate), mLST8 (mammalian lethal with SEC13 protein 8), and mTOR. It regulates growth, translation, and metabolism by sensing nutrients and energy, promoting biosynthesis, and inhibiting catabolic processes like autophagy. mTORC2, a complex of mTOR, DEPTOR (DEP-domain-containing mTOR-interacting protein), mSIN1 (mammalian stress-activated protein kinase-interacting protein 1), Rictor (rapamycin-insensitive companion of mTOR), Protor /PRR5 (Proline-rich protein 5), and mLST8 regulates cell proliferation, migration and survival (Proud, 2019; Roux and Topisirovic, 2018; Saxton and Sabatini, 2017). AMPK is a serine/threonine protein kinase complex and function as a cellular energy sensor. It is activated under energy-deficit conditions, e.g., low glucose, low ATP levels, hypoxia, and damaged mitochondrial respiration. Activated AMPK is the main activator of autophagy (Kim et al., 2016; Mihaylova and Shaw, 2011) (Figure.1-3).

Under nutrient-sufficient conditions, mTORC1 inhibits autophagy through phosphorylation of ULK1 on its ser residues (Ser 757 and Ser 637), thus disrupting the association between ULK1 and AMPK (Kim et al., 2011). Under glucose starvation, activated AMPK promotes autophagy by phosphorylating ULK1 on additional Ser residues (Ser 317 and Ser 777) (Kim et al., 2011), and inhibiting mTORC1 either by direct phosphorylating its component, Raptor or by indirectly activating TSC1/2 (tuberous sclerosis complex subunit 1 or 2), upstream inhibitors of mTORC1 (Gwinn et al., 2008; Kim and Guan, 2015). The activated ULK1 subsequently phosphorylates ATG13-FIP200 complex to initiate the formation of autophagosomes (Alers et al., 2012; Kim et

al., 2011) (Figure.1-3).

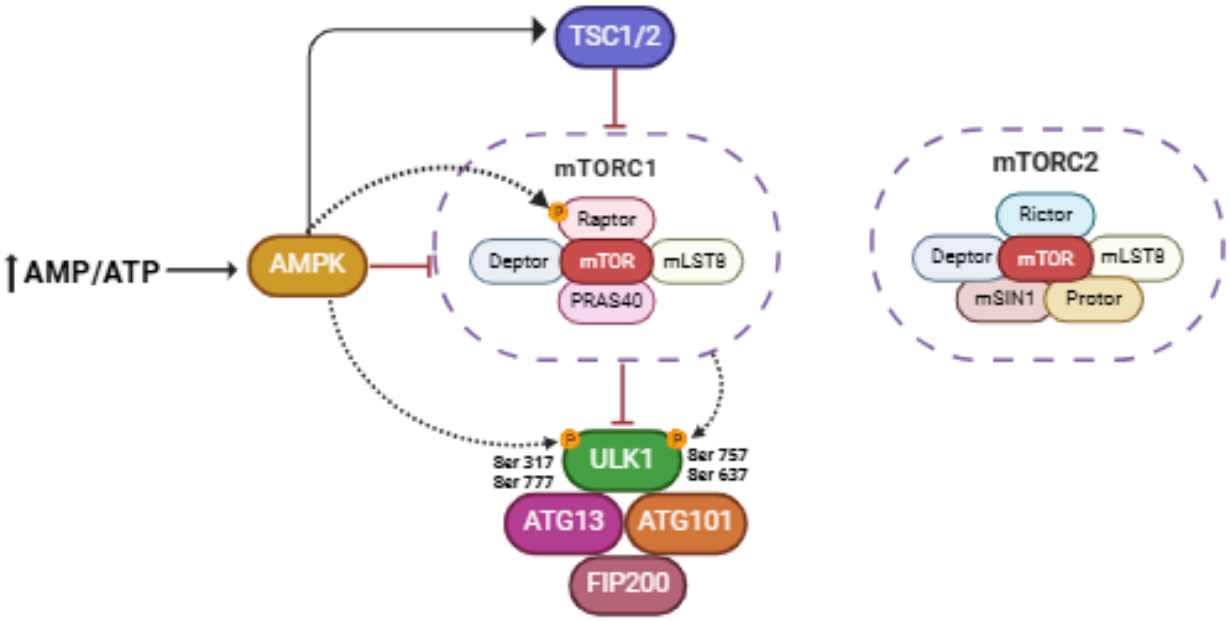

Figure.1-3 Regulation of autophagy by mTORC1 and AMPK Kinases.

Under nutrient-sufficient conditions, activated AMPK activates ULK1 through phosphorylation, inhibits mTORC1 by phosphorylating Raptor, and activates the TSC1/2 complex. Together, these events lead to the activation of the ULK1 complex and the initiation of autophagy. The components of mTORC1 and mTORC2 are also displayed. “P” represents phosphorylatable residue and illustrations for this figure are created using BioRender.com.

1.1.4 Translation During Autophagy

Cap-dependent translation is the primary and most efficient translation mechanism for most eukaryotic mRNAs (messenger RNAs) under normal conditions (Lacerda et al., 2017). The process involves the ribosome recognizing the 5’ cap of mRNAs for efficient initiation, coordinated by the eukaryotic Initiation Factor 4F (eIF4F) complex. This eIF4F complex is consist of the 5’ cap-binding protein eIF4E, which binds eIF4F to the cap structure; eIF4G, a

scaffolding protein that mediates mRNA binding to the 43S pre-initiation complex (a ribosomal assembly consisting of the small 40S ribosomal subunit, initiation factors, and the initiator tRNA); and the RNA helicase eIF4A, which unwinds local secondary structure of the mRNAs to facilitate the 43S ribosomal complex to access the mRNA template. Together, these components initiate translation by binding to the mRNA cap structure and positioning ribosomes near the 5' end, thus promoting cap-dependent translation. eIF4F complex assembly is regulated by mTORC1, which phosphorylates eIF4E-Binding Proteins (4E-BPs), preventing their binding to eIF4E. Since both 4E-BPs and eIF4G compete for the same binding site on eIF4E, this allows eIF4G to bind and stabilize eIF4E on the 5' cap, thereby initiating translation. However, when mTORC1 was inhibited, hypophosphorylated 4E-BPs bind to eIF4E with high affinity, preventing eIF4E from associating with eIF4G and eIF4A to form the eIF4F complex, thus repressing cap-dependent translation (Roux and Topisirovic, 2018),(Fonseca et al., 2016) Therefore, cap-dependent translation is repressed during autophagy, a process in which mTORC1 is inhibited.

While the ER membrane, from which the phagophore emerges, is void of ribosomes (Biazik et al., 2015), the regions surrounding it are demonstrated being densely populated with ribosomes by multiple studies using electron microscopy (EM) (Bernales et al., 2006; Biazik et al., 2015; Eskelinen et al., 2011; Yla-Anttila et al., 2009). This suggests the possibility of translationally competent ribosomes in proximity to forming autophagosomes that could furnish a rapid, local supply of key proteins involved in autophagosome biogenesis. Ribosomes have been documented to be selectively sequestered into autophagosomes for degradation during starvation, called ribophagy. During this process, the receptor NUFIP1 (Nuclear Fragile X Mental Retardation-Interacting Protein 1) forms a heterodimer with its partner protein ZNHIT3 (Zinc

Finger HIT Domain-Containing Protein 3) to recruit ribosomes to autophagosomes through binding to LC3B (Wyant et al., 2018). However, a recent publication raised the concern for the selectivity of ribophagy, stating that ATG8 conjugation is not required for ribophagy (An and Harper, 2018). Additionally, to the best of our knowledge, it has not been assessed whether some of the ribosomes degraded through ribophagy remain functional or can be recruited to the vicinity of autophagosomes for local translation of mRNAs.

When subjected to stress, cells utilize myriad pathways to reduce energy consumption (e.g., translation) to conserve resources and promote survival by inhibiting mTORC1 (Klann et al., 2020), which induces autophagy. In autophagy an entire organelle is formed *de novo* within minutes, and hundreds of autophagosomes are formed in a cell within few hours under stress stimulation (Noda et al., 2009). Together this evidence raises the possibility that continued mRNA translation in the vicinity of the phagophore may be necessary for a continuous supply of key autophagy-related proteins to sustain autophagy during prolonged stress.

1.1.5 Autophagy of Stress Granules and Mitochondria

1.1.5.1 Autophagy of Stress Granules

Stress granules are well-characterized non-membrane ribonucleoprotein particles that are assembled in response to stress stimuli (Ryan and Rubinsztein, 2024) and are involved in many neurodegenerative diseases like Amyotrophic lateral sclerosis (ALS) (Li et al., 2013). The stresses stall translation initiation, causing the dissociation of translation initiation complexes from polysomes. These complexes then interact with RNA, proteins, and RNA-protein complexes to form messenger ribonucleoprotein particles (mRNPs) that condense into discrete foci (Marcelo et al., 2021). Stress granules are also characterized by their dynamic nature,

rapidly forming in response to stress and quickly disassembling once the stressful conditions resolve (Buchan and Parker, 2009). The core components of stress granules include ribonucleoprotein particles, translational factors, the 40S ribosomal subunit (Kedersha et al., 2002), and RNA-binding proteins (RBPs) such as G3BP1 (G3BP Stress Granule Assembly Factor 1) (Yang et al., 2020). The stress granules function as the foci where translation is arrested, as translation initiation complexes, RNA, proteins, and RNA-protein complexes and RBPs involved in translation are assembled into SGs under stress conditions. They also serve as the temporary storage sites for mRNAs that are released from disassembled polysomes during stress, which can be re-released and rejoin the polysomes to resume translation once the stress is relieved (Marcelo et al., 2021).

The turnover of stress granules has been reported to occur through two distinct mechanisms: ubiquitin-proteasome-mediated mechanism, in which Zinc Finger AN1-type Containing 1 (ZFAND1) interacts with 26S proteasome and ubiquitin-selective unfoldase p97, recruiting them to arsenite-induced stress granules to facilitate their clearance (Lai et al., 2024; Turakhiya et al., 2018), and via autophagy, mediated mainly by receptor CALCOCO2/NDP52 (Xie et al., 2015a; Yang et al., 2023a) and SQSTM1/p62 (Chitiprolu et al., 2018; Mateju et al., 2017).

1.1.5.2 Autophagy of Mitochondria

Mitochondria are dynamic organelles that constantly fuse and divide (Westermann, 2010). Mitochondrial hyperfusion, triggered by mild stress or reduced mitochondrial fission, is characterized by enhanced fusion and the formation of long, filamentous mitochondria (Gao and Hu, 2021). This process helps mitigate stress by sustaining ATP production and avoiding mitophagy (Rambold et al., 2011). However, the prolonged stress reverses mitochondrial

hyperfusion and leads to mitochondrial fragmentation and apoptosis (Das and Chakrabarti, 2020; Westrate et al., 2014). Mitochondrial fission, triggered by stress, eliminates damaged mitochondria from the healthy pool. The split or damaged mitochondria are degraded through autophagy, while healthy mitochondria fuse with other functional ones to enhance efficiency (Tilokani et al., 2018).

Mitophagy is the autophagic clearance of dysfunctional mitochondria (Youle and Narendra, 2011), which generate reactive oxygen species (ROS) that can cause cellular stress, dysfunction, and even cell death (Shefa et al., 2019). Mitophagy is preceded by mitochondrial fission, which divides elongated mitochondria into smaller fragments that are suitable for encapsulation (Westermann, 2010). PTEN-induced kinase 1 (PINK1) and an E3 ubiquitin ligase (Parkin) have been documented to be play important roles in the mitophagy (Jin and Youle, 2012; Wang et al., 2023). Mutation in PINK1 or Parkin genes are linked to Parkinson's disease (Cookson, 2012). PINK1 accumulates on outer membrane of damaged mitochondria, and recruits activated Parkin, which in turn ubiquitinates outer mitochondrial membrane proteins. These ubiquitinated mitochondria are then recognized by selective autophagy receptors, e.g., NBR1 and subsequently targeted to autophagosomes for degradation (Eiyama and Okamoto, 2015; Sun et al., 2022; Wang et al., 2023; Zhu et al., 2021). Collectively, mitochondrial fission, fusion, and mitophagy play a critical role in maintaining mitochondrial health and quality (Figure.1-4).

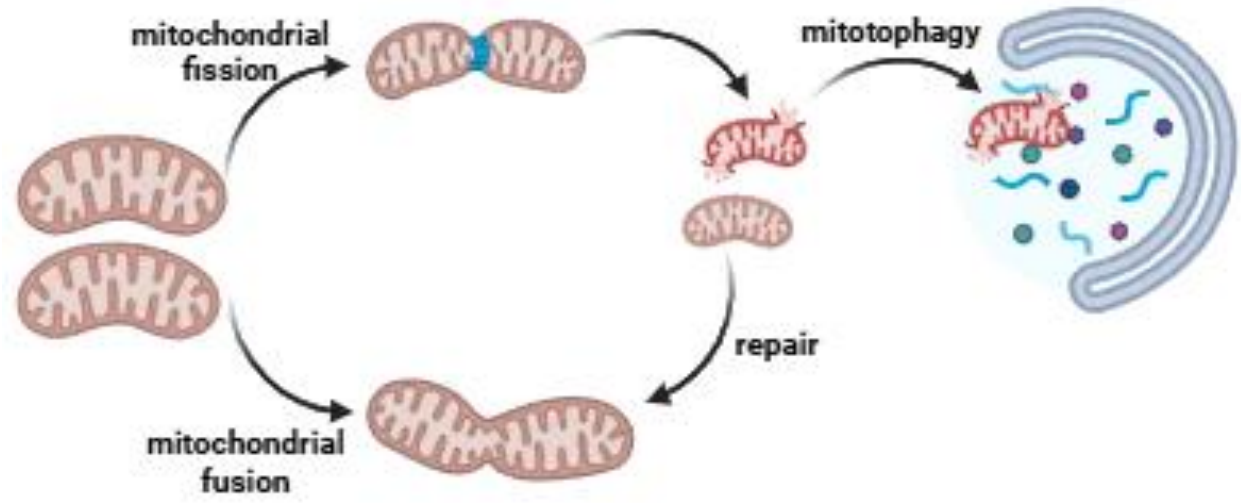

Figure.1-4 Mitochondria dynamics.

The mitochondrial fission, fusion and mitophagy process involved in the quality control of mitochondrial function. Illustrations for this figure are created using BioRender.com.

1.1.6 Autophagy and Disease

Misregulation of autophagy—whether excessive or insufficient—has been associated with a wide range of diseases. In neurodegenerative disorders, impaired autophagic clearance of toxic protein aggregates, e.g., β-amyloid and tau aggregates that contributes to neuron damage of Alzheimer's disease (Hampel et al., 2021), while disrupted mitophagy leads to accumulation of damaged mitochondria and thus neurodegeneration in Parkinson's disease (Guo et al., 2018; Li et al., 2023). In autoimmune and inflammatory conditions such as Crohn's disease, mutations in ATG16L1 impair microbial autophagy in intestinal cells, resulting in chronic inflammation (Kuballa et al., 2008; Wildenberg et al., 2017). In systemic lupus erythematosus (SLE), dysregulated autophagy in dendritic cells causes abnormal antigen presentation and autoantibody

production(Moulton et al., 2017; Yang et al., 2015). In metabolic diseases, impaired autophagy in the insulin-responsive tissues (liver and adipose tissue) disrupts insulin signaling, whereas autophagy enhancement improves insulin sensitivity in diabetic models (Menikdiwela et al., 2020; Yamamoto et al., 2018). Autophagy also plays a complex, stage-dependent role in cancer: in early tumorigenesis, it suppresses tumor growth by clearing damaged organelles, while in later stages, it supports tumor survival by supplying nutrients and energy under stress conditions (White, 2015). Consequently, autophagy inhibitors such as chloroquine are being explored as adjuvants to enhance the efficacy of chemotherapy (Jain et al., 2023). Studying the underlying mechanisms that regulate autophagy will enhance our understanding and may facilitate the development of effective therapies for these diseases.

1.2 General and Local Translation

1.2.1 General mRNA Translation

It was commonly believed that most proteins are synthesized and targeted to different organelles through the following steps in eukaryotic cells (Reid and Nicchitta, 2015): DNAs are transcribed in the nucleus to produce mature mRNAs, which are subsequently transported to the cytosol for translation initiation by ribosomes that freely diffuse throughout the cytoplasm. The translating mRNP (messenger ribonucleoprotein particle) complex, containing a topogenic signal sequence at the N-terminus of the nascent polypeptide chain, is recognized by the signal recognition particle (SRP), a conserved complex of RNAs and proteins. The SRP then binds to SRP receptors on the ER membrane, directing the mRNP complex to the ER, where translation continues with ribosomes attached to the ER (Walter and Johnson, 1994). The proteins synthesized at the ER are typically secreted or membrane proteins, which are then targeted to

different compartments, such as endosomes or peroxisomes, based on specific signals within their protein sequences (Reid and Nicchitta, 2015). If the translating mRNA complex lacks signal sequence, it remains in the cytosol until translation is complete, and the synthesized proteins will stay in the cytosol as cytosolic proteins. Since the translation of mRNAs encoding secreted, glycosylated, and/or transmembrane proteins happens on the rough ER (Ast et al., 2013), which indicates localization of these mRNAs to ER is translation dependent and mediated by SRP.

However, increasing evidence shows that translation initiation can occur directly on the ER, with mRNAs encoding cytosolic proteins localized to the ER membrane and translated de novo by ER-bound ribosomes (Jagannathan et al., 2014; Reid and Nicchitta, 2015) and mRNAs encoding cytosolic proteins observed to be translated on ER in living cells (Halstead et al., 2015). Consistently, mRNAs encoding non-membrane or non-secreted proteins are frequently found localized on the ER (Jagannathan et al., 2014; Pyhtila et al., 2008; Reid and Nicchitta, 2015; Voigt et al., 2017), using techniques such as multiplexed error-robust fluorescence in situ hybridization (MERFISH) (Xia et al., 2019), proximity-specific ribosome profiling (Jan et al., 2015), and engineered ascorbate peroxidase-based proximity biotinylation of endogenous proteins and RNA Immunoprecipitation (APEX-RIP) (Kaewsapsak et al., 2017). This may be partly due to the ability of ER-bound mRNAs to partially escape the suppression of cap-dependent translation under stress conditions (Lerner and Nicchitta, 2006; Unsworth et al., 2010).

Translation initiation typically begins when the 5' cap structure on the mRNA is recognized by eIF4E, which recruits other factors like eIF4G and eIF4A to form the eIF4F complex. This

canonical, cap-dependent pathway is responsible for the majority of translation under normal conditions. However, non-canonical (cap-independent) translation pathways also exist and play a critical role in maintaining selective protein synthesis under stress conditions such as nutrient deprivation, oxidative stress, and hypoxia—when cap-dependent translation is usually downregulated. In cap-independent translation pathways, the requirement for the 5′ cap stuctute and the canonical eIF4F complex was bypassed. One major cap-independent pathway is internal ribosome entry site (IRES)-mediated translation, in which certain mRNAs with IRES elements in their 5′ untranslated regions (5' UTRs) that directly recruit ribosomes, allowing translation to proceed without cap recognition (Spriggs et al., 2005). This mechanism has been utilized by viruses such as HCV (Hepatitis C virus) (Rosenfeld and Racaniello, 2005) and certen cellular mRNAs, such as c-Myc (Cellular Myelocytomatosis Oncogene) (Chappell et al., 2000). Another important mechanism involves eIF2α-independent translation pathway. Under stress conditions, eukaryotic initiation factor 2 subunit alpha (eIF2α) is phosphorylated and inactivated, thereby inhibiting the formation of the eIF2-GTP–$tRNA_i$^Met complex essential for cap-dependent initiation. In such cases, alternative initiation factors like eIF5B and eIF3D may deliver the initiator tRNA for selective mRNAs (Wek, 2018). A third cap-independent mechanism involves upstream open reading frames (uORFs), which are short sequences in the 5′ UTR that generally repress translation of the downstream main coding sequence (Calvo et al., 2009). Under eIF2α phosphorylation, ribosomes may bypass these uORFs and initiate at the downstream start codon through delayed reinitiation. This mechanism regulates the translation of stress-response genes such as ATF4 (activating transcription factor 4), whose protein levels increase under stress (Vattem and Wek, 2004). Recent findings suggest that bypassing the uORFs of autophagy-related genes like ATG5 and ATG13 enhances autophagy activity (Yang et al., 2023b). While

these alternative mechanisms are crucial during cellular stress, most eukaryotic mRNAs—including many ATG mRNAs—are still predominantly translated through the canonical cap-dependent pathway.

1.2.2 mRNA Localization and Local Translation

In 1983, mRNAs coding cytosolic β-actin were found to be asymmetrically localized in ascidian eggs and embryos, revealing the process of mRNA localization, a novel mechanism for sorting mRNAs into distinct subcellular compartments (Jeffery et al., 1983). mRNAs have been documented to be localized to various organelles, including the ER, mitochondria (e.g., ATM1 mRNA, encoding Atm1 protein, inner mitochondrial membrane proteins accumulated near mitochondria (Leighton and Schatz, 1995)), and non-membrane-bound structures such as P-bodies and stress granules (Niessing et al., 2018).

Localizing mRNAs rather than proteins offers several advantages: First, mRNA localization is more energy- and time-efficient because a single RNA molecule can be translated multiple times and localized mRNA translation provides a rapid supply of specific proteins, bypassing delays in protein trafficking (Moor et al., 2017). Second, localized translation can help directing proteins to specific compartments without disturbing cell fates and embryonic patterning (Driever and Nusslein-Volhard, 1988; Ephrussi et al., 1991; Gavis and Lehmann, 1992). Additionally, locally synthesized proteins may differ from pre-existing proteins, because they may undergo post-translational modifications or chaperone-assisted folding (Lin and Holt, 2007). Overall, mRNA localization fine-tunes mRNA levels in both space and time in response to environmental stimulation.

mRNA localization is primarily achieved through active transport along cytoskeletal filaments (e.g., actin filaments, microtubules) and passive diffusion. The active transport is primary mode of mRNA localization in eukaryotic cells, in which the mRNA's "zip code", a sequence with unique secondary structures, is recognized and bound by RBPs, forming the mRNPs. This mRNPs are then transported to their target locations by RBP-recruited motor proteins, such as myosin, dynein and kinesin. The zip code is crucial for RBP recognition and varies in structure and length across cell types and organisms (Biswas et al., 2019). While commonly found in the 3' untranslated regions (3' UTR), zip codes can also locate in the 5' UTR and coding regions (Buxbaum et al., 2015; Jansen, 2001). The passive diffusion and anchoring of mRNAs, commonly seen in bacteria, direct them to ribosome-rich poles or the membrane, often with the assistance of RNA chaperones (Buskila et al., 2014; Castellana et al., 2016).

It is generally thought that mRNA translation is repressed during transport. Several RBPs involved in mRNA localization also play an important role in the translation repression of trafficking mRNAs. (Besse and Ephrussi, 2008). For example, the 3'UTR sequence of ACTB mRNA (encodes β-actin) was bound by ZBP1 (Zipcode Binding Protein 1) to prevent the 60S ribosomal subunit from joining the 40S subunit to form the 80S complex during trafficking (Biswas et al., 2019; Huttelmaier et al., 2005). Additionally, RBPs can repress the translation of trafficking mRNAs through multiple mechanisms such as inhibiting cap-dependent initiation through recruiting eIF4E-BP to sequester eIF4E (Jung et al., 2006; Richter and Sonenberg, 2005), blocking translation elongation (Chen et al., 2014), or sequestering mRNAs into translation-silent granules, such as stress granules (Bassell and Warren, 2008). However, increasing evidence reveal that during mRNA trafficking co-translation occurs and is translation dependent (Chouaib et al., 2020; Safieddine et al., 2021; Wang et al., 2016). For example, the

localization of ASPM (Abnormal Spindle-like Microcephaly-associated Protein) mRNAs to the centrosome during mitosis was inhibited by translation inhibitor puromycin, and depends on the coding sequence of the ASPM mRNAs, indicating that the localization of ASPM mRNAs occurs in a co-translational manner (Safieddine et al., 2021).

RBP-mediated translation repression is relieved once the mRNAs reach their final subcellular destination or upon specific activation signals at the destination. The translation of localized mRNAs can be activated either by initiating cap-dependent translation or by relieving translation repression mediated by RBPs. In the former mechanism, external stimuli activate mTOR signaling pathways to phosphorylate eIF4E-BP, reducing its affinity for eIF4E, or activate ERK (extracellular signal-regulated kinase) to phosphorylate eIF4E, both of which can initiate cap-dependent translation. In the latter mechanism, RBPs can be phosphorylated, causing them to dissociate from mRNAs, or be displaced through competitive binding by other proteins (Besse and Ephrussi, 2008). While the exact mechanism of translation initiation for localized mRNAs remains unclear, the concept of "translation factories" is widely accepted. According to this concept, translation machinery including core translation initiation factors (e.g., eIF4E, eIF4G, eIF4A, eIF3, eIF2), ribosomes, RBPs and trafficking mRNAs, along with their synthesized proteins, accumulate in specific subcellular regions, creating translation hotspots or foci where local translation occurs (Chouaib et al., 2020; Cioni et al., 2019; Koppers et al., 2019; Safieddine et al., 2021).

1.2.3 The Localization of ATG mRNAs to the ER

Most autophagy-related proteins are cytosolic proteins, and as a result, it is commonly believed that most ATG mRNAs are translated by ribosomes in the cytosol and then targeted to the sites

where autophagosomes are formed. However, a recent study found that LC3 mRNAs are recruited to omegasomes through direct binding to the ER transmembrane Sigma-1 Receptor (S1R), with this interaction being translation-dependent. S1R interacts with a specific region within the 3' UTR of LC3 mRNAs and ribosomes to promote the local translation of LC3 mRNAs on ER-derived omegasomes. This S1R-dependent translation of LC3B promotes its efficient lipidation and accelerates autophagosome formation in response to stress (Chen et al., 2024; Knupp et al., 2024). In consistent, S1R, an RNA-binding ER membrane protein (Lee et al., 2020), has been documented to be involved in autophagy despite unclear mechanisms: mutant S1R results in defective autophagy (Dreser et al., 2017; Vollrath et al., 2014), while S1R activation induces autophagic degradation (Christ et al., 2019). Additionally, SIR is essential to the formation of omegasomes (Kumar et al., 2021).

However, colocalization of LC3B mRNAs with the ER membrane, marked by WIPI2, was observed only by smFISH (single molecule fluorescence in situ hybridization) imaging, and there is no direct evidence of nascent translation of LC3 mRNAs near the ER membrane. Additionally, the FLAG-LC3B mRNA lacking the S1R-binding region, which was used to study the role of the 3' UTR in LC3B mRNA, did not decay and may have caused overexpression of LC3B mRNAs (Knupp et al., 2024). Therefore, the conclusion that the translation of LC3B mRNAs occurs near S1R+/ omegasome+ structures requires further validation.

1.3 The Roles of RACK1 and eIF5A in mRNA Translation and Autophagy

1.3.1 The Role of RACK1 in mRNA Translation and Autophagy

Receptor for Activated C Kinase 1 (RACK1) is coded by GNB2L1 (Adams et al., 2011; Sharma et al., 2013). Its molecular weight is approximately 36 kDa, and it belongs to the WD-repeat protein family, characterized by conserved amino acid repeats ending in a Trp-Asp (W-D) dipeptide and forming a seven-bladed propeller structure, crucial for protein-protein interactions (Li and Roberts, 2001; Neer et al., 1994; Stirnimann et al., 2010). Similarly, RACK1 acts as a scaffold and adaptor protein in multiple signal transduction pathways by interactions with other proteins and ligands, such as activated Protein Kinase C-βII (PKCβII) (Belozerov et al., 2014; Dobrikov et al., 2018; Long et al., 2014). RACK1 is also a ribosome-associated protein that binds the 40S subunit near the mRNA exit tunnel (Coyle et al., 2009; Sengupta et al., 2004) and modulates the translation of a subset of mRNAs by interacting with the 40S subunit and its associated proteins (Gallo et al., 2018; Nilsson et al., 2004), though it is not essential for general translation (Majzoub et al., 2014). For example, under synaptic stimulation, RACK1 recruits PKCβII to the mRNP complex to phosphorylate polyA-mRNA-bound proteins and regulate localized translation in neurons (Angenstein et al., 2002). RACK1 binds the β-actin mRNA/ ZBP1 complex on ribosomes, releasing β-actin mRNA from ZBP1 and alleviating translation repression (Ceci et al., 2012). Additionally, RACK1 proteins have been identified in various cellular sites, including the cytosol, rough ER, and nucleus (Angenstein et al., 2002). They can relocate to different subcellular sites in response to different stimuli. For instance, PKC activation leads to the translocation of RACK1 from perinuclear structures to other intracellular sites, while exposure to ethanol causes RACK1 to move to the nucleus (Ron et al., 1999).

An increasing amount of research indicates that RACK1 plays a role in regulating autophagy through its interaction with several key autophagy-related proteins. RACK1 has been found to interact with ATG5, a key component of the E3-like ATG12~ATG5–ATG16L1 protein complex, and this interaction is indispensable for autophagy, and is enhanced by classic autophagy inducer (e.g., mTOR inhibitor and starvation) (Erbil et al., 2016). RACK1 colocalizes with early autophagic structures on the ultrastructural level, and its deletion impairs starvation-induced autophagy in Drosophila (Erdi et al., 2012). AMPK-mediated phosphorylation of RACK1 at Thr50 promotes its binding to the autophagy-initiation complex (Atg14L-Beclin 1-Vps34-Vps15), facilitating complex assembly and Vps34-mediated conversion of phosphatidylinositol (PtdIns) to PI(3)P, which serve as the platform to recruit PI(3)P-binding proteins like DFCP1 and WIPI1, without affecting ULK1 activation (Zhao et al., 2015). Additionally, RACK1 knockdown promotes non-canonical autophagy by enhancing the association of mRNAs like LC3 and Bcl-xL (B-cell lymphoma-extra large, Beclin1 complex inhibitor, antiapoptotic proteins) with polysomes while inhibiting Beclin1-mediated canonical autophagy (Kim et al., 2017). RACK1 represses the translation of Potassium Inwardly Rectifying Channel Subfamily J Member 10 (Kcnj10) mRNAs by associating with their 5' UTR sequences (Oudart et al., 2023), thereby regulating translation by sensing 5' UTR sequences (Gallo et al., 2018). While RACK1 has been shown to interact with various mRNAs and play a role in translational regulation, its specific role in autophagy, particularly in the spatial regulation of Atg mRNA localization and translation, remains unexplored.

1.3.2 The Role of eIF5A in mRNA Translation and Autophagy

Eukaryotic Translation Initiation Factor 5A (eIF5A) is a conserved acidic protein with a MW of 16.7 kDa and two isoforms, EIF5A1 and EIF5A2. It is controversial about whether eIF5A is essential for global translation elongation and termination (Saini et al., 2009; Schuller et al., 2017), or mediates the selective translation of a set of mRNAs (Mandal et al., 2016). To date, eIF5A is the only known protein in nature containing a hypusine residue (Dever et al., 2014), formed through posttranslational modification of a specific lysine. eIF5A is also a well-recognized RBP, with the interaction between eIF5A and RNA depending on both the presence of hypusine and the core motif of the target RNAs (Xu and Chen, 2001; Xu et al., 2004).

Hypusinated eIF5A promotes autophagy by enhancing translation of TFEB (transcription factor EB), an autophagy transcription factor with a triproline motif. TFEB requires hypusinated eIF5A for efficient peptide bond formation due to proline's rigidity. The eIF5A-TFEB-autophagy pathway is independent of mTOR (Zhang et al., 2019). eIF5A is also essential for LC3 lipidation by mediating ATG3 translation, overcoming ribosome pausing caused by its DDG motif (Lubas et al., 2018). Induction of autophagy (e.g., by starvation or Torin1) leads to promotion of eIF5A's association with ribosomes without affecting its protein levels, thereby aiding in the translation of several proteins, including ATG3 (Lubas et al., 2018). eIF5A was also confirmed as a component of the stalled translation initiation complex that accumulates at stress granules and hypusine-modified eIF5A is essential for assembly of stress granules by promoting stress/arsenite -induced polysome disassembly (Li et al., 2010). In conclusion, eIF5A is a key regulator of translation, particularly in autophagy and stress responses, by selectively translating

mRNAs like TFEB and ATG3. eIF5A is also essential for stress granule formation and ribosome function under stress, highlighting its role in translation regulation and autophagy.

1.4 Hypotheses and Objectives

1.4.1 Hypotheses

We hypotheses that several key autophagy-related mRNAs are localized to the vicinity of forming autophagosomes, where they are translated *in situ* to provide core autophagy-related proteins for autophagosome maturation during sustained autophagy. The localization of these core Atg mRNAs to forming autophagosome could be regulated by some key regulatory factors such as RACK1 and RBPs, e.g., eIF5A. Additionally, blocking the localization and local translation of Atg mRNAs to the forming autophagosomes is hypothesized to impair the autophagy of stress granules and damaged mitochondria.

1.4.2 Objectives

The overall objective of this thesis is to investigate the localization and local translation of Atg mRNAs in proximity to autophagosomes, and to explore the molecular mechanisms underlying these processes. Several specific objectives are as following:

1. **To investigate the Atg mRNAs that are localized to autophagosomes.** APEX2-based proximity labeling combined with pulldown assays, and RNA-seq allows the identification of mRNAs in proximity to autophagosomes and phagophores. These enriched Atg mRNAs near autophagosomes and phagophores will be further validated with FISH (Fluorescence in situ

hybridization) imaging, and RT-qPCR, and this provides insights into the spatial distribution of Atg mRNAs during sustained autophagy.

2. **To examine whether Atg mRNAs localized to autophagosomes undergo local translation.** SILAC (Stable Isotope Labeling by Amino acids in Cell culture)-based proteomics, (L-azidohomoalanine) AHA Click-iT assays, and ribosome profiling will be used to identify newly synthesized proteins in proximity to autophagosomes. This will help clarify whether these key Atg mRNAs are recruited to autophagosomes for *in situ* translation to supply proteins for autophagosome formation and maturation during autophagy.
3. **To investigate roles of the regulatory factors RACK1 and eIF5A in localization of Atg mRNAs to the proximity of autophagosomes and their *in-situ* translation**. RACK1 or eIF5A knockdown with small interfering RNAs (siRNAs), combined with Reverse Transcription Quantitative Polymerase Chain Reaction (RT-qPCR) of APEX2 proximity labeling-based pulldowns, RT-qPCR of RACK1 or eIF5A immunoprecipitations, and polysome profiling of APEX2 proximity labeling-based pulldowns of RNAs from cells transfected with RACK1 siRNAs or eIF5A siRNAs will help identify whether recruitment of core autophagy-related mRNAs to autophagosomes and their local translation near autophagosomes were affected by RACK1 or eIF5A knockdown.
4. **To evaluate effects of RACK1 and EIF5A on autophagy of stress granules and damaged mitochondria**: Effects of knockdown of RACK1 or EIF5A with siRNAs on the autophagic process, stress granule dynamics, and the elimination of damaged mitochondria will be evaluated. This will provide insight into the relevance of local translation for sustained autophagy.

Ultimately, this thesis aims to demonstrate the localization of key Atg mRNAs to forming phagophores and the local translation of these key Atg mRNAs at the site of forming autophagosomes is crucial for sustained autophagy. Understanding the underlying regulatory mechanisms will provide new insights into the control of autophagy and its dysregulation in diseases.

Chapter 2. Materials and Methods

2.1 Materials and Reagents

Table 2. Reagents and equipment

Antibodies	**Vendor**	**Cat#**
LC3A	Cell Signaling Technology	4599
LC3B	Sigma-Aldrich	L7543
ATG2A	MBL	PD041
ATG3	Cell Signaling Technology	3415
ATG5	Cell Signaling Technology	8540
ATG7	Cell Signaling Technology	8558
ATG12	Cell Signaling Technology	4180
ATG16L1 (D6D5)	Cell Signaling Technology	8089
ACTB	Sigma-Aldrich	A5441
4E-BP1 (53H11)	Cell Signaling Technology	9644S
PHOSPHO-4E-BP1 (s65)	Cell Signaling Technology	9456
RACK1 (B-3)	Santa cruz	sc-17754
p62 Antibody	Sigma-Aldrich	P0067

Streptavidin-AF488	Thermo Fisher scientific	S32354
ZFYVE1 /DFCP1	novusbio	NBP1-84267-25ul
IHC-plus™ Polyclonal Rabbit anti-Human ZFYVE1 / DFCP1 Antibody	lsbio	LS-B15646-50
Mouse IgG1 K Isotype Control Purified	eBioscience	14-4714-82
Rabbit IgG isotype control antibody	genetex	GTX35035
GAPDH	Santa cruz	sc-32233
NBR1	Abnova	H00004077-M01
NDP52	Cell Signaling Technology	9036S
OPTN/ Optineurin (C-Term) Polyclonal Antibody	Caymanchem	100000
NUFIP1 Polyclonal antibody	Proteintech	12515-1-AP
RPS3A Antibody	Bethyl Laboratories	A305-001A-T
RPL10A Antibody	Bethyl Laboratories	A305-062A-T
Vinculin Antibody	Abcam	Ab129002
VPS34	Proteintech	12452-1-AP
eIF5A	Thermo Fisher scientific	PA5-29204

Tomm20 Polyclonal Antibody	Thermo Fisher scientific	PA5-39247
Oligonucleotides		
RACK1 Silencer Select siRNA s20340	ThermoFisher	4392420
Silencer Select Negative Control siRNA 2	ThermoFisher	4390824
NUFIP Silencer Select siRNA s25623	ThermoFisher	4392420
RACK1 3'UTR siRNA ID 556309	ThermoFisher	4399665
eIF5A Silencer Select siRNA ID10892	ThermoFisher	
Recombinant DNA	**Vender**	**Cat#**
pEGFP-N1-RACK1	Addgene	41088
mCherry-DFCP1	Addgene	86746
GFP-DFCP1	Addgene	38269
WIPI2-Halo WT	Addgene	175025
APEX2-DFCP1	Gift from Dr. Christian Behrends' lab	

APEX2-NPM1	Gift from Dr. Christian Behrends' lab at Ludwig-Maximilians-Universität	
APEX2-LC3B	Gift from Dr. Christian Behrends' lab at Ludwig-Maximilians-Universität	
APEX2-LC3B^{G120A}	Gift from Dr. Christian Behrends' lab at Ludwig-Maximilians-Universität	
WIPI1-GFP	Addgene	38272
APEX2- perilipin2	Addgene	170573
APEX2-Cyto-V5	Addgene	170572
Other reagents	**Vendor**	**Cat#**
Dynabeads™ MyOne™ Streptavidin C1	Invitrogen	65001
Click-IT™ AHA (L-Azidohomoalanine)	Invitrogen	C10102
Alexa Fluor™ 488 Alkyne	Invitrogen	A10267
Click-iT® Cell Reaction Buffer Kit	Thermo Fisher Scientific	C10269
Click-iT Protein Reaction Buffer Kit	Thermo Fisher Scientific	C10276

Antifade Mounting Medium with DAPI	VECTASHIELD	H-1200-10
Mounting medium (W/o DAPI)	VECTASHIELD	H-1000
RPMI, no methionine	Gibco	A1451701
µ-slide 8 well chambered coverslip	Ibidi	80826
6-FAM-dC-puromycin	Jena Bioscience	NU-925-6FM-S
6-FAM	Invitrogen	C1360
Opti-MEM/ Reduced Serum Medium	Giboco	31985070
Lipofectamine™ RNAiMAX Transfection Reagent	Invitrogen	13778075
M-MuLV Reverse Transcriptase	NEB - New England Biolabs	M0253L
GoTaq® qPCR Master Mix	Promega	A6002
Enhanced PEI (polyethylenimine)	Biobar	R-R02
PVDF transfer membrane	Thermo Scientific	88518
Immun-Blot Low fluorescence PVDF membrane	Biorad	1620261
HaloTag® Ligands (Coumarin)	Promega	G8582
Dynabeads Protein G	Thermo Fisher	10004D

Human ATG3 mRNA probe with Quasar® 570 Dye	Biosearch technologies	SMF-1063-5
Human ATG12 mRNA probe with Quasar® 570 Dye	Biosearch technologies	SMF-1063-5
Stellaris® FISH Probes, Human ACTB with Quasar® 670 Dye	Biosearch technologies	VSMF-2003-5
dNTP Mix 10mM	bio basic	DD0056
Salmon sperm DNA	Thermo Fisher	15632011
Baker's yeast RNA	Sigma Aldrich	R6750-100MG
Chemiluminescent Nucleic Acid Detection Module Kit	Thermo Fisher	89880
Mass-spec grade trypsin	Worthington Biochemical	LS02122
Sep-Pak tc18 1cc cartridges	Waters	WAT054960
Seahorse XF Cell Mito Stress Test Kit	Agilent	103015-100
HRP substrate	EMD Millipore	WBLUR0100A
Chemical reagents	**Vendor**	**Cat#**
2-Mercaptoethanol	Bio-Rad	1610710
4× Laemmli sample buffer	Bio-Rad	161–0747

Sucrose	Fisher Scientific	BP220-1
Biotin-tyramide	Sigma Aldrich	SML2135
Doxycycline hyclate	Sigma Aldrich	D9891
Torin1	Tocris Bioscience	4247
INK128 (MLN-0128)	ChemieTek	CT-INK128
BafilomycinA1	Millipore sigma	196000-1SET
Trolox	Cayman chemicals	10011659
Sodium ascorbate	Sigma Aldrich	A7631-100G
Sodium azide	Fisher Scientific	AAJ2161022
TRIzol	Invitrogen	15596018
Cycloheximide/CHX	Sigma Aldrich	C7698
H_2O_2	Fisher Scientific	H325100
Hygromycin B	Thermo Fisher	10687010
Formamide	Fisher Scientific	BP227-500
Harringtonine	Cayman chemicals	15361
D-glucose	Invitrogen	D16-500
Sodium pyruvate	Invitrogen	11360-070
Glutamine	Invitrogen	25030-081

Sodium arsenite	Sigma-Aldrich	71287
Stellaris® RNA FISH Hybridization Buffer	Biosearch technologies	SMF-HB1-10
HaloTag® Ligands (Coumarin)	Promega	G8585
Duolink In Situ Wash Buffers, Fluorescence	Sigma Aldrich	DUO82049
Duolink® In Situ PLA Probe Anti-Rabbit PLUS	Sigma Aldrich	DUO82002
Duolink® In Situ PLA® Probe Anti-Mouse MINUS	Sigma Aldrich	DUO82004
Duolink Antibody Diluent (1×)	Sigma Aldrich	DUO82008
Duolink® In Situ Mounting Medium with DAPI	Sigma Aldrich	DUO82040
Duolink Blocking Solution (1×)	Sigma Aldrich	DUO82007
Duolink® In Situ Detection Reagents Orange	Sigma Aldrich	DUO92007
Cell lines	**Vendor**	**Cat#**
HeLa WT	ATCC	CCL2
HEK293T	ATCC	CRL-3216

HEK293T expressing LC3B-mCherry-GFP	Dr. Ryan Russel's lab at uOttawa	
APEX2-DFCP1 expressing HeLa cells	Dr. Christian Behrends' lab at Ludwig-Maximilians-Universität	
APEX2-LC3B expressing HeLa cells	Dr. Christian Behrends' lab at Ludwig-Maximilians-Universität	
Equipment	**Vendor**	**Cat#**
Density gradient fractionation system	Brandel	SYN-202
DynaMag™-2 Magnet	Invitrogen	12321D
Quorum spinning disk confocal microscopy	Leica (provided by uOttawa CBIA core)	
Zeiss LSM800 AxioObserver Z1	Zeiss (provided by uOttawa CBIA core)	
BioComp model 108 Gradient Master	BioComp	
Seahorse Flux Analyzer XF24	Aglient	
Li-Cor Odyssey Fc imaging system	Li-Cor Biotechnology	

Chemi Doc MP Imaging System	Bio-Rad	
CFX384 Real-Time PCR System [C-1000 Touch Thermal Cycler]	Bio-Rad	
Synergy H1Multi-Mode Plate Reader [monochromator & filter optical system (HTRF & Green/Blue); dual reagent dispensers]	Synergy	
ZOE Fluorescent Cell Imager	Bio-Rad	

Table 3. Primer sequences

Primer name	**Sequence**
ATG3-F	ACTGGAAGTGGCTGAGTACC
ATG3-R	CTGTAGCCCATTGCCATGTTG
ATG12-F	CTATGAGTGTTTTGGCAGTGATGG
ATG12-R	TTCAGAGCTGTCTCTTCCGTG
ATG16L1-F	CGAGAGATGGAGCTGTTGGG
ATG16L1-R	CCCAGGTGCACTGAATGTCT
VPS34-F	CATGTTTCGCCAAGGGATGC
VPS34-R	TGGTGAGCTTGGCAAGACG

DFCP1-F	CTTCATGGCTCAGTCGGTGT
DFCP1-R	TGCAGCTCAGAATCTGGGAG
18s-F	GTTCAGCCACCCGAGATTGA
18s-R	CCCATCACGAATGGGGTTCA
28s-F	AGCCGACTTAGAACTGGTGC
28s-R	GGCAGAAATCACATCGCGTC
MAP1LC3B/B2-F	GAGAAGCAGCTTCCTGTTCTGG
MAP1LC3B/B2-R	GTGTCCGTTCACCAACAGGAAG
MTCO2-F	AACCAAACCACTTTCACCGC
MTCO2-R	CGATGGGCATGAAACTGTGG
EGFR-F	TTGCCGCAAAGTGTGTAACG
EGFR-R	GAGATCGCCACTGATGGAGG
H1.1-F	AGGCAACGGGTGCATCTAAA
H1.1-R	GATTTCCTTGTTGCCGCAGG
ATG7-F	CGTTGCCCACAGCATCATCTTC
ATG7-R	CACTGAGGTTCACCATCCTTGG
ATG5-F	GCAGATGGACAGTTGCACACAC
ATG5-R	GAGGTGTTTCCAACATTGGCTCA

ATG2B-F	CTTCAGATGGAGTTGGAGGAGAC
ATG2B-R	AGTGGCTCCTTTCAGTCCTACG
p62-F	TGTGTAGCGTCTGCGAGGGAAA
p62-R	AGTGTCCGTGTTTCACCTTCCG
ATG4-F	CCTTCGCCTGGGCATAAA
ATG4-R	GTATGAGGGTCCAAGAAGATGAG
NBR1-F	CCTGAGAGCTTGCTCCAGTCTA
NBR1-R	CTTGGTTCCTGGCTGAAGGTGA
NDP52-F	CCAGTTCTGCTATGTGGATGAGG
NDP52-R	GTGCTGCTCAATCTCTTCCACC
RACK1-F	AATACCCTGGGTGTGTGCAA
RACK1-R	GCCAGGTTCCATACCTTGACC
EIF5A-F	TTCGAAGACTGGCAAGCACG
EIF5A-R	TGGATGCCAATCAGCTGGAAG

2.2 Cell Culture

HeLa (CCL2, ATCC) and HEK293T (CRL-3216, ATCC) cells were cultured in complete medium (Dulbecco's Modified Eagle's Medium/ DMEM containing 10% fetal bovine serum and 1% penicillin-streptomycin) in an incubator set at 37°C with 5% CO_2. For all stress granule

experiments, cells stably expressing Ras-GTPase-activating protein-binding protein 2 (G3BP2)-eGFP (enhanced Green Fluorescent Protein) were induced with 0.5 mM sodium arsenite for 30 min followed by a PBS wash and recovery in complete DMEM medium for up to 2 h.

2.3 Plasmid Transfection Using Polyethylenimines (PEIs)

Cells were rinsed with Phosphate-Buffered Saline (PBS) and replaced with fresh complete medium. Proper volume of media without Fetal Bovine Serum (FBS) were added into sterile Eppendorf tube (e.g., for 6 well plate, place 6 tubes with 200 µL DMEM without FBS or Opti-MEM in each of them) and mixed with planned amount of plasmid DNAs. Then polyethylenimine (PEI) (ratio: 4 µL PEI to 1µg plasmid DNAs) were then mixed with DNA transfection mixture and incubated at room temperature for ~15min to 30min with occasional vortexing to allow formation of liposomes. DNA-liposomes were added to the cell culture medium and incubated with cells at 37°C in a CO_2 incubator for 48 h until harvesting cells.

2.4 siRNA Knockdown with Lipofectamine

Cells were transfected with siRNAs using Lipofectamine™ RNAimax. One day before transfection, cells were plated in complete medium (DMEM with 10% FBS medium without antibiotics) in such a concentration that they would be 50% confluent at the time of transfection. For each transfection, siRNA - RNAiMAX complexes were prepared by following the standard protocol. Briefly, the siRNA and the Lipofectamine RNAiMAX were diluted in appropriate volume of Opti-MEM medium. The two diluted products were then mixed and incubated for 5 minutes at room temperature to allow complex formation to occur. The siRNA - RNAiMAX complexes were then added to each well containing cells and medium. The plates were gently

rocked so as to mix the contents followed by incubation at 37°C in a CO2 incubator for 72h until it was time to harvest the cells for further downstream analysis.

2.5 Western Blotting

Cells were lysed with Radio-Immunoprecipitation Assay (RIPA) buffer to isolated proteins, which were normalized to the same amount following (bicinchoninic acid) BCA assay. Equal amount of proteins were collected and diluted in buffer and 4× Laemmli sample buffer with 10% 2-Mercaptoethanol and boiled for 5 mins at 99 °C. Samples were then separated by Sodium Dodecyl Sulfate–Polyacrylamide Gel Electrophoresis (SDS–PAGE) at 100 V for 15 mins for stacking and 150 V for 1 h for resolving. Samples were transferred on a positively charged polyvinylidene difluoride (PDVF) membrane for 1.5 h at 100 V. Membranes were washed with 1× TBST/ Tris-Buffered Saline with Tween-20 (3 × 5 mins) and blocked with non-fat milk dissolved in 1× TBST for 1 h at room temperature. Post incubation, membranes were rinsed once with 1x TBST and then incubated at 4 °C overnight with the appropriate dilutions of the primary antibody. Following the O/N incubation, membranes were washed with TBST (3 × 5 mins) and incubated for 1 h with appropriate secondary antibody conjugated to HRP (Horseradish Peroxidase). Membranes were then washed with TBST (3 × 5 min) and incubated with HRP substrate before imaging with Li-Cor Odyssey Fc imaging system (Li-Cor Biotechnology). After imaging, the mean intensity of target protein was quantified with Fiji software.

2.6 In Vitro APEX2 Proximity Labeling

APEX2-DFCP1 plasmids, APEX2-DFCP1 and APEX2-LC3B expressing HeLa cells were gifts from Dr. Christian Behrends. APEX2 expressing cells were seeded in 15 cm plates until they were 90% confluent. 24 h before collection, APEX2 expression was induced with doxycycline

(40 µg/mL). On the day of collection, cells were treated with Torin 1 for 4 h to induce autophagy. APEX2 labeling was then initiated by changing the medium to fresh complete DMEM medium containing 500 mM Biotin-Phenol/ biotin-tyramide (BP). The cells were incubated at 37°C under 5% CO_2 for 30 min following which they were incubated with 1 mM H_2O_2 and gently agitated for 1 min at room temperature (RT). The unlabeled controls were processed identically, except that the H_2O_2 addition step was omitted.

The reaction was quenched by replacing the medium with equal volume of quenching buffer (5 mM Trolox, 10 mM sodium ascorbate and 10 mM sodium azide in DPBS/ Dulbecco's Phosphate-Buffered Saline) and gently agitating the plates for 10 min. Cells were further washed with cold sterile PBS (2 times, each last 5 min). Post washing, cells were either fixed for immunofluorescence staining with streptavidn-Alexa488 antibody to label biotinylated molecules or collected by scrapping, transferred to 1.5-mL Eppendorf tubes and pelleted by centrifugation at 300×g for 3 min at 4°C before being stored at -80°C for further experiments.

2.7 Streptavidin Purification of Biotinylated RNAs

TRIzol was added to APEX2 proximity biotinylated or unlabeled (controls) cell pellets. Cellular RNAs were extracted following manufacturer's protocol. Dynabeads™ MyOne™ Streptavidin C1 Beads were used to enrich biotinylated RNAs. 10 µL beads were used for every 25 mg of total RNAs. Beads were washed with 1× Binding and Washing (B & W) Buffer (5 mM Tris-HCl (pH 7.5), 0.5 mM EDTA/ Ethylenediaminetetraacetic acid and 1 M NaCl) thrice, followed by washing with Solution A (Diethyl pyrocarbonate/ DEPC-treated 0.1 M NaOH and DEPC-treated 0.05 M NaCl) twice, and again washing them with Solution B (DEPC-treated 0.1 M NaCl) once. The beads were then suspended in 500 µl of 2× B & W Buffer and incubated with 500 ul RNAs

(diluted in nuclease-free water) on a rotator for 2 h at 4°C. After rotation, biotinylated RNA-coated beads were then washed with 1× B & W Buffer and eluted with magnet rack for 3 times. The eluted beads with the biotinylated RNAs were resuspended in 7 μL of RNase-free water for downstream applications.

2.8 RT-qPCR on Biotinylated RNAs

10 μL M-MuLV Reverse Transcriptase Reaction system was used to synthesize complementary DNA (cDNA) from beads-coated biotinylated RNAs and input RNAs (1 μg). After the RT reaction, cDNAs from biotinylated RNAs were separated from beads using the magnet rack. The cDNAs were diluted for 10-fold for further qPCR analysis. Custom primers for qPCR were ordered from IDT. The SYBR™ Green Master Mix was used for the qPCR. qPCR conditions were as follows: 95 °C for 2 min, (95 °C for 30 sec, 55 °C (varies primer to primer) for 30 sec, 72 °C for 45 sec) × 50 cycles, 72 °C for 10 min.

2.9 Immunofluorescence Analysis

Cells were seeded on cover slip. On the day of collection, cover slips were fixed with 4% PFA for 10 min at RT and washed with PBS for 3 thrice. Fixed cells were permeabilized with permeabilization buffer (20 mM NH_4Cl, and 0.2% Triton in PBS) for 30 min at room temperature. Cells were subsequently blocked with 1% BSA for 1 h before being incubated with primary antibody overnight at 4°C. Next day, cells on coverslip were washed with PBS and incubated with fluorophore-tagged secondary antibody for 1 h at room temperature. Cells were then washed and mounted on a slide with VECTASHIELD mounting medium and sealed with clear nail varnish.

2.10 Polysome Profiling Fractionation

APEX2 expressing cells were processed through proximity labelling as described above (BP +/- H_2O_2). The cells were treated with 100 µg/µL of Cycloheximide (CHX) for 5-10 min before applying quenching buffer. The cells were scraped and pelleted at 400×g at 4°C (supernatant was discarded). Cell Pellets were resuspended in 450 µL of 1st lysis buffer (5 mM 1M Tris-HCl pH 7.5, 1.5 mM KCl, 2.5 mM MgCl2, 1× Protease Inhibitor, 20U/mL RNase Inhibitor, 1 mM Dithiothreitol (DTT), prepared in RNase-free conditions) and vortexed for 5 seconds. 50 µL of 2nd lysis buffer (0.5% Triton X-100, 0.5% Sodium deoxycholate) was subsequently added to the cell suspension prior to another 5 seconds of vortexing. The cells in lysis buffers were then incubated on ice for 15 min. Cell lysates were then collected by centrifugation at 14,000 RPM at 4°C for 15 min to pellet out the debris. Optical Density at 260 nanometers (OD260) of each sample was measured and all samples were normalized to the lowest absorbance to a total volume of 500 µL per sample (for consistency of samples to be loaded for ultracentrifugation). 10% of lysate samples (50 µL) were kept in -80°C as input.

60% sucrose was diluted in polysome buffer containing 20 mM HEPES/ 4-(2-hydroxyethyl)-1-piperazineethanesulfonic acid (PH7.6), 0.1 M KCl, 5 mM $MgCl_2$, 1× Protease Inhibitor, 20 U/mL RNase Inhibitor, 0.1 mM DTT, and prepared in RNase-free conditions to make 5 % (w/v) and 50 % (w/v) sucrose solutions. Sucrose gradients were prepared using the BioComp model 108 Gradient Master with 5% (w/v) and 50% (w/v) sucrose solution at the mode of 7-47 % sucrose gradient.

500 µL were removed from the top of each sucrose gradient and 450 µL of 500 µL balanced cell lysate samples were slowly loaded on top of the sucrose gradients to prevent disrupting the

gradient. The tubes were balanced using the hypotonic lysis buffer and then centrifuged at 190,000 × g (~39,000 RPM) at 4°C for 2 h with SW41Ti rotor. After centrifuge, sucrose gradient was separated into ribosome-free sub fractions (sub), light polysome fractions (light) and heavy polysome fractions (heavy) using density gradient fractionation system by monitoring their absorbance at 254 nm. The polysome profile of each sample was recorded with UA-6 absorbance detector. The separated sucrose gradient fractions were subsequently collected and stored at -80 °C prior to further processing.

2.11 Streptavidin-based Purification of Biotinylated RNAs from Distinct Ribosome Fractions

1.8 mL out of 2 mL of sucrose gradient samples (containing RNAs and proteins) from ribosome-free sub fractions, light polysome fractions or heavy polysome fractions were incubated with 5-10 µL of MyOne™ Streptavidin C1 beads and rotated for 2 h at 4°C. The leftover 0.2 mL of sucrose was used as input. Biotinylated samples coated with Streptavidin C1 beads were then washed with 1X B &W Buffer and eluted with magnet rack for 3 times. TRIzol was then added to the eluted samples and inputs to extract biotinylated RNAs from streptavidin beads for RT-qPCR.

2.12 FISH Staining

Cells were seeded on glass coverslips and transfected with plasmid for 48 h. Cells were fixed in 4% PFA in PBS for 10 min at room temperature (RT) and washed with PBS, the coverslips were subsequently permeabilized and blocked for 1 h at RT with (0.2% Triton X-100, 1% BSA, 100 µg/mL salmon sperm DNA and 250 µg/mL RNA from yeast extract in PBS). The coverslips were then washed once with Stellaris Wash Buffer A at RT followed by incubation with Stellaris

fluorescent-labelled mRNA probes (against *ATG3*, *ATG12*, and *β-actin*) diluted in hybridization buffer (90% Stellaris Hybridization buffer, 10% formamide) at 37°C overnight in the dark. On the next day the coverslips were washed with Wash Buffer A, mounted on a slide with VECTASHIELD mounting medium with DAPI and sealed with clear nail varnish.

2.13 Nascent Protein Labeling with Click-iT® AHA (L-Azidohomoalanine)

L-Azidohomoalanine (AHA) is an amino acid analog of methionine that can be incorporated into newly synthesized proteins. AHA also contains an azido moiety that can "click" to an alkyne moiety (Wang et al., 2017; Zhang et al., 2014). Cells were cultured in complete DMEM medium overnight. On the day of AHA labeling, seeding media was aspirated off, cells were washed once with warm PBS and replaced with methionine-free RPMI medium and incubated again (37°C, 5% CO_2) for 1.5 h to deplete methionine reserves. AHA (50 μM) was then added to the culture medium (control group had vehicle added to it) and incubated with cells for another 30 mins. The cells were then washed twice with PBS and fixed with 4% PFA in PBS for 15 minutes at RT. Cells were then permeabilized with 0.2% Triton-X-100 in PBS containing 20 mM NH4Cl for 15 minutes. After PBS washing, cells were blocked with 3% BSA in PBS for 1 h at RT and washed thrice with 1% BSA in PBS. The cells were then used for the click reaction with the alkyne-tagged Alex Flour 488 using the Click-iT® Cell Reaction Buffer Kit.

2.14 Stable Isotope Labeling by Amino Acids in Cell Culture (SILAC) in APEX2-Expressing Cells

APEX2-DFCP1 expressing cells were incubated in DMEM along with Torin1 and consisting of $^{13}C_6$- $^{15}N_2$ L-Lysine-2HCl and $^{13}C_6$ -$^{15}N_4$ L-Arginine-HCl, for 30 min, before being biotinylated with BP and H_2O_2, following which they were lysed with RIPA buffer and subjected to

streptavidin bead pulldown. For 100% labeling, cells were incubated in DMEM consisting of $^{13}C_6$- $^{15}N_2$ L-Lysine-2HCl and $^{13}C_6$ -$^{15}N_4$ L-Arginine-HCl and passaged for five doubling events, the incorporation of heavy amino acids was tested using mass spectrometry analysis.

2.15 SILAC-Labeled Biotinylated Protein Pulldown and Sample Preparation for Mass Spectrometry

Biotin-streptavidin pulldown samples were prepared for mass spectrometry analysis in an 'on-bead' digestion method. Briefly, a magnetic stand was used to remove excess liquid from the beads suspension. The eluted beads were resuspended in 9 µL of 20mM Tris-HCl (pH 8) with 1.6 µL of 25mM DTT and then incubated for 30 minutes at room temperature. After adding 1.2 µL of 50mM iodoacetamide and incubated for 10 minutes, 10 µL of 100 ng/µL mass-spec grade trypsin was then added to achieve a final concentration of 45 ng/µL. The mixture was then incubated on the rotator at 37 °C overnight. The next day, the beads were removed with a magnetic stand, and additional 500ng of trypsin was added for 4 hours incubation at 37 °C with gentle vortexing. Digestion was stopped with formic acid (F.A.) at a final concentration of 2%. For desalting, Sep-Pak tc18 1cc cartridges were conditioned in 900 µL of 100% acetonitrile (ACN) followed by 300 µL of 50% ACN and 0.5% acetic acid (HAcO). Cartridges were then equilibrated with 900 µL of 0.1% trifluoroacetic acid (TFA). Samples were adjusted to a final concentration of 0.4% TFA, passed through the cartridges, desalting with 900 µL of 0.1% TFA, washing with 90 µL of 0.5% HAcO, and elution with 500 µL of 50% ACN, 0.5% HAcO. LCMS Analysis was processed by following this protocol (Pelletier et al., 2020) and generated data was recorded using Xcalibur software (ThermoFisher Scientific).

2.16 Live-Cell Imaging

Cells were seeded on a 8-welled µ-Slide chambered polymer coverslips at a density of 15,000 cells per well. A live imaging chamber maintained at 5% CO_2 and 37°C on a Quorum spinning disk confocal microscope (Leica DMI6000B inverted model) was used. Multiple cells in the field of view were selected for imaging and phenol red-free DMEM medium containing INK128 (50 nM) with or without CHX was added. Cells were imaged every 30 min for up to 6 hours. DAPI signals (405 nm laser and DAPI emission filter set, 460/50 nm), GFP signals (490 nm laser and FITC emission filter set, 525/50 nm), and mCherry signals (561 nm laser and Cy3 emission filter set, 605/52 nm) were detected. A 63X oil immersion objective/1.4 NA was used. Images were captured with a sCMOS camera: Photometrics Prime BSI (1966x1966).

2.17 Colocalization Spots Analysis with Imaris Software

Z-stack images with GFP, mCherry, and DAPI channels were imported into the Imaris8 Software. The spots from GFP, mCherry, and DAPI channels were 3D rendered with Imaris Spots and the number of single mCherry positive dots and single DAPI positive nucleus, along with the fluorescence intensity change of GFP and mCherry over 6h imaging period were quantified and exported from the Statistics (Abu Bakar et al., 2023). Colocalization of GFP positive spots and mCherry positive spots was analyzed by the distance between these signals, using the colocalization plugin of Imaris software. Spots were considered colocalized if the distance between the spots in the GFP and mCherry channels was less than or equal to half the sum of their diameters. Based on this, the number of double fluorescent spots (LC3-mCherry positive and LC3-GFP positive) were quantified.

2.18 Immunoprecipitation

Torin1 treated wild type (WT) HeLa cells were lysed with NP40 lysis buffer (50 mM Tris-HCl pH 7.5, 150 mM NaCl, 1% NP40, 1 Roche Complete Protease Inhibitor Cocktail Tablet) for 20 min at 4 °C and centrifuged at 5000× g for 10 min. Protein concentration was measured with BCA assay. 10 µL of protein G-Dynabeads were added to into every lysate and vortexed for no more than 20 mins at 4 °C to gets rid of any proteins from cell lysate that sticks to the beads. Every 1000 µg pre-cleared lysate was further incubated with 4 µg RACK1 or mouse IgG antibody for 3 h at 4 °C before incubation with 25 µL wet volume of protein G-Dynabeads (1 h, 4 °C) to form the immune complex. Subsequently, beads were collected by using a magnetic rack and washed with 1mL wash buffer (50mM Tris-base, pH 7.5 and 150mM NaCl, 0.1% NP-40) thrice. Half eluted samples were suspended in 1X SDS-sample buffer and boiled at 99 °C for 10 min to release the proteins while denaturing them. The supernatants were eluted with magnet rack right after boiling and loaded onto a gel along with the inputs for western blot. The left-over eluted samples were further used for mass spectrometry or RNA extraction, followed by RT-qPCR or RNA sequencing.

2.19 RNA Immuno-Blot Assay

2 µL of APEX2-biotinylated RNAs and un-biotinylated RNAs were pipetted onto a positively charged nylon membrane (Roche, Mannheim, Germany). RNAs were cross-linked to the nylon membrane with UV light (120 mJoule for 1min of both sides at 254 nm) (Miller et al., 2018). Biotinylated RNAs were detected using the Chemiluminescent Nucleic Acid Detection Module Kit, which includes Stabilized Streptavidin-HRP Conjugate and Substrate Working Solution. The

kit features an enhanced luminol HRP substrate for sensitive detection of biotinylated signals. Detection was followed by imaging with a Charge-Coupled Device (CCD) camera.

2.20 Proximity Ligation Assay (PLA)

Proximity Ligation Assay (PLA) is a sensitive and specific method for in situ detection of endogenous interactions between proteins in cells. If two target proteins interact or are in close proximity, the oligonucleotide-conjugated antibodies, each specific to and bound to one of the proteins, will enable the oligonucleotides to ligate, forming a circular DNA molecule that can be amplified and detected (Romero-Fernandez et al., 2023). Duolink® In Situ Detection Reagents Orange kit (including Ligase, Ligation buffer, DNA polymerase, and Amplification Orange buffer) was used. Cells seeded on coverslips were fixed with 4% PFA and permeabilized before being blocked with Duolink Blocking buffer for 60 min at 37°C. The coverslips were incubated with primary antibodies diluted in Duolink® Antibody Diluent for 1 h at room temperature. Coverslips were washed 2 times for 5 min in Wash Buffer A and then incubated with PLA probes (MINUS and PLUS probes) corresponding to the primary antibodies (Duolink® In Situ PLA Probe Anti-Mouse MINUS and Duolink® In Situ PLA Probe Anti-Rabbit PLUS) for 1 h at 37°C. Then, coverslips were washed twice for 5 min with Wash Buffer A and then incubated with a DNA ligase diluted in Ligation buffer for 30 min at 37°C. Coverslips were again washed twice for 5 min with Wash Buffer A and incubated with a DNA polymerase diluted in Amplification buffer for 100 min at 37°C. Finally, coverslips were washed twice for 10 min with 1× Wash Buffer B followed by a single wash with 0.01× Wash Buffer B for 1 minute before being mounted with Duolink® In Situ Mounting Media with DAPI. Fluorescence was visualized with a confocal microscope with Z-stack.

2.21 Lentiviral Vector Production and Transduction

HEK293T cells stably expressing APEX2-DFCP1 were generated via lentiviral transduction. Lentivirus was produced through co-transfection of WT HEK293T cells with the packaging plasmids psPAX2 and pMD2.G, along with the APEX2-DFCP1 plasmid. The media was harvested 48 h and 72 h post transfection and filtered through a 0.45 μM PES membrane. The produced lentivirus was concentrated by ultracentrifuging the media at 20,800 rpm with SW32Ti rotor for 2 h. HEK293T cells were seeded in 6 well plates 24 h before being infected with the concentrated lentivirus suspension along with 8 μg/mL of polybrene. After 48 h, media was changed, and infected cells were selected with puromycin (2 μg/mL) and the fluorescence of infected cells was confirmed under ZOE Fluorescent Cell Imager.

2.22 Seahorse XF Cell Mito Stress Test

Mitochondrial respiration activity was determined with OCR (Oxygen Consumption Rate) using the Seahorse Flux Analyzer XF24 (Agilent Technology) and the Seahorse XF Cell Mito Stress Test Kit according to the manufacturer's protocol (Gu et al., 2021). Briefly, 5,000 HEK293T cells were seeded on XF24-well cell culture microplates and next day they were transfected with siRNA and incubated for another 72 h. On the day of running the Seahorse assay, cells were treated with/without CHX along with or without Torin1 ± Bafilomycin A1.

Basal respiration was measured in XF DMEM supplemented with 1 mM sodium pyruvate, and 10 mM D-glucose and 2 mM glutamine after incubation at 37°C in an incubator without CO_2 for 1 h. Periodic oxygen consumption measurements were performed with inhibitors that specifically target components of the electron transport chain to derive multiple parameters of mitochondrial respiration. Metabolic states were measured after subsequent addition of 3 μM oligomycin, 1 μM

FCCP (carbonyl cyanide 4 (trifluoromethoxy) phenylhydrazone), 1 μM antimycin A, and 2 μM rotenone. Wave software (Agilent Technologies) was used to analyze OCR data and OCR was calculated from the slope of change in oxygen concentration over time. OCR data were normalized by protein concentration and the average values were taken for each experiment. Six replicates were performed for each treatment and total four biological replicates of experiments were performed.

2.23 Mitochondrial Morphology Analysis

Cells were seeded on cover slips, transfected with indicated siRNAs after 16 h, and incubated for another 72 h. On the day of collection, cells were treated with Torin1 (500nM) for 2 h together with FCCP (20 μM) for 0.5 h before being fixed with 1% PFA for 10 min at RT and washed with PBS for 3 thrice. Fixed cells were permeabilized with permeabilization buffer (20 mM NH4Cl, and 0.2% Triton-X100 in PBS) for 30 min at room temperature. Cells were subsequently blocked with 1% BSA for 1 h before incubating with primary antibody against Tomm20, overnight at 4°C. Next day, cells were washed with PBS and incubated with Alexa fluor 488-tagged secondary antibody for 1 h at room temperature. Cells were then washed and mounted on a slide with VECTASHIELD mounting medium and sealed with clear nail varnish.

Mitochondria Analyzer plugin of FIJI software was employed to analyze the mitochondrial morphology. The block sizes and C-values were optimized through Threshold Optimize, which were followed by “Threshold” and “Analysis” to quantify key mitochondrial parameters, including mean area per mitochondria, mean perimeter per mitochondria, and mitochondria count per cell (Chaudhry et al., 2020; Hemel et al., 2021).

2.24 Nascent Protein Labeling with 6-FAM-dc-Puromycin

WT HeLa cells were seeded on glass coverslips. When cells got 50% confluent, they were transfected with a plasmid encoding mCherry-DFCP1 by PEI and cultured for another 48 h. Cells were then incubated with complete DMEM containing Torin1 (250 nM) for 2 h followed by labelling with 6-FAM-dc-puromycin (10 nM) or 6-FAM-DC (10 nM) for 20 mins in the incubator. The coverslips were fixed with 1% PFA for 10 mins at RT and washed thrice with PBS. Slides were then mounted with antifade mounting media with DAPI and sealed with nail varnish. A Leica DMI6000B Quorum Spinning Disk confocal microscope was used for imaging. 490 nm and 561 nm laser were used to excite GFP and mCherry, respectively. 63 × oil objective/1.4 NA was used. The emissions of fluorescence were captured by an sCMOS camera (Photometrics Prime BSI 1966x1966).

2.25 Streptavidin Purification of APEX2-Biotinylated Nascent Proteins

APEX2-DFCP1 expressing cells were cultured in methionine-free RPMI medium with Torin1 (250 nM) for 1.5 h. The cells were then treated with AHA (50 μM) or vehicle for 30 mins, and subsequently proximity labelled as previously described (BP ± H_2O_2) for 30 min. Quenching buffer was added to stop the reaction. Cells were then washed twice with PBS, scrapped with cell lifters, and transferred to 1.5-mL Eppendorf tubes for pelleting by centrifugation. Cell pellets were lysed with 50-100 μL of the lysis buffer (containing 0.5% sodium deoxycholate and 0.5% Triton X-100 in PBS) followed by centrifugation at 10000× g for 15 mins to isolate protein supernatants. The proteins were clicked to Alexa Fluor™ 488 Alkyne (5 μM) using the Click-iT® Protein Reaction Buffer Kit. APEX2 biotinylated proteins were pulled down by the Streptavidin C1 beads for analysis by western blotting. Transferred PVDF membrane was

incubated with HRP-conjugated anti-Alexa 488 overnight before reacting with HRP substrate for imaging.

2.26 APEX2-sequencing

APEX2 biotinylated RNAs were pulled down by streptavidin beads and extracted with TRIzol before being sent to sequencing service provider Innomics for RNA sequencing with DNBSEQ platform at reading length of PE 100bp. RNA-seq libraries were constructed following the Standard DNBSEQ Eukaryotic Transcriptome Resequencing protocols.

The raw data from the DNBSEQ platform was processed using nf-core/rnaseq v3.14.0 (doi: https://doi.org/10.5281/zenodo.1400710) of the nf-core collection of workflows (Ewels et al., 2020). Sequences were aligned to the human GRCh38 genome and v45 GENCODE annotations using STAR 2.7.9a (Dobin et al., 2013) and quantified using Salmon 1.10.1 (Patro et al., 2017), generating gene based read counts and Transcripts Per Million (TPM) files.

2.27 Statistics

The data are displayed as mean ± standard deviation (SD). Statistical significances were calculated in GraphPad Prism with either Student's t-test, or one-way ANOVA/ Analysis of Variance, or two-way ANOVA as per requirement. P values less than 0.05 were considered statistically significant.

Chapter 3. Nascent Translation During Sustained Autophagy

3.1 Background

Since mTORC1 phosphorylates 4E-BPs, preventing their binding to eIF4E, which allows eIF4G to bind and stabilize eIF4E on the 5' cap, thereby promoting translation initiation (Klann et al., 2020). Under stress, autophagy can be induced by inhibiting mTORC1, accompanied by the repression of cap-dependent translation. The formation of autophagosomes engages over 35 autophagy-related proteins in a cascade that results in the covalent modification of LC3 proteins with the lipid PE, to form LC3-II. Autophagy receptors like p62/ SQSTM1, NBR1 and LC3-II are also degraded by lysosomal hydrolases together with engulfed cargoes, consistent with their relatively short half-lives (Bjorkoy et al., 2005; Johansen and Lamark, 2011). Additionally, LC3 and its lipid modification are essential, with rare exceptions, for autophagy and thus the accumulation of LC3-II and its subsequent turnover in autophagosomes correlates with the number of autophagosomes and autophagy activity (Klionsky et al., 2021).

3.2 Results

3.2.1 Overall cellular translation was inhibited during autophagy.

Torin1, a small molecule mTOR inhibitor, was commonly used to induce bulk autophagic flux (Thoreen et al., 2009). The Torin1-induced autophagy was confirmed by the increase protein levels of LC3-II that further increased when lysosomal degradation and lysosome-autophagosome fusion were inhibited by Bafilomycin A1 (BAF) (Figure.3-1a). Polysome profiling is a powerful technique for studying protein translation regulation, allowing for the analysis of individual mRNAs or genome-wide translation (Chasse et al., 2017). It separates

polysomes, ribosomes, subunits, and free mRNAs through sucrose gradient centrifugation of a cytoplasmic lysate. Torin1 also reduced global translation as indicated by a loss of ribosome occupancy on mRNAs in polysome fractionation experiments, as seen in the polysome profile plot (Figure.3-1b).

DFCP1 has also been documented to label omegasomes through specific interactions with PI3P and found expressed on mitochondria and Golgi apparatus (Gao et al., 2019). Due to the inconsistency in the expression pattern of DFCP1, we validated DFCP1 as a marker of forming autophagosomes. With double fluorescent plasmid transfection, DFCP1 was found to localize to omegasomes (phagophore precursors) when autophagy is induced, as DFCP1-mCherry was found located around ER-BFP (Blue Fluorescent Protein) positive signals (Figure.3-1c), and co-localized with WIPI1-GFP, a common marker of phagophores (Figure.3-1d) under Torin1 treatment.

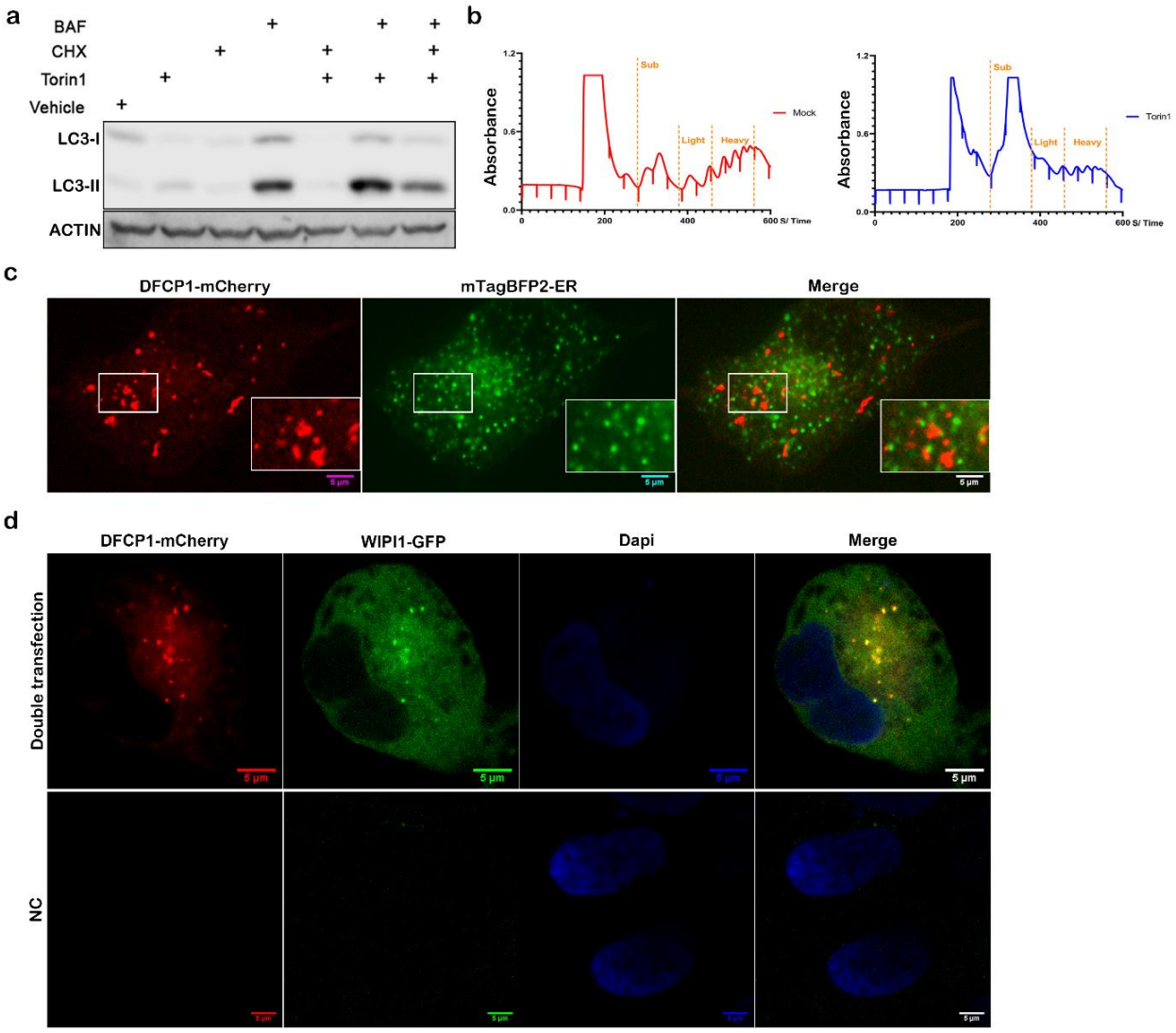
a
BAF
CHX
Torin1
Vehicle
LC3-I
LC3-II
ACTIN
b
Absorbance
Sub
Light
Heavy
Mock
Torin1
S/ Time
c
DFCP1-mCherry
mTagBFP2-ER
Merge
5 μm
d
DFCP1-mCherry
WIPI1-GFP
Dapi
Merge
Double transfection
NC
5 μm

Figure.3-1 Cellular translation was inhibited during autophagy.

(a) Torin1 induced autophagy. Western blot of LC3-I/ II and β-actin protein levels in cells treated with Torin1 (250 nM), ± BAF (500 nM), ± CHX (100 μg/mL) for 6 h. (b) Torin1 inhibited cellular protein synthesis. Representative A260 absorbance reading of ribosome profiles from mock-treated or Torin1-treated HeLa cells. Orange dashes outline the heavy and light polysome fractions, as well as the sub-polysome fractions. (c) Representative fluorescence microscopy image of cells transfected with DFCP1-mCherry and ER-BFP to identify the colocalization between DFCP1 and ER under Torin1 treatment. (d) Fluorescence microscopy image showing the colocalization of DFCP1-mCherry and WIPI1-GFP. Cells were co-transfected with DFCP1-mCherry and WIPI1-GFP plasmids and treated with Torin1 (250 nM) for 4 h and accompanied with the negative control.

3.2.2 Specificity of APEX2-based proximity labeling

APEX2, an engineered ascorbate peroxidase, catalyzes the oxidation of biotin-phenol (BP) in a reaction potentiated by a 1-minute pulse of H_2O_2. This generates short-lived biotin radicals that covalently ligate to nearby molecules within a 20 nm radius of APEX2, enabling the enrichment of APEX2 nearby molecules using streptavidin beads and their subsequent identification (Fazal et al., 2019; Lam et al., 2015) (Figure.3-2).

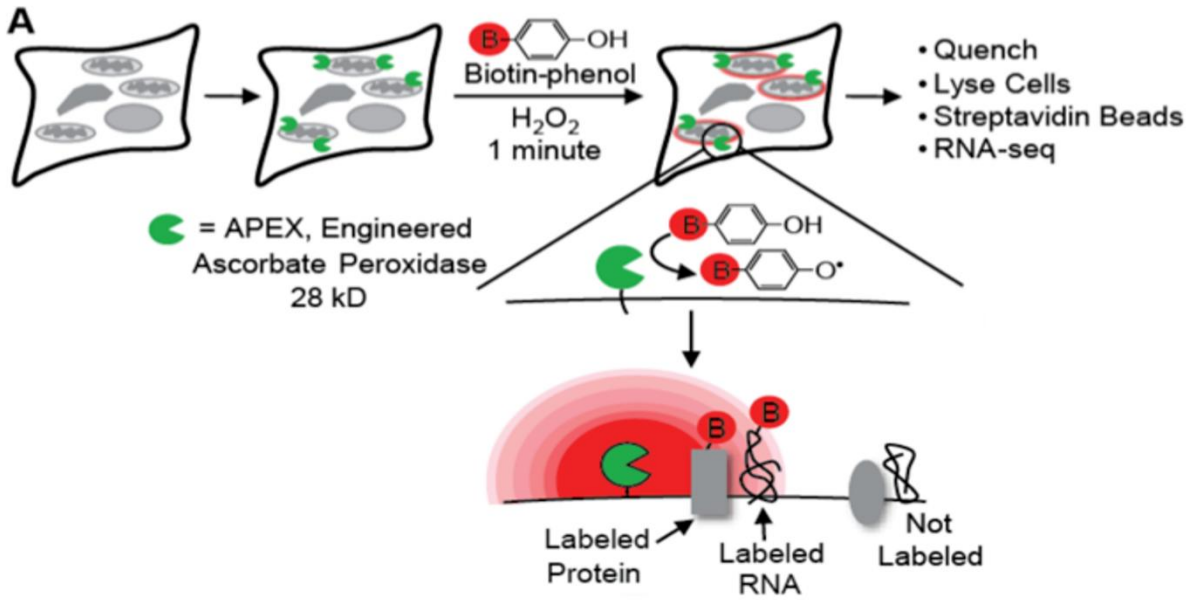

Figure.3-2 Model of APEX2-based proximity biotinylation.

(a) Endogenous RNAs and proteins of live cells within a few nanometers of APEX2 were proximity biotinylated by APEX2 under the catalyzation of H_2O_2 and BP. The biotinylation reaction was quenched and cells were lysed to pulldown biotinylated molecules using streptavidin beads. The figure is adapted from (Fazal et al., 2019) with open access from Copyright © 2019 Elsevier Inc.

With the APEX2 proximity labelling, molecules in proximity to APEX2-DFCP1 or -LC3B were biotinylated and followed being labeled with Alexa Fluor 488-streptavidin (Figure.3-3a). After APEX2-DFCP1 mediated biotinylation, cellular RNAs in proximity to APEX2-DFCP1 were detected in a manner dependent on activation of APEX2 by H_2O_2 and subsequent reaction with streptavidin-HRP (Figure.3-3b). These formed discrete biotinylated foci, which colocalized with cellular DFCP1 or LC3B signals (both endogenous and transfected), respectively, thereby confirming the specificity of this proximity-based biotinylation labeling, while no discrete foci

were spotted in APEX2-DFCP1 or -LC3B cells without H_2O_2 labelling (Figure.3-3c). p62, in addition to being an autophagy receptor, is also recruited to omegasomes and participates in the early steps of autophagosome formation (Itakura and Mizushima, 2011). In agreement with this, a fraction of p62 positive punctate co-localized with molecules biotinylated by APEX2-DFCP1 (Figure.3-3d). In addition, the protein levels of APXE2-DFCP1 and endogenous DFCP1 in APEX2-DFCP1 expressing cells were similar with or without Torin1 ± BAF treatment (Figure.3-3e). This suggests that, under autophagy conditions, neither endogenous nor transfected DFCP1 protein levels were significantly affected, indicating the stability of the APEX2-based system for further use. More biotinylated proteins by APEX2-DFCP1 were observed in pulldown comparing to input samples under Torin1 conditions, which validated successful proximity labeling-based pulldown under Torin1 treatment (Figure.3-3f). In cells expressing APEX2-myc-DFCP1, the APEX2-biotinylated signals (labeled with streptavidin) colocalized with myc-DFCP1. This indicates that the biotinylation was specific to the transfected APEX2-myc-DFCP1 protein, ensuring that the proximity labeling method selectively targeted the intended proteins (Figure.3-3g). In addition, ATG14 proteins were successfully pulled down by APEX2-DFCP1-based proximity labeling and pulldown (Figure.3-3h). These results provide additional evidence for the specificity of the APEX2 proximity labeling approach.

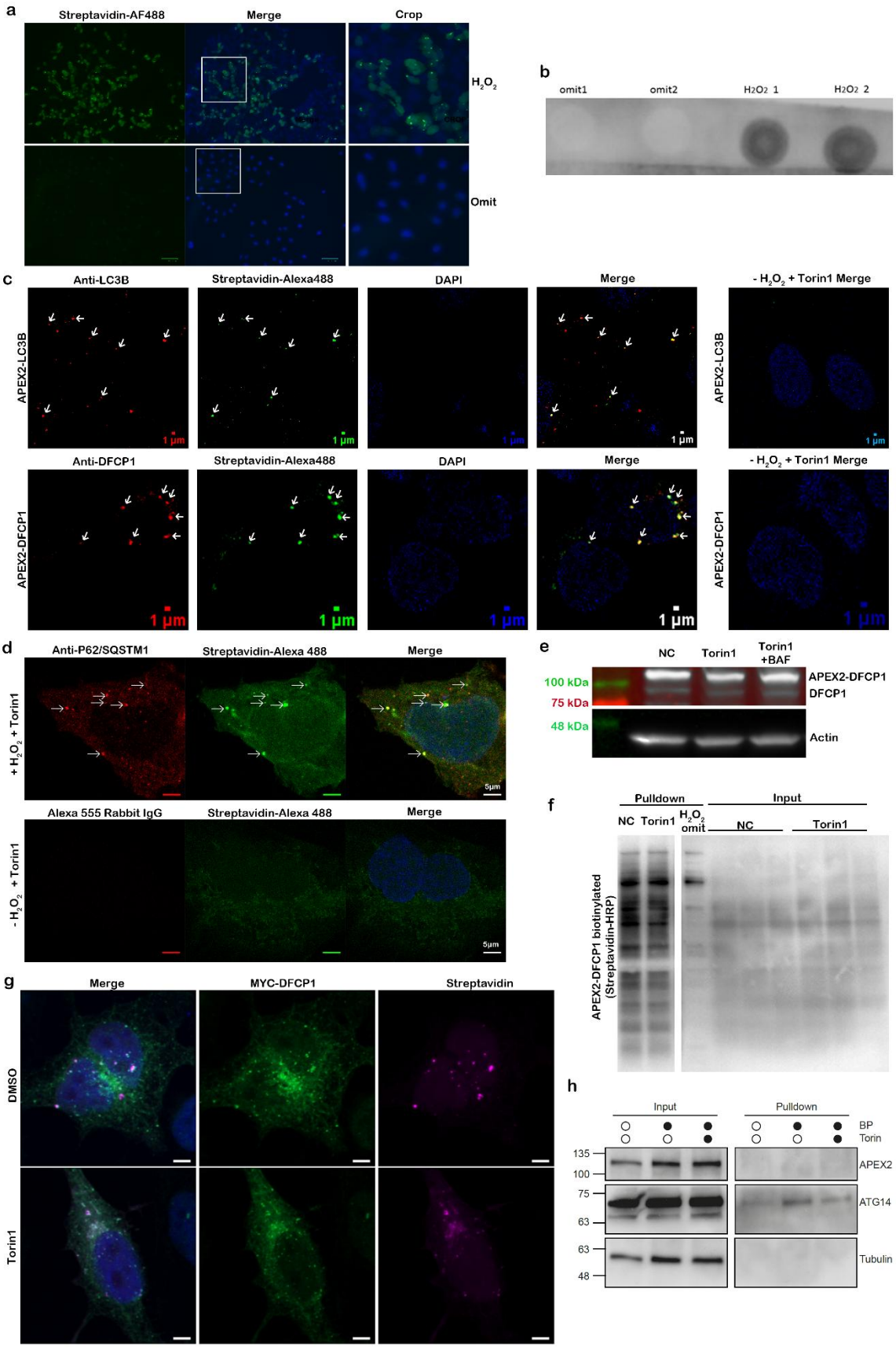
a
Streptavidin-AF488
Merge
Crop
H2O2
Omit
b
omit1
omit2
H2O2 1
H2O2 2
c
Anti-LC3B
Streptavidin-Alexa488
DAPI
Merge
- H2O2 + Torin1 Merge
APEX2-LC3B
Anti-DFCP1
APEX2-DFCP1
1 μm
d
Anti-P62/SQSTM1
Streptavidin-Alexa 488
+ H2O2 + Torin1
Alexa 555 Rabbit IgG
- H2O2 + Torin1
5μm
e
NC
Torin1
Torin1 +BAF
100 kDa
75 kDa
48 kDa
APEX2-DFCP1
DFCP1
Actin
f
Pulldown
Input
NC
Torin1
H2O2 omit
APEX2-DFCP1 biotinylated (Streptavidin-HRP)
g
Merge
MYC-DFCP1
Streptavidin
DMSO
Torin1
h
Input
Pulldown
BP
Torin
135
100
75
63
48
APEX2
ATG14
Tubulin

Figure.3-3 Specificity of APEX2-based proximity labeling.

(a) Fluorescence microscopy of biotinylated molecules (streptavidin-Alexa Fluor 488) in APEX2-DFCP1 expressing HEK293T cells. APEX2-DFCP1 expressing cells were labeled with BP± H_2O_2. (b) Biotinylation of RNAs in proximity to DFCP1. RNAs of APEX2-DFCP1 expressing cells after labelling with BP± H_2O_2 were extracted and detected by reaction with Streptavidin-HRP. (c) APEX2-DFCP1 and APEX2-LC3B specifically biotinylated their nearby molecules. Fluorescence microscopy of biotinylated molecules (streptavidin-Alexa488) in proximity to APEX2-DFCP1 in HEK293T cells and APEX2-LC3B in HeLa cells after treatment with Torin1 for 2 h. Endogenous DFCP1, LC3B and p62 signals were identified with anti-DFCP1, anti-LC3B and anti-p62/SQSTM respectively. (d) APEX2-DFCP1 specifically biotinylated their nearby molecules. Fluorescence microscopy of biotinylated molecules (streptavidin-Alexa Fluor 488) in proximity to APEX2-DFCP1 in HEK293T cells after treatment with Torin1 for 2 h. Endogenous p62 signals were identified with anti-p62/SQSTM. APEX2-DFCP1 expressing cells were labeled with BP± H_2O_2. (e) The comparison of protein levels of APXE2-DFCP1 and endogenous DFCP1 in APEX2-DFCP1 expressing cells with or without Torin1 (500 nM) +/- BAF (500 nM) treatment for 2 h. (f) Successful proximity labeling and pulldown by APEX2-DFCP1 under Torin1 conditions. The biotinylated proteins in input and pulldown in representative APEX2-DFCP1 proximity labeling experiments with/ without Torin1 (500 nM). Protein samples of input and pulldown from same group (e.g., Torin1) were displayed separated but on the same PVDF membrane. (g) APEX2-DFCP1 specifically biotinylated their nearby molecules. Fluorescence microscopy of biotinylated molecules (streptavidin) and myc-DFCP1 in APEX2-myc-DFCP1 cells with or without Torin1 treatment and labelling with BP± H_2O_2. (h) ATG14 proteins were precipitated after biotinylation in APEX2-DFCP1 expressing cells.

3.2.3 Translation is required to maintain the levels of several Atg proteins during sustained autophagy

CHX is a reversible, specific inhibitor of eukaryotic translation that binds to the E site on 60S ribosomal subunits, inhibiting eEF2-mediated translocation, halting elongation (Obrig et al., 1971; Poehlsgaard and Douthwaite, 2005; Schneider-Poetsch et al., 2010), and stalling translation by freezing polysomes on mRNAs (Bastide et al., 2018; Dermit et al., 2020). Previous attempts to use CHX to study the impact of translation on autophagy, were confounded by the use of serum-starvation to activate autophagy (Watanabe-Asano et al., 2014). CHX stops the incorporation of amino acids into proteins, which also increases the free amino acid pool, thereby re-activating mTORC1 and reducing autophagy (Watanabe-Asano et al., 2014). To avoid this confounding effect, mTOR inhibitors (INK128, Torin1) were used to ensure complete inhibition of mTORC1 during CHX treatment, which was confirmed by the sustained dephosphorylation of eIF4E-BP (Figure.3-4a, b).

To identify proteins involved in autophagy that continue to be translated during sustained autophagy, HeLa cells were treated with Torin1 and BAF, the vacuolar H+ ATPase (V-ATPase) inhibitor, which inhibited both autolysosome acidification and autophagosome-lysosome fusion, to negate the influence of protein turnover caused by lysosomal degradation (Mauvezin and Neufeld, 2015). The cellular protein levels of ATG3, ATG5, ATG12, and ATG7 were significantly reduced when translation was inhibited by CHX under Torin1 and BAF treatment, compared to treatment with Torin1 or BAF alone (Figure.3-4c, d). Protein level of ATG2, which connects the omegasome membrane to the ER membrane and functions in coordination with ATG9 to delivers phospholipids from the ER membrane to the cytoplasmic layer of omegasome

membrane (Osawa et al., 2019), was also decreased by CHX but with the P value of 0.056 (Figure.3-4c, d). The levels of ATG16L1 were not significantly altered by CHX (Figure.3-4c, d). Notably, the levels of several autophagy receptors including p62/SQSTM, NBR1, OPTN, NDP52 (CALCOCO2), and autophagosome marker, LC3A-II were also significantly depleted when translation was inhibited (Figure.3-4e, f). These data suggest that the translation of several key proteins involved in autophagy is essential for maintaining their levels and supporting the autophagic process. This becomes particularly crucial when general translation is inhibited, as in the case of sustained autophagy.

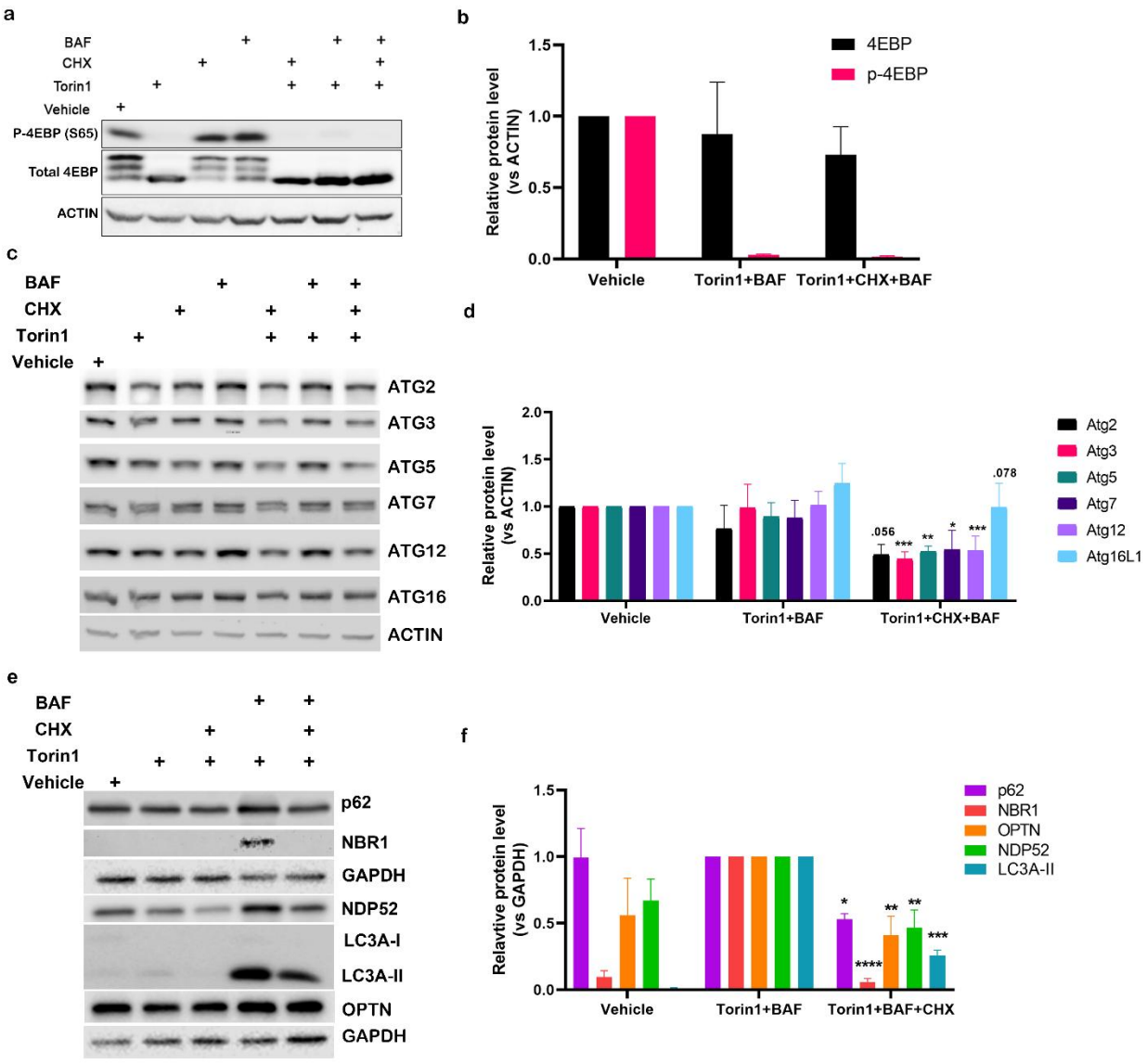
a
BAF
CHX
Torin1
Vehicle
P-4EBP (S65)
Total 4EBP
ACTIN
b
Relative protein level (vs ACTIN)
4EBP
p-4EBP
Vehicle
Torin1+BAF
Torin1+CHX+BAF
c
ATG2
ATG3
ATG5
ATG7
ATG12
ATG16
ACTIN
d
Relative protein level (vs ACTIN)
Atg2
Atg3
Atg5
Atg7
Atg12
Atg16L1
e
p62
NBR1
GAPDH
NDP52
LC3A-I
LC3A-II
OPTN
GAPDH
f
Relavtive protein level (vs GAPDH)
p62
NBR1
OPTN
NDP52
LC3A-II
Torin1+BAF+CHX

Figure.3-4 Translation is required to maintain the levels of several Atg proteins during sustained autophagy.

(a, b) Western blots and quantification of eIF4EBP, 4EBP, and β-actin protein levels in cells that were untreated or treated with Torin1 (250 nM), ± BAF (500 nM), ± CHX (100 μg/mL) for 6 hours. (c) Western blots analysis of ATG2, ATG3, ATG5, ATG7, ATG12, ATG16L1 and β-actin protein levels in cells untreated or treated with Torin1 (250 nM), ± BAF (500 nM), ± CHX (100 μg/mL) for 6 h. (d) Quantification of ATG2, ATG3, ATG5, ATG7, ATG12, ATG16L1, and β-actin protein levels from the blots in panel (c), with the statistical significance calculated by comparing to Torin1+BAF group using a two-way ANOVA analysis (n=3). (e) Western blots of p62/SQSTM, NBR1, NDP52, OPTN, LC3A-II and GAPDH proteins from cells untreated or treated with ± Torin1 (250 nM), ± BAF (500 nM), or ± CHX (100 μg/mL) for 6 h. (f) Quantification of protein levels from the blots in panel (e), and significance was calculated by comparing to Torin1+BAF group with a two-way ANOVA analysis (n=3). Statistical significance is indicated as ****P<0.0001; ***P<0.001; **P<0.01; *P<0.05.

3.2.4 Translation is required for synthesis of autophagosome/ autophagolysosome during sustained autophagy

To further evaluate the requirement of translation for sustained autophagy, HEK293T cells expressing a GFP-mCherry-LC3B autophagy dural reporter were treated with another effective mTOR inhibitor, INK128, along with or without CHX. Upon fusion of the autophagosome with the lysosome, GFP fluorescence is quenched by the low pH of the lysosome, leaving only

mCherry fluorescence. This allows for the differentiation and quantification of autophagosomes and autophagolysosomes, respectively (Mizushima et al., 2010). Inhibition of translation led to a reduction in the number of both autophagosomes and autophagolysosomes (Figure.3-5a, b, c), a result that was not attributable to changes in the fluorescence intensity of GFP or mCherry (Figure.3-5d, e). These data further suggest that translation of several proteins involved in autophagy is essential for maintaining their levels and is required for sustained autophagy.

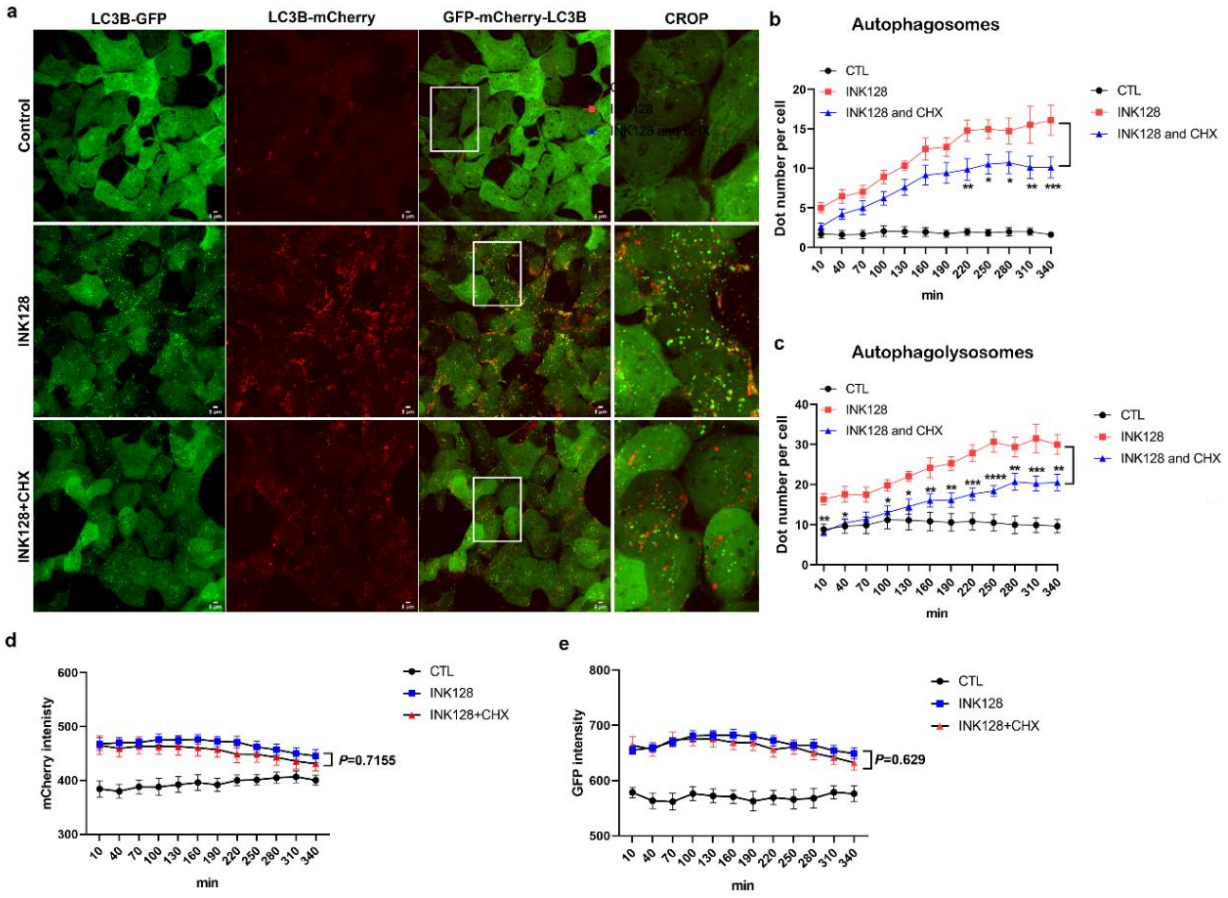

Figure.3-5 Translation is required for the formation of autophagosomes and autophagolysosomes during sustained autophagy.

(a) Representative microscopy images of HEK293T cells stably expressing the GFP-mCherry-LC3B autophagy reporter, either untreated or treated with INK128 (50 nM) ± CHX (100 μg/mL) for 6 h. The quantification of autophagosomes (b) and autophagolysosomes (c). The number of dots per cell was counted from over 250 cells for each data point (each time point), and statistical analysis between treatment groups was performed using a two-way ANOVA. The intensity of mCherry (d) and GFP (e) fluorescence in GFP-mCherry-LC3B expressing cells, either untreated or treated with INK128 ± CHX for 6 h. Statistical significance is indicated as ****P<0.0001; ***P<0.001; **P<0.01; *P<0.05.

3.3 Discussion

During autophagy, many cellular debris were degraded together with their receptors, such as p62/SQSTM1, NBR1. Therefore, the continuous synthesis of these autophagy-related proteins and receptors is essential for sustained autophagy. However, consistent with previous findings, we found the overall cellular protein synthesis was inhibited during autophagy induced by mTOR inhibitors (Torin1 and INK128). Since the inhibition of mTOR dephosphorylates 4E-BPs, which then bind eIF4E, preventing its association with eIF4G, this represses the assembly of the eIF4F complex and inhibits cap-dependent translation (Clohessy et al., 2012).

Despite that CHX has been reported to activate mTOR to inhibit autophagy (Watanabe-Asano et al., 2014), our study revealed that Torin1-mediated dephosphorylation of 4E-BPs was not significantly affected by CHX, indicating that the mTOR inhibitor, Torin1 induced autophagy through mTOR inhibition, was not repressed by CHX. Additionally, CHX treatment significantly

reduced the protein levels of several key autophagy-related proteins, and inhibited the synthesis of autophagosomes and autophagolysosomes, indicating that the continuous translation of these proteins is essential for sustaining autophagy. Therefore, general translation repression during sustained autophagy highlights the necessity of translating key autophagy-related proteins to support this process.

DFCP1 has been reported to relocate to PI3P-rich autophagosome precursor on the ER under starvation (Axe et al., 2008; Uemura et al., 2014), it also localizes to ER or Golgi apparatus in fed cells (Ismail et al., 2023), and Tomm20-positive filamentous mitochondria (Nanao et al., 2015). In our study, DFCP1-mCherry positive signals were found located around ER-BFP, and co-localized to well-known phagophores marker, WIPI1-GFP under Torin1 treatment, indicating the specificity of DFCP1 as a marker of forming autophagosomes.

APEX2 is used to catalyze the oxidation of biotin-phenol to the short-lived (<1 ms) biotin-phenoxyl radical in the presence of H_2O_2, therefore, the molecules (e.g., proteins and RNAs) in proximity to APEX2 will be biotinylated. The specificity of APEX2-based biotinylation reaction of APEX2-DFCP1 and APEX2-LC3B expressing cells was confirmed by labeling DFCP1 and LC3B with fluorescence conjugated antibody, which was found to colocalized to APEX2-biotinylated molecules. Not all LC3B or DFCP1 signals colocalized to the biotinylated molecules, which was not unexpected and could be caused by the DFCP1/LC3B signals are consists of both endogenous DFCP1/ LC3B proteins and transfected APEX2-DFCP1/LC3B proteins. Accordingly, APEX2-biotinylated signals (tagged with streptavidin) colocalized with myc-DFCP1 in APEX2-myc-DFCP1 expressing cells, further validating the specificity of APEX2-based proximity labeling without interference by endogenous DFCP1. ATG14 proteins,

components of the VPS34 complex, participate in the early stages of autophagosome formation and were successfully pulled down using APEX2-DFCP1-based proximity labeling and pulldown. All of these indicate that the APEX2-based proximity labeling successfully biotinylated its nearby RNAs and proteins and these APEX2 expressing cell lines were ready to be used for further proximity labeling.

Chapter 4. Atg mRNAs were Localized to Phagophores for Local Translation

4.1 Background

Autophagosomes are commonly recognized as emerging from the PI3P enriched smooth ER, which is devoid of ribosomes directly attached to it (Biazik et al., 2015). However, increasing number of studies using EM suggest that the regions surrounding omegasomes and phagophores are densely populated with ribosomes (Kishi-Itakura et al., 2014). Ribosomes can also localize to forming autophagosomes for degradation through a process called ribophagy (Wyant et al., 2018). However, to the best of our knowledge, it has not been assessed whether all of these ribosomes are damaged and nonfunctional, or some of these ribosomes are functional and recruited near forming autophagosomes for local mRNA translation.

Besides ATG9, the only core autophagy-related protein that is transmembrane, the other core autophagy-related proteins are neither membranous nor secreted proteins (Hurley and Young, 2017; Klionsky et al., 2011), suggesting that the Atg mRNAs should not be recruited to the ER by the SRP of translating Atg proteins. Intriguingly, increasing studies suggest that mRNAs encoding cytosolic proteins are translated on both ER-bound ribosomes and cytosolic free ribosomes (Jagannathan et al., 2014; Reid and Nicchitta, 2015). In addition, many mRNAs that do not encode membrane or secreted proteins have been observed to localize to the ER for reasons that remain unclear (Reid and Nicchitta, 2015; Voigt et al., 2017).

Our previous findings in last chapter indicate that nascent translation is essential for the maintenance of sustained autophagy. This raises the question of whether there is localized translation of Atg mRNAs near autophagosomes, providing autophagy-related proteins in a

timely and efficient manner to directly support the autophagic process. Exploring this possibility could provide deeper insights into how translation regulation is spatially coordinated with autophagy at the cellular level, and whether localized protein synthesis plays a key role in sustaining autophagic flux under stress conditions.

4.2 Results

4.2.1 Atg mRNAs localize in proximity to phagophores and autophagosomes.

To identify which mRNAs are localized in proximity to DFCP1-positive phagophores and LC3B-positive structures, APEX2-DFCP1 and APEX2-LC3B expressing cells were used. mRNAs in proximity to APEX2-DFCP1 and LC3B were biotinylated, enriched with streptavidin-coated beads, and quantified by RT-qPCR. Phagophores form from smooth ER, which lacks ribosomes, so mRNAs encoding secreted or transmembrane proteins found on the rough ER should not be labeled by APEX2-DFCP1. Indeed, mRNA encoding the transmembrane protein EGFR (Epidermal Growth Factor Receptor), was not enriched in proximity to DFCP1 or LC3B (Figure.4-1a, b). Similarly, mRNA encoding the nuclear protein, Histone H1.1 was not enriched at these sites (Figure.4-1a, b). However, mRNAs encoding proteins participating in autophagosome formation, such as ATG3, ATG12, VPS34, DFCP1, and p62/SQSTM, were found to be enriched in proximity to DFCP1, despite the fact that these proteins lack transmembrane domains (Figure.4-1a). Notably, some of these mRNAs were also enriched in proximity to APEX2-LC3B (Figure.4-1b). In addition, 18S rRNA, a marker of ribosomal activity, was found to be enriched near DFCP1 (Figure.4-1a), suggesting that mRNAs may be actively translated in proximity to the phagophore.

To further confirm, using an orthogonal method, that mRNAs encoding proteins required for autophagy localize in proximity to forming autophagosomes, we used single-molecule FISH probes targeting *ATG3* or *ATG12* mRNA conjugated to Quasar® 570 Dye. Both *ATG3* and *ATG12* mRNAs frequently co-localized with or were immediately adjacent to the phagophore marker, WIPI1 (Figure.4-1c, d). *ATG3* mRNAs also co-localized with DFCP1 positive organelles (Figure.4-1e). In contrast, *ACTB* mRNA encoding β-Actin co-localized much less frequently with WIPI1 proteins (Figure.4-1c, d). These results reinforce the proximity-labeling pulldown data (Figure.4-1a, b), demonstrating that mRNAs encoding several proteins involved in autophagy preferentially localize in proximity to phagophores and autophagosomes.

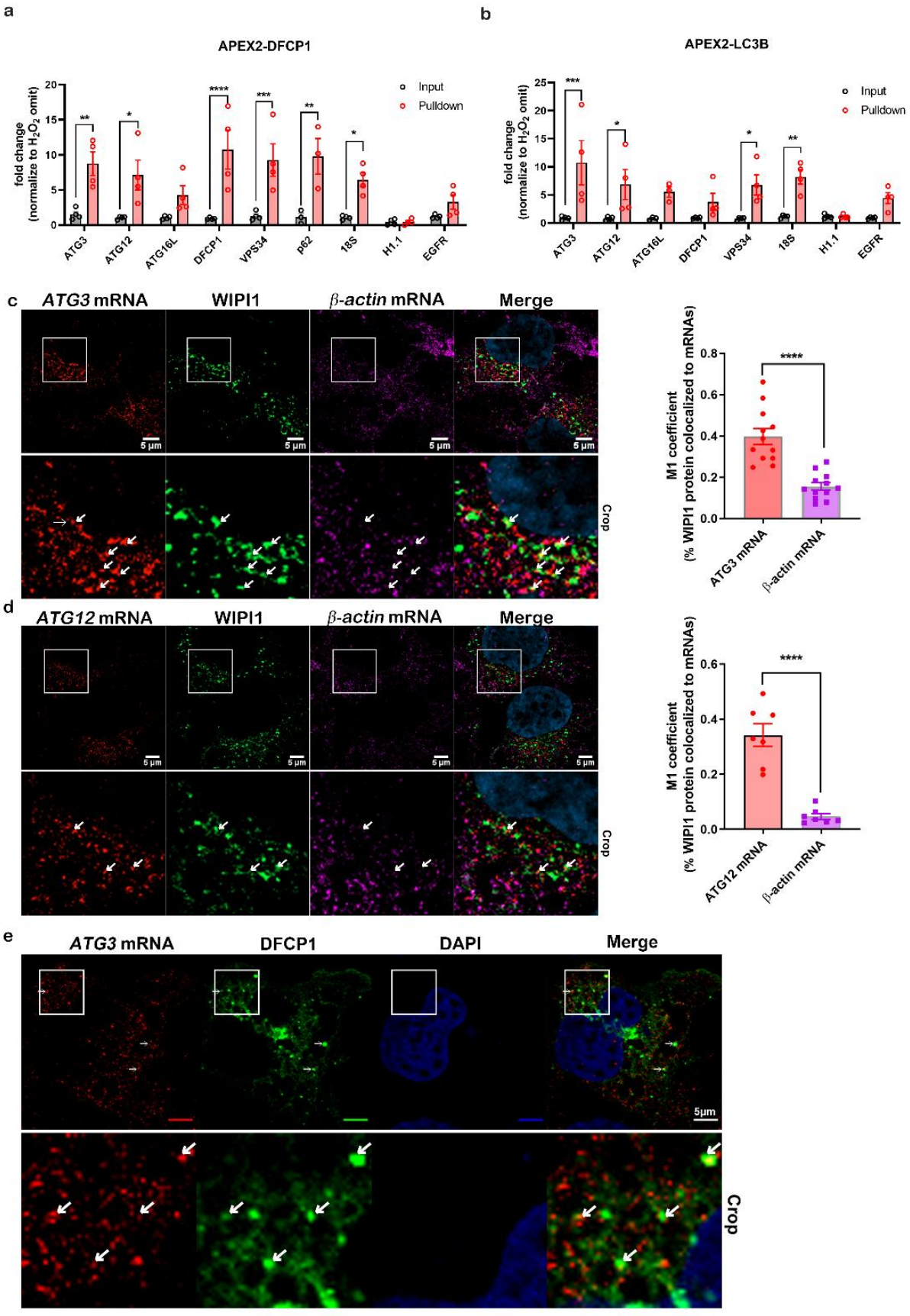
a
APEX2-DFCP1
fold change (normalize to H_2O_2 omit)
Input
Pulldown
ATG3
ATG12
ATG16L
DFCP1
VPS34
p62
18S
H1.1
EGFR
b
APEX2-LC3B
c
ATG3 mRNA
WIPI1
β-actin mRNA
Merge
Crop
M1 coefficient (% WIPI1 protein colocalized to mRNAs)
ATG3 mRNA
β-actin mRNA
d
ATG12 mRNA
ATG12 mRNA
e
DFCP1
DAPI
5μm

Figure.4-1 mRNAs encoding proteins required for autophagy localize in proximity to phagophores and autophagosomes.

(a, b) RT-qPCR analysis showing specific enrichment of mRNAs encoding proteins required for autophagy in proximity to DFCP1 and LC3B in cells treated with Torin1 (250 nM) for 4 h. Data are presented as the mean ± standard error of the mean (SEM), and a two-way ANOVA was used for statistical analysis (n = 4). (c) *ATG3* and (d) *ATG12* mRNAs colocalized more with WIPI1 proteins comparing to *β-actin* mRNAs. RNA FISH staining for *ATG3* (red), *ATG12* (red) and *β-actin* (magenta) mRNA was performed in HeLa cells transfected with WIPI1-GFP and treated with Torin1 (250 nM) for 4 h. The white arrows indicated examples of Atg mRNAs, but not *β-actin* mRNAs, colocalizing with WIPI1. Manders' colocalization coefficient was used to quantify the percentage of mRNAs colocalized to WIPI1 proteins, and unpaired t-test was used for statistical analysis. Each dot represents one image, with >40 cells quantified. (e) FISH staining of *ATG3* mRNAs in cells transfected with DFCP1-GFP. Statistical significance is indicated as **** P<0.0001.**** P<0.0001; *** P<0.001; ** P<0.01; * P<0.05.

4.2.2 Atg mRNAs are specifically recruited to DFCP1 and LC3B to a greater extent than NPM1, cyto-V5, and perilipin.

To confirm these Atg mRNAs are specifically recruited to regions containing DFCP1 and LC3B under stress, rather than randomly, we used two independent cytoplasmic APEX2-fused proteins (Apex2-Perilipin2, Apex2-Cytoplasmic-V5 tag) and an RNA-binding nucleo-cytoplasmic protein (Apex2-NPM1) as negative controls. These constructs exhibited proximity labeling localizing as

expected, but not with the phagophore marker DFCP1 (Figure.4-2a). In contrast, APEX2-DFCP1 proximity-labeling co-localized with DFCP1-mCherry (Figure.4-2a), confirming the specificity of the labeling method. The mRNAs encoding core autophagy-related proteins were enriched in proximity to DFCP1 (Figure.4-1a), but not in proximity to a diffuse cytoplasmic protein (Cytoplasmic V5-tag) or Perilipin (Figure.4-2b). Similarly, these mRNAs were not enriched in proximity to NPM1 (Figure.4-2b). This demonstrates that the enrichment of these mRNAs in proximity to DFCP1 is not due to random labeling of the cytoplasm or RNA-binding sites.

To expand this principle, we performed RNA-seq on mRNAs in proximity to DFCP1, CytoV5 and Perilipin. The Atg mRNAs of heatmap were selected based on the study by Hayashi Yamamoto et al (Yamamoto et al., 2023). The p-value was determined by comparing the ratio of (count+1) from three replicates of H_2O_2 labeling versus H_2O_2 omission, using a Independent T-test (Appendix A). We displayed Atg RNAs with a p-value < 0.05 in the APEX2-DFCP1 RNA-seq samples. The enrichment level was calculated as the average ratio of (count+1) from three replicates of APEX2 H_2O_2 labeling versus H_2O_2 omission. It was found that mRNAs encoding an extensive list of proteins involved in autophagosome formation, cargo recruitment and maturation were enriched in proximity to DFCP1 to a greater extent than CytoV5, Perilipin or NPM1 when normalzied to a negative control without H_2O_2-induction of proximity-labeling (Figure.4-2c). Additionally, a total of 63086 RNAs were identified with the RNA seq of APEX2-proximity based pulldowns. The pathways analysis of RNAs with Log2FC>0.2 and average count of H_2O_2 >600 from APEX2-DFCP1 RNA-seq data was also performed (Appendix B). The autophagy, and related pathways such as (ER-Golgi trafficking, ubiquitination) are selectively enriched among these mRNAs (Figure.4-2d).

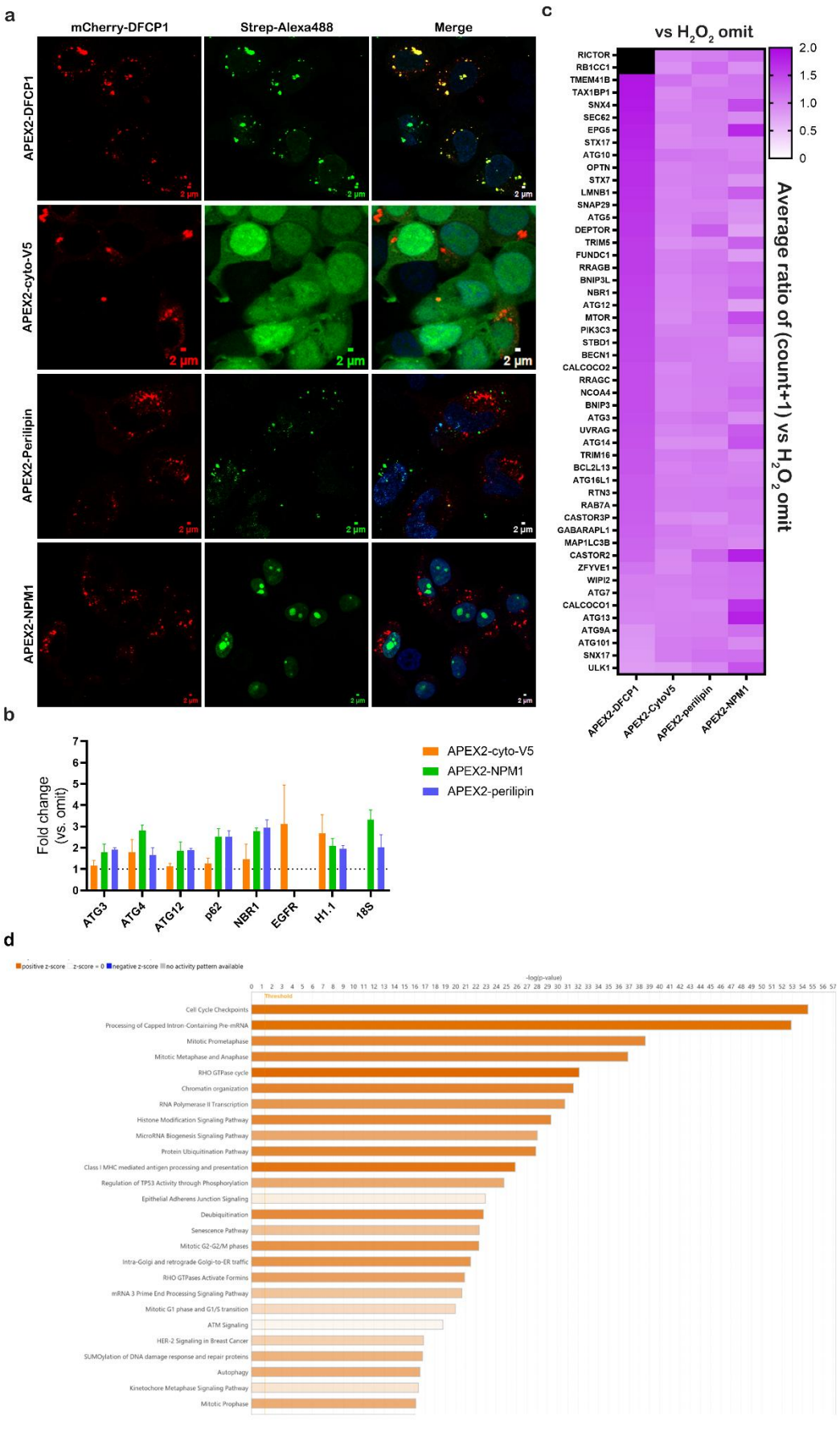
a
mCherry-DFCP1
Strep-Alexa488
Merge
APEX2-DFCP1
APEX2-cyto-V5
APEX2-Perilipin
APEX2-NPM1
2 µm
b
Fold change (vs. omit)
APEX2-cyto-V5
APEX2-NPM1
APEX2-perilipin
ATG3
ATG4
ATG12
p62
NBR1
EGFR
H1.1
18S
c
vs H2O2 omit
RICTOR
RB1CC1
TMEM41B
TAX1BP1
SNX4
SEC62
EPG5
STX17
ATG10
OPTN
STX7
LMNB1
SNAP29
ATG5
DEPTOR
TRIM5
FUNDC1
RRAGB
BNIP3L
NBR1
ATG12
MTOR
PIK3C3
STBD1
BECN1
CALCOCO2
RRAGC
NCOA4
BNIP3
ATG3
UVRAG
ATG14
TRIM16
BCL2L13
ATG16L1
RTN3
RAB7A
CASTOR3P
GABARAPL1
MAP1LC3B
CASTOR2
ZFYVE1
WIPI2
ATG7
CALCOCO1
ATG13
ATG9A
ATG101
SNX17
ULK1
APEX2-DFCP1
APEX2-CytoV5
APEX2-perilipin
APEX2-NPM1
2.0
1.5
1.0
0.5
0
Average ratio of (count+1) vs H2O2 omit
d
positive z-score
z-score = 0
negative z-score
no activity pattern available
-log(p-value)
Threshold
Cell Cycle Checkpoints
Processing of Capped Intron-Containing Pre-mRNA
Mitotic Prometaphase
Mitotic Metaphase and Anaphase
RHO GTPase cycle
Chromatin organization
RNA Polymerase II Transcription
Histone Modification Signaling Pathway
MicroRNA Biogenesis Signaling Pathway
Protein Ubiquitination Pathway
Class I MHC mediated antigen processing and presentation
Regulation of TP53 Activity through Phosphorylation
Epithelial Adherens Junction Signaling
Deubiquitination
Senescence Pathway
Mitotic G2-G2/M phases
Intra-Golgi and retrograde Golgi-to-ER traffic
RHO GTPases Activate Formins
mRNA 3 Prime End Processing Signaling Pathway
Mitotic G1 phase and G1/S transition
ATM Signaling
HER-2 Signaling in Breast Cancer
SUMOylation of DNA damage response and repair proteins
Autophagy
Kinetochore Metaphase Signaling Pathway
Mitotic Prophase

Figure.4-2 mRNAs encoding proteins required for autophagy specifically localize in proximity to phagophores and autophagosomes to a greater extent than CytoV5, Perilipin or NPM1.

(a) DFCP1 colocalized to biotinylated signals by APEX2-DFCP1 but not that of APEX2-cyto-V5, -NPM1, and -perilipin. APEX2 expressing cells transfected with mCherry-DFCP1 were treated with Torin1 (250 nM, 4 h) and H_2O_2- catalyzed biotinylation and followed by streptavidin-Alexa488 labelling to react with biotinylated molecules. (b) RT-qPCR analysis showing no enrichment of Atg mRNAs in proximity to APEX2-cyto-V5 (n=4), APEX2-NPM1 (n=3), and APEX2-perilipin (n=3). (c) Heatmap of candidate Atg genes in APEX2-seq data from different subcellular locales (DFCP1, cyto-V5, NPM1, and perilipin). The enrichment level was calculated as the average ratio of (count+1) of three replicates of APEX2 H_2O_2 labelling vs H_2O_2 omit. (d) Pathway analysis of RNAs with Log2FC>0.2 and average count of H_2O_2 >600 from APEX2-DFCP1 RNA-seq data.

4.2.3 Atg mRNAs are specifically recruited to phagophores and autophagosomes

RNAs in proximity to APEX2-DFCP1 and APEX2-LC3B were pulled down from cells expressing APEX2-DFCP1, or APEX2-LC3B that were not treated with Torin1. However, no significant enrichment of ATG mRNAs was observed in the pulled-down RNAs (Figure.4-3a, b). This suggests that the recruitment of mRNAs encoding autophagy proteins to DFCP1 or LC3B locales requires Torin1 treatment, and that these mRNAs are specifically recruited to phagophores or autophagosomes, which are induced by Torin1.

To test this, experiments were repeated in *FIP200*$^{-/-}$ cells and WT cells transfected with APEX2-DFCP1 plasmids. The FIP200 knockouts were validated by Sanger sequencing as below indicating the mutations on both alleles in FIP200 (The Sanger sequence is displayed as the Appendix C). *FIP200*$^{-/-}$ cells fail to form ULK1 nucleation sites and block formation of phagophores in response to mTOR inhibition (Hara and Mizushima, 2009). *FIP200*$^{-/-}$ cells nonetheless do not impair non-canonical autophagy pathways and their production of LC3B-II, meaning that untreated *FIP200*$^{-/-}$ cells do have LC3B-II, but this does not increase when autophagy is induced. In agreement, LC3B-II was present in *FIP200*$^{-/-}$ cells, but was not increased by Torin1 treatment (Figure.4-3c). APEX2-DFCP1 proximity labeling failed to enrich mRNAs encoding proteins involved in autophagy in APEX2-DFCP1$^{FIP200-/-}$ cells (Figure.4-3d), supporting this being a site of autophagosome genesis. The requirement of FIP200 for localization of mRNAs to DFCP1 also indicates that this is not a site involved in non-canonical autophagy processes (Durgan and Florey, 2022), like microautophagy, LC3-associated endosomes and packaging of extracellular vesicles (Gardner et al., 2023; Guo et al., 2017).

Another autophagy-deficient cell line, APEX2-LC3B (G120A mutant) was used, which was known as lipidation deficient mutant (Tanida et al., 2008), and thus cannot localize to phagophores. Therefore signifiant less LC3B-II synthesis was observed after Torin1 induction in APEX2-LC3B^{G120A} cells (Figure.4-3e). The RNAs in inproximity to APEX2-LC3B^{WT} and APEX2-LC3B^{G120A} were biotinylated and pulldown for qRT-PCR. The enrichment of several key Atg mRNAs to APEX2-LC3B^{G120A} was also reduced comparing to that to APEX2-LC3B^{WT} (Figure.4-3f), indicating the localization to phagephores was required for the recruitment of these Atg transcripts to LC3B. This further suggest these Atg transcripts were specifically recruited to phagophores.

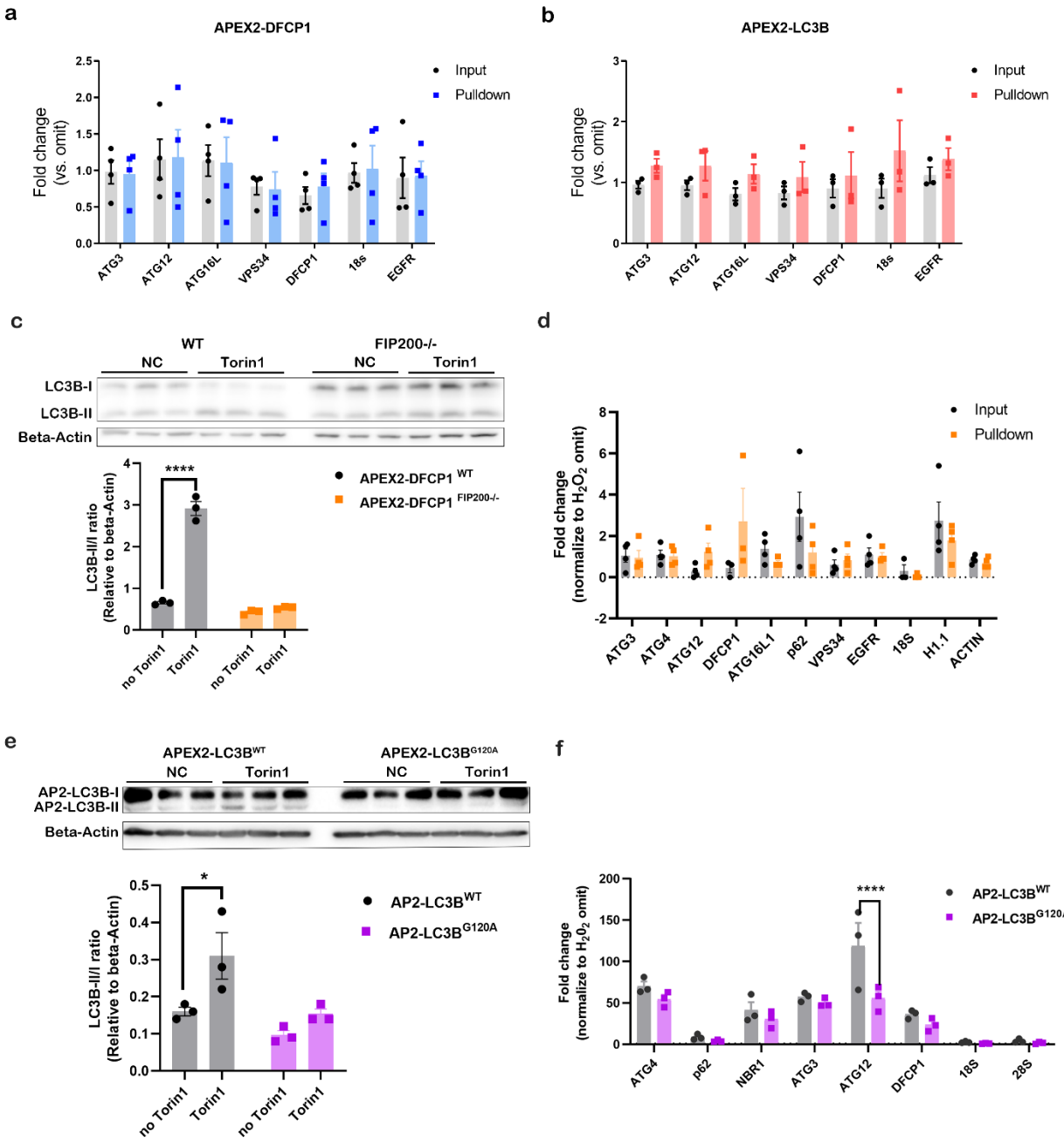
a
APEX2-DFCP1
Fold change (vs. omit)
Input
Pulldown
ATG3
ATG12
ATG16L
VPS34
DFCP1
18s
EGFR
b
APEX2-LC3B
c
WT
FIP200-/-
NC
Torin1
LC3B-I
LC3B-II
Beta-Actin
LC3B-II/I ratio (Relative to beta-Actin)
****
APEX2-DFCP1 WT
APEX2-DFCP1 FIP200-/-
no Torin1
d
Fold change (normalize to H2O2 omit)
ATG4
p62
ATG16L1
H1.1
ACTIN
e
APEX2-LC3BWT
APEX2-LC3BG120A
AP2-LC3B-I
AP2-LC3B-II
*
AP2-LC3BWT
AP2-LC3BG120A
f
NBR1
28S

Figure.4-3 Atg mRNAs are specifically recruited to DFCP1/ LC3B under autophagy. (a, b) RT-qPCR analysis showing no enrichment of Atg mRNAs in proximity to DFCP1 and LC3B in cells without Torin1 treatment. Data are mean ± SEM and analysed with Two-way ANOVA (n=4 for APEX2-DFCP1 and n=3 for APEX2-LC3B). (c) WB of LC3B protein and the quantification of LC3B-II/I ratio of APEX2-DFCP1$^{FIP200-/-}$ and APEX2-DFCP1^{WT} cells with/ without 4 h of Torin1 (250 nM) treatment. (d) RT-qPCR analysis showing no enrichment of Atg mRNAs to APEX2-DFCP1 when FIPI200 was knocked out. A two-way ANOVA analysis was used. (e) WB bands and quantification of LC3B-I/-II in APEX2-LC3B^{WT} and APEX2-LC3B^{G120A} cells with/ without Torin1 treatment. (f) RT-qPCR analysis showing reduced enrichment of Atg mRNAs to APEX2-LC3B^{G120A}. *P<0.05; ****P<0.0001.

4.2.4 Nascent protein synthesis in proximity to phagophores

To assess nascent protein synthesis near forming autophagosomes, APEX2-DFCP1-expressing cells were briefly pulsed with a Click-iT amino acid analogue (AHA, L-azidohomoalaine), followed by biotinylation and pulldown to isolate molecules in proximity to APEX2-DFCP1. AHA was then detected on SDS-PAGE gels by coupling it to Alexa Flour488. Validating the specificity of this assay, minimal signal was observed in the absence of AHA or in the absence of H_2O_2 which activates APEX2 proximity labeling (Figure.4-4a). Nascently-translated proteins were present in proximity to APEX2-DFCP1 (Figure.4-4a), and this was blocked when translation was inhibited with CHX (Figure.4-4a). More biotinylated proteins were observed in pulldown comparing to input proteins of APEX2-DFCP1 cells treated with or without CHX, indicating successful proximity labeling and pulldown under CHX conditions (Figure.4-4b). While we cannot exclude that nascent proteins were synthesized and transported to sites of

autophagosome formation during the brief pulse, this suggests that nascent protein synthesis occurs near phagophores.

In support of this, when nascent translation was visualized by microscopy using a fluorescent aminoacyl-tRNA analogue (puromycin-FAM) incorporation method (Wong et al., 2024), nascent translation was observed dispersed throughout cells with some discrete foci. A subset of nascent translation foci (puromycin-FAM positive signals) co-localized with or were in close proximity to DFCP1 (Figure.4-4c) or ATG13, component of ULK1 complex (Figure.4-4d) by fluorescence microscopy after brief pulses. This suggests that among sites where mRNA is translated, some are in proximity to forming autophagosomes.

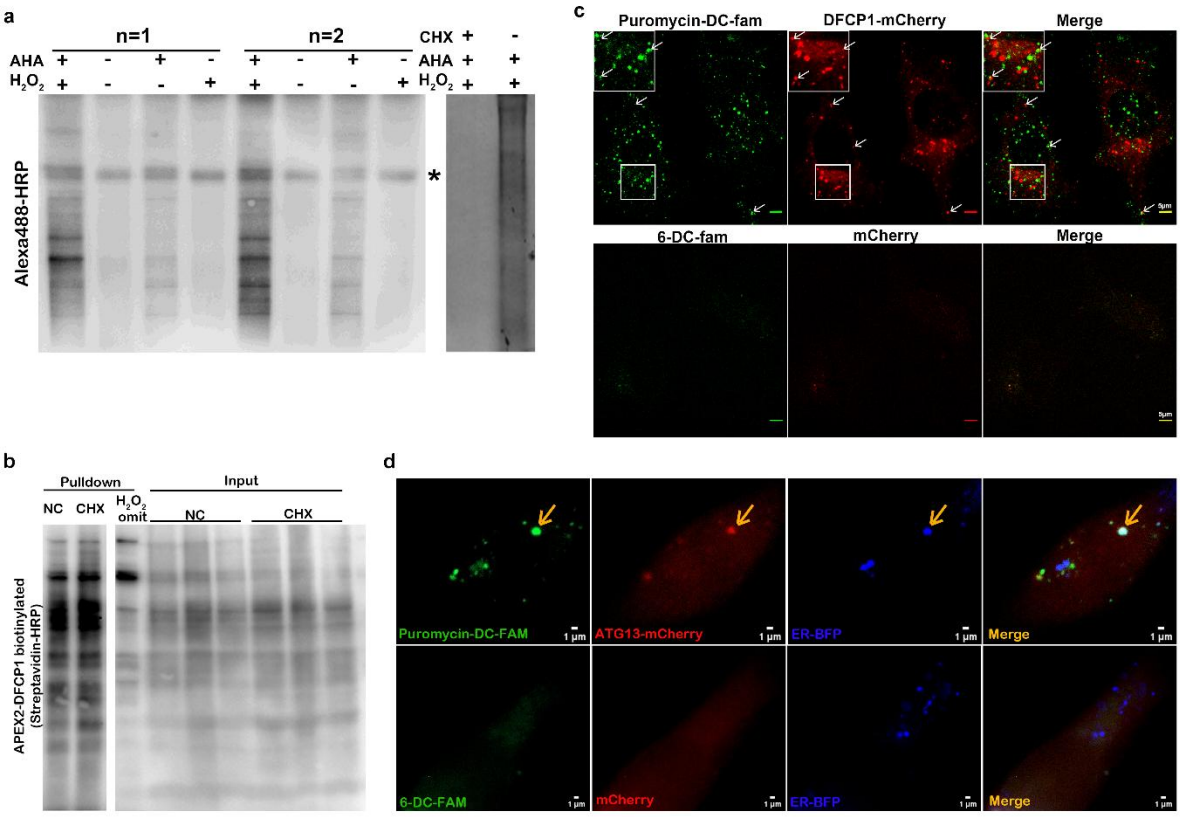

Figure.4-4 Nascent translation occurs in proximity to forming autophagosomes.

(a) Detection of AHA-labelled nascent proteins clicked to Alexa488 and detected with western blot using anti-Alexa488 antibody and HRP-conjugated secondary antibody. APEX2-DFCP1 expressing cells treated with/ without CHX (100 μg/mL) were pulsed with/without AHA and proteins in proximity to APEX2-DFCP1 were biotinylated and pulled down. *Non-specific band. (b) Successful proximity labeling and pulldown by APEX2-DFCP1 under CHX treatment condition. The biotinylated proteins in input and pulldown in representative APEX2-DFCP1 proximity labeling experiments with/ without CHX (100 μg/mL). Protein samples of input and pulldown from same group were displayed separated but on the same PVDF membrane. (c) Puromycin-FAM-labelled nascent proteins localized in proximity to DFCP1-mCherry in HEK293 cells detected by microscopy. (d) Puromycin-labelled nascent peptides colocalized to forming autophagosome marker ATG13 proteins and ER, indicating the nascent protein translation in proximity to forming autophagosomes.

4.2.5 Nascent translation near forming autophagosomes is not affected by ribophagy.

NUFIP1 was documented as an autophagy receptor to recruit ribosomes to autophagosomes for degradation (Wyant et al., 2018), although this role is being questioned recently (An et al., 2020). Depletion of NUFIP1 with siRNA (Figure.4-5a), did not affect the abundance of nascent peptides in proximity to DFCP1 (Figure.4-5b, c), or the proportion of nascent peptides (AHA-Alexa488 clicked) that colocalized with mCherry-DFCP1 (Figure.4-5d, e). This indicates that the accumulation of nascent proteins around DFCP1 is not dependent on ribophagy, and translation may occur in proximity to forming autophagosomes.

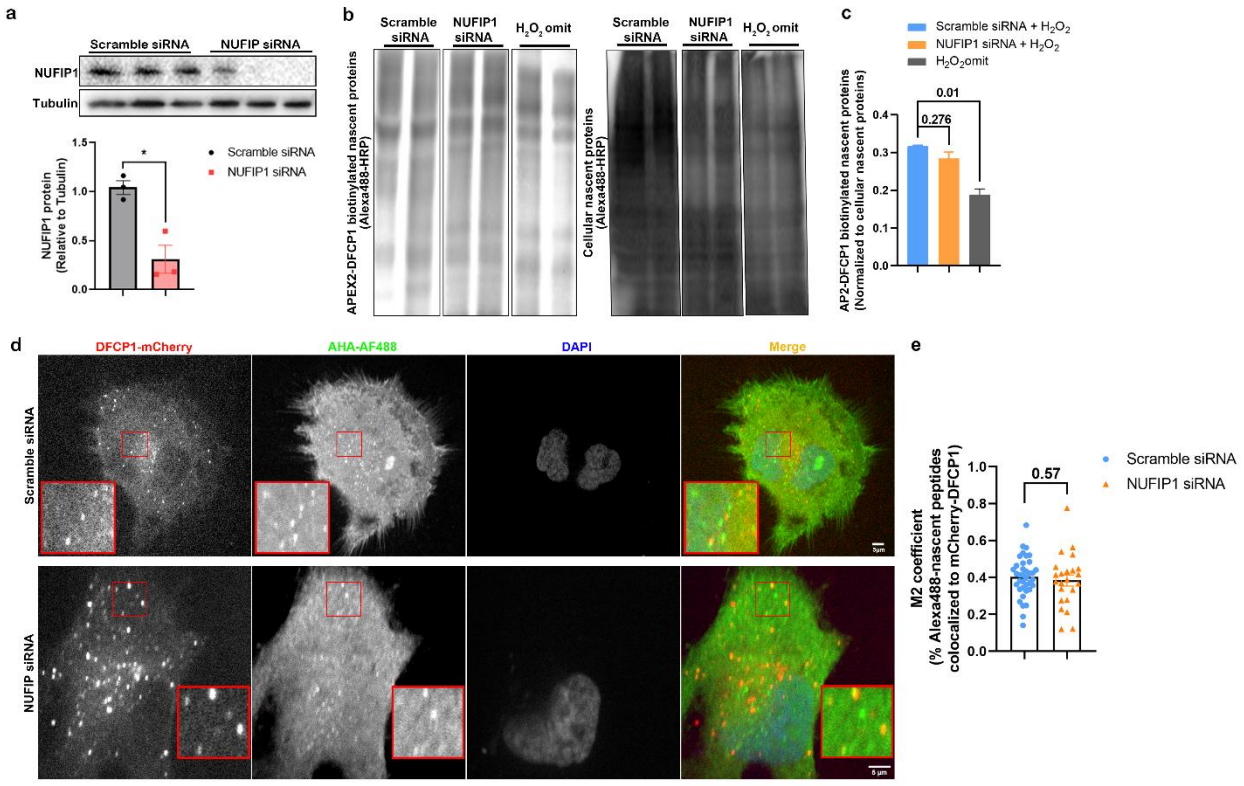
a
Scramble siRNA
NUFIP siRNA
NUFIP1
Tubulin
NUFIP1 protein (Relative to Tubulin)
Scramble siRNA
NUFIP1 siRNA
b
Scramble siRNA
NUFIP1 siRNA
H2O2 omit
APEX2-DFCP1 biotinylated nascent proteins (Alexa488-HRP)
Cellular nascent proteins (Alexa488-HRP)
c
Scramble siRNA + H2O2
NUFIP1 siRNA + H2O2
H2O2 omit
AP2-DFCP1 biotinylated nascent proteins (Normalized to cellular nascent proteins)
0.01
0.276
d
DFCP1-mCherry
AHA-AF488
DAPI
Merge
Scramble siRNA
NUFIP siRNA
e
M2 coefficient (% Alexa488-nascent peptides colocalized to mCherry-DFCP1)
0.57
Scramble siRNA
NUFIP1 siRNA

Figure.4-5 Nascent translation in proximity to forming autophagosomes is not affected by ribophagy.

(a) Knockdown of NUFIP proteins with NUFIP siRNAs. Western blot of NUFIP protein in cells transfected with NUFIP siRNAs. n=3 and t-Test was used. (b) Detection of nascent protein synthesis (AHA-Alexa488) in APEX2-DFCP1 proximity-labeled pulldown (left panel) and total cell lysate (right panel) from cells transfected with scramble siRNAs or NUFIP siRNAs. Alexa488-labelled proteins were detected with anti-Alexa488 incubation and reaction to HRP-substrates. The protein bands of different groups were separated but on the same PVDF membrane. (c) Graph quantifies nascent proteins in proximity to APEX2-DFCP1 normalized to cellular overall nascent proteins. One-way ANOVA analysis was used for significance analysis, n=2. (d) Representative fluorescent image of Alexa488-tagged nascent proteins colocalized to DFCP1-mCherry in cells transfected with scramble or NUFIP siRNAs. (e) Manders' colocalization coefficient/MCC of Alexa488-tagged nascent proteins colocalized to mCherry-DFCP1. Unpaired t-test was used for significance and each dot represents one image.

4.2.6 mRNAs encoding proteins essential for autophagy are translated near phagophores.

If proteins are nascently translated in proximity to DFCP1, and several key Atg mRNAs were localized to phagophore and autophagosomes, then these Atg mRNAs should be in translation-competent ribosomes. We performed proximity labeling with APEX2-DFCP1 expressing cells, then polysomes were fractionated into heavy and light polysome, and monosome fractions (Ingolia et al., 2009; Ingolia et al., 2011) (Figure.4-6a). Heavy and light polysome fractions

could be ablated by EDTA which disrupts ribosome association with mRNA (Pan and van Breukelen, 2011) (Figure.4-6b). From these fractions, we pulled down biotinylated RNAs proximal to DFCP1 and performed RT-qPCR. mRNAs encoding proteins involved in autophagosome formation, like *ATG2*, *ATG3*, *ATG4*, *ATG5*, *VPS34*, *DFCP1*, *ATG12* and *p62/SQSTM* were found enriched in heavy polysome fractions in proximity to APEX2-DFCP1, while *β-actin*, mitochondrial *MTCO2 (Mitochondrially Encoded Cytochrome C Oxidase II)*, and nuclear *H1.1(histone H1)* mRNAs were not (Figure.4-6c). This evidence strongly suggests that mRNAs encoding several proteins essential for autophagy are selectively and actively translated in proximity to phagophores.

SILAC is a metabolic labeling method that incorporates non-radioactive, stable isotopes of amino acids (usually arginine and lysine) directly into newly synthesized proteins (Hung et al., 2014). To determine which mRNAs encoding essential autophagy proteins are actively translated in proximity to phagophores on a large scale, we gave a short pulse of SILAC heavy amino acids to cells, labeled and pulled-down proteins in proximity to DFCP1 and then performed mePROD mass spectrometry (Klann et al., 2020). The significant enriched proteins were many involved in autophagy-related pathways, indicating that the APEX2-DFCP1 biotinylated the nearby proteins of DFCP1 successfully and specifically (Figure.4-6d). VPS34, ATG5, ATG12, ATG3, p62/SQSTM, and ATG16L were identified as nascent proteins in proximity to DFCP1, with significant heavy/light amino acid (H/L) ratios (Figure.4-6e). A total of 2564 proteins were identified with the 0.5h SILAC labeling. And out of them only 21 proteins are significantly enriched after normalizing to the omit sample in the raw MS data of SILAC labeling displayed in Appendix D.

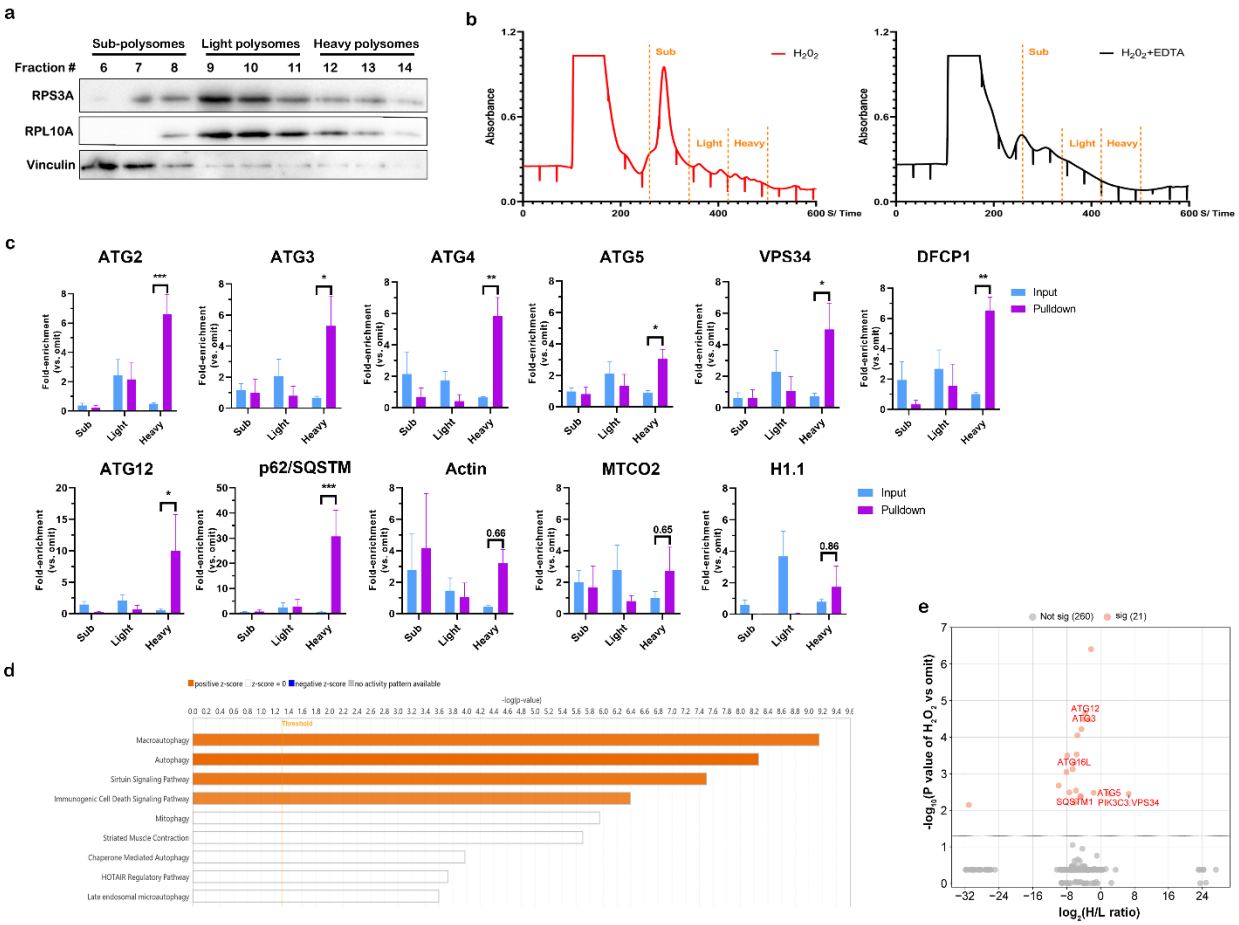
a
Sub-polysomes
Light polysomes
Heavy polysomes
Fraction # 6 7 8 9 10 11 12 13 14
RPS3A
RPL10A
Vinculin
b
Absorbance
Sub
Light
Heavy
H2O2
H2O2+EDTA
S/ Time
c
ATG2
ATG3
ATG4
ATG5
VPS34
DFCP1
ATG12
p62/SQSTM
Actin
MTCO2
H1.1
Fold-enrichment (vs. omit)
Sub
Light
Heavy
Input
Pulldown
0.66
0.65
0.86
d
positive z-score
z-score = 0
negative z-score
no activity pattern available
-log(p-value)
Threshold
Macroautophagy
Autophagy
Sirtuin Signaling Pathway
Immunogenic Cell Death Signaling Pathway
Mitophagy
Striated Muscle Contraction
Chaperone Mediated Autophagy
HOTAIR Regulatory Pathway
Late endosomal microautophagy
e
Not sig (260)
sig (21)
-log10(P value of H2O2 vs omit)
log2(H/L ratio)
ATG12
ATG3
ATG16L
ATG5
SQSTM1
PIK3C3:VPS34

Figure.4-6 mRNAs encoding proteins required for autophagy are translated in proximity to forming autophagosomes.

(a) Western blots of RPS3A, RPL10A, and Vinculin of three ribosome fractions from cells treated with Torin1. (b) Representative polysome profiling plot from Hela cells treated with Torin1 ± EDTA indicating sub, light and heavy polysome fractions. (c) RT-qPCR analysis showing specific enrichment of Atg mRNAs in polysome fractions in input total samples as well as in proximity to DFCP1 (S=sub-polysome, L=light polysome, H=heavy polysome). APEX2-DFCP1 expressing cells treated with Torin1 (250 nM, 4 h) were labeled with BP± H_2O_2. The cell lysates went through heavy polysome fractionation, pulldown with streptavidin beads and RT-qPCR to quantify polysome-associated mRNAs in proximity to DFCP1. n=3, and two-way ANOVA analysis was used. (d) Pathway analysis of significantly enriched proteins in proximity to DFCP1 comparing to that of H_2O_2 omit samples. (e) APEX2-DFCP1 cells underwent a short pulse of SILAC heavy amino acids for 30 min, proximity-labelling based pulldown, and subsequent mePROD mass spectrometry to identify nascent proteins in proximity to DFCP1. A volcano plot displaying log2 (Heavy /Light ratio) of pulldown proteins from H_2O_2 group and the p value of H_2O_2 versus H_2O_2 omit of heavy-isotype labelled samples, analyzed with independent t-tests. Orange dots represent heavy isotype-labeled proteins that are significantly enriched in proximity to DFCP1.

4.3 Discussion

Several key Atg transcripts were found to be significantly enriched in proximity to DFCP1 and LC3B with APEX2-based proximity labeling. FISH staining further validated that *ATG3* and *ATG12* mRNAs were localized near the phagophore marker WIPI1, in comparison to the

negative control β-actin mRNA. Additionally, *ATG3* mRNAs were found to colocalize with DFCP1-positive organelles. These strongly suggest the enrichment of Atg mRNAs near phagophore marker DFCP1/WIPI1 and autophagosome marker LC3B.

We note that several other GO-terms seemingly unrelated to autophagy are also enriched in the dataset of RNA-seq with APEX2-DFCP1 expressing cells. It is possible that a broader set of mRNAs are localized near phagophores, either for translation or degradation. Interestingly, several eIF3D (Eukaryotic Translation Initiation Factor 3 Subunit D) target transcripts, such as INSR (Insulin Receptor) and IGF1R (Insulin-like Growth Factor 1 Receptor), were found to be enriched in the APEX2-DFCP1 RNA-sequencing data. Moreover, in the SILAC mass spectrometry data, a significant portion of the eIF3 complex was enriched, including key interactors and effectors of eIF3D, such as (heterogeneous nuclear ribonucleoprotein K) hnRNPK, eIF4G (Ma et al., 2023; Shin et al., 2023). This further underscores the potential role of eIF3D in the recruitment of specific mRNAs to DFCP1-positive regions. Notably, eIF3D has been shown to bind to the mRNA 5' cap and promote translation of selective mRNAs independently of eIF4E (Lamper et al., 2020; Lee et al., 2015; Ma et al., 2023). Since eIF4E and its regulator, eIF4E-BP, are major mediators of cap-dependent translation that are inhibited by mTOR inhibitor, eIF3D may represent an alternative mechanism for activating the translation of specific mRNAs following mTOR inhibition during autophagy (Shin et al., 2023).

Using APEX2 proximity labeling-based RNA sequencing, we found that several key Atg transcripts were significantly more enriched in DFCP1-positive regions compared to cytoplasmic proteins, such as Perilipin2 and a Cytoplasmic-V5 tag, as well as the RNA-binding nucleo-cytoplasmic protein NPM1. This suggests that these key Atg transcripts were specifically

recruited to DFCP1-positive forming regions, rather than being randomly biotinylated by the APEX2 system. In addition, the recruitment of these key Atg transcripts to DFCP1 or LC3B was blocked in the absence of the autophagy inducer Torin1, upon knockout of FIP200 (a central component of the ULK1 complex, crucial for autophagy initiation), or without LC3B lipidation. These further suggests that these key Atg transcripts were specifically recruited to phagophores and autophagosomes to participate canonical autophagy process.

Nascent translation foci, labeled with puromycin-FAM and AHA, were observed to localize near DFCP1, suggest nascent translation occurs around DFCP1 positive forming phagophores. Additionally, we found that key Atg mRNAs were actively translated near DFCP1, as determined by fractionation of heavy polysomes. Using SILAC labeling of proteins involved in nascent translation, we identified several Atg peptides that were heavily labeled around DFCP1-positive regions. These findings collectively suggest that several core mRNAs encoding proteins involved in autophagy are selectively translated near the forming autophagosomes. Previous studies have suggested that ribosomes are located in the vicinity of forming autophagosomes (Dunkle and Cate, 2010; Eskelinen et al., 2011; Yla-Anttila et al., 2009), supporting the idea that translationally competent ribosomes are present near these structures. This validates the presence of ribosomes in close proximity to forming autophagosomes, where they play a crucial role in the translation of key Atg mRNAs, ensuring a rapid, local supply of proteins essential for autophagosome biogenesis.

Notably, ribosomes can also be degraded by autophagy in both yeast and mammalian cells, but it remains unclear whether these ribosomes are bound to mRNAs or are functional. The ribosomes degraded by autophagy are poly-ubiquitinated however, and are hypothesized to be damaged,

inappropriately assembled, or non-functional (Frankel et al., 2017). Our data suggests that the accumulation of nascent proteins around DFCP1 is not affected by knockdown of ribophagy receptor NUFIP1. Therefore, our evidence suggests that ribophagy and local translation of Atg mRNAs near forming autophagosomes are two independent processes. Consistent with our observation, a recently published study by Knupp et al. also reported that LC3B mRNAs localize near (or colocalize with) to omegasomes (visualized as WIPI2+ puncta) with smFISH and could be immunoprecipitated by WIPI2. Additionally, components of E3-like complex ATG5 and ATG16L1 did not colocalize with LC3B mRNAs (Knupp et al., 2024).

Collectively, the aforementioned evidence suggests that several key autophagy-related mRNAs are selectively and actively translated in close proximity to the phagophores under autophagy, highlighting a localized and regulated process essential for autophagy initiation and progression.

Chapter 5. Roles of RACK1 and eIF5A in Localization and Local Translation of Atg mRNA Near Forming Autophagosomes

5.1 Background

In our study in previous chapters, several key Atg mRNAs were found to localize to ER-derived phagophores for translation. Since most core Atg proteins are cytosolic (Bento et al., 2016), these Atg mRNAs should not be recruited to the ER via interaction with the SRP receptor. This suggests that a specific factor may be involved in recruiting mRNAs encoding autophagy-related proteins to forming autophagosomes for *in situ* translation.

Intriguingly, RACK1, part of the ribosomal 40S subunit, is previously shown to bind to the complex of VPS15, ATG14L, and Beclin1, placing it at the site of phagophore formation (Zhao et al., 2015) and is also known to control the translation of mRNAs encoding proteins involved in autophagy (Kim et al., 2017). Upon autophagy induction by starvation or mTOR inhibition, RACK1 has been shown to interact with ATG5, a key component of the ATG12~ATG5-ATG16 complex, which catalyzes LC3 lipidation and regulates autophagic vesicle formation (Erbil et al., 2016).

eIF5A, as an RBP, has been documented to promote translation of ATG3 by overcoming ribosome pausing caused by its DDG motif through its enhanced association with ribosomes under autophagy. Therefore, eIF5A facilitates ATG3-mediated LC3B lipidation and autophagosome formation (Lubas et al., 2018). However, it remains unclear whether eIF5A is involved in recruiting Atg mRNAs to phagophores. Collectively, roles of RACK1 and eIF5A in

recruiting key Atg mRNAs to forming autophagosomes for *in situ* translation were explored in our following studies.

5.2 Results

5.2.1 Translating ribosomes are essential for localizing Atg mRNAs to phagophores and autophagosomes

Recruitment of mRNAs encoding autophagy proteins into the vicinity of DFCP1 and LC3B, was abrogated when translating ribosomes were displaced from mRNAs with puromycin (Figure.5-1a), which induces premature termination of translation and releases the nascent peptides (Aviner, 2020). Recruitment of *28S* rRNA to DFCP1 was also significantly inhibited by puromycin (Figure.5-1a). While *EGFR mRNA* was enriched in DFCP1 proximity labeling samples, but to a lesser extent than mRNAs encoding autophagy proteins (Figure.5-1a). This enrichment was likely due to the co-translational insertion of EGFR into the ER membrane as a type I transmembrane protein (Oksvold et al., 2002). Interestingly, recruitment of several of these mRNA to DFCP1 was also abolished by Homoharringtonine (Figure.5-1b), which arrests ribosomes at the start codon and disrupts polysomes (Fresno et al., 1977; Latallo et al., 2023). Collectively, this suggests that autophagy-related mRNAs require active, ongoing translation, and potentially a ribosome-associated factor, for their recruitment to or retention at DFCP1-positive regions.

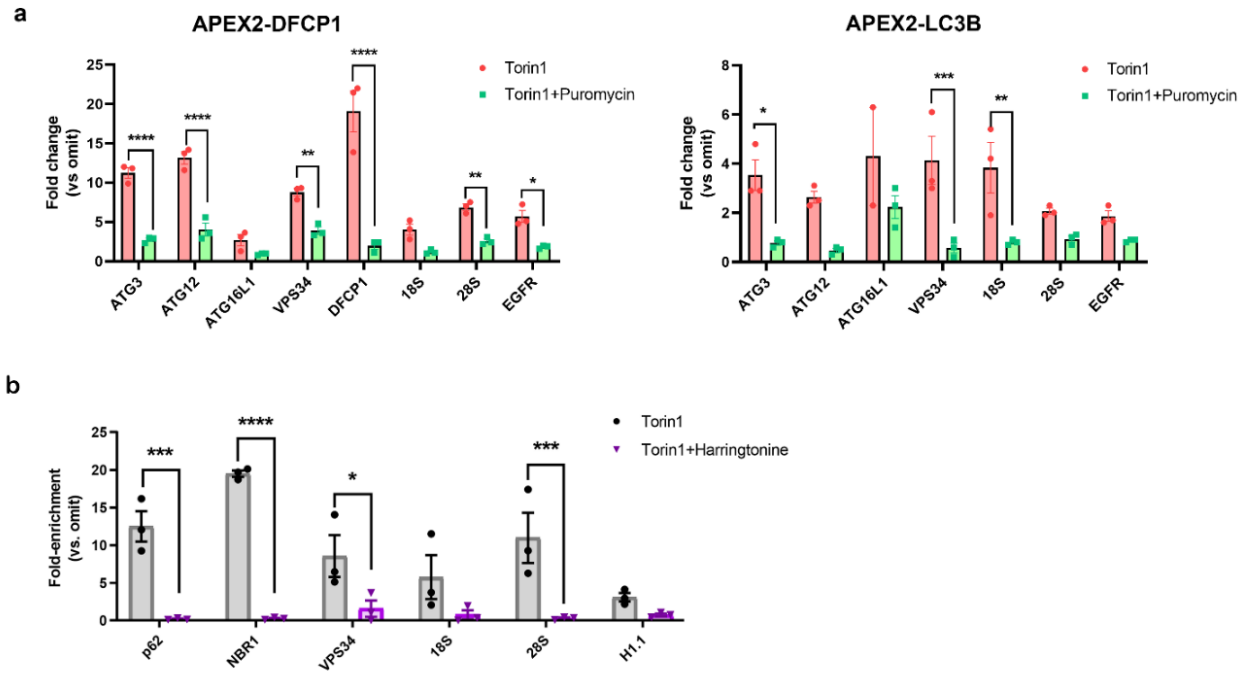

Figure.5-1 Translating ribosomes are essential for localizing Atg mRNAs to phagophores and autophagosomes.

(a) RT-qPCR analysis of APEX2-DFCP1 and APEX2-LC3B proximity-labeling pulldowns, showing specific enrichment of Atg mRNAs in proximity to DFCP1 and LC3B, was inhibited by puromycin treatment. Cells were treated with Torin1 (250 nM, 4 h) ± puromycin (100 µg/mL, 1 h) before being labelled with BP ± H_2O_2. A two-way ANOVA analysis was used for statistical analysis. (b) RT-qPCR analysis of APEX2-DFCP1 proximity-labeling pulldowns, showing specific enrichment of Atg mRNAs in proximity to DFCP1 was abolished by Homoharringtonine. Cells were treated with Torin1 (500 nM) for 2 h and followed by Homoharringtonine (2.5 µg/ml) treatment for an additional 1 h before being labelled with BP ± H_2O_2. N=3 and a two-way ANOVA analysis was used for statistical analysis. ****P<0.0001; ***P<0.001; **P<0.01; *P<0.05.

5.2.2 RACK1 co-localizes with phagophores and autophagosomes and associates with Atg mRNAs

Fluorescence microscopy of cells co-transfected with RACK1-GFP and DFCP1-mCherry plasmids demonstrated that RACK1 localized in the cellular cytoplasm under Torin1 treatment and colocalized with or is immediately adjacent to many punctate of DFCP1 (Figure.5-2a). In consistent, endogenous RACK1 proteins were found in the vicinity of DFCP1 proteins but not Histone H3 proteins with proximity ligation assay (PLA) (Figure.5-2b). RACK1 proteins also colocalized with LC3B-positive mature autophagosomes, as observed by IF (Figure.5-2c). Additionally, the fluorescence microscopy for endogenous RACK1 using a validated antibody demonstrated that it colocalizes with or is immediately adjacent to *ATG12* mRNA (FISH) and WIPI2 (Figure.5-2d).

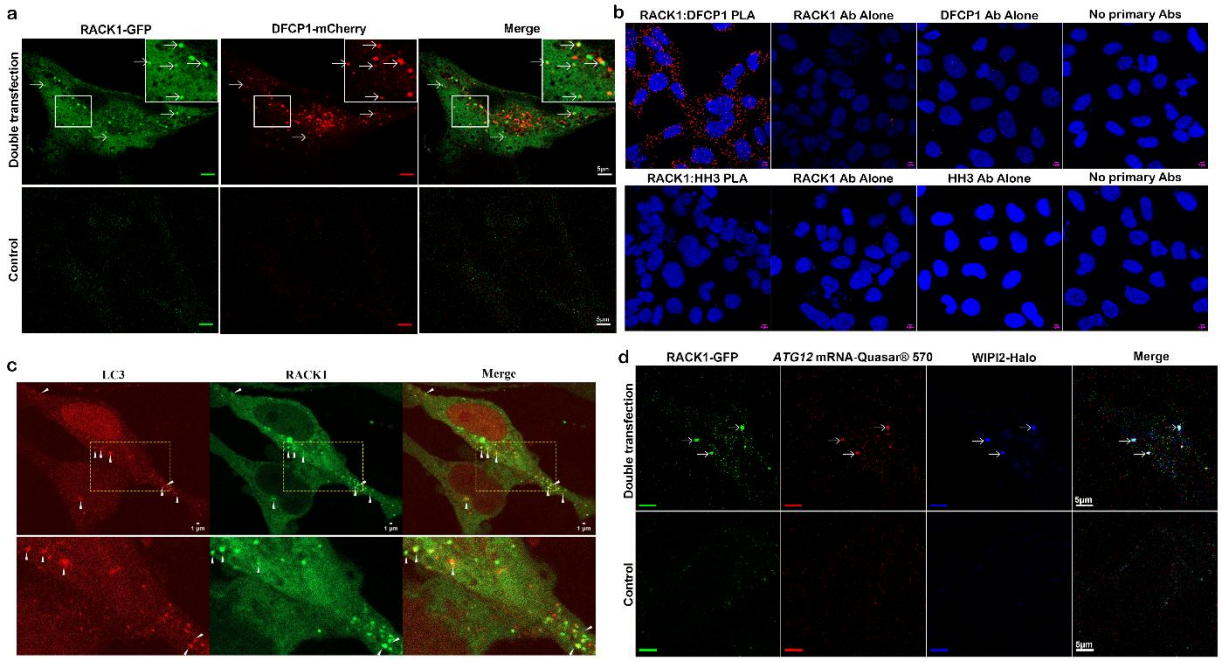

Figure.5-2 RACK1 co-localizes with phagophores and autophagosomes.

(a) Fluorescence microscopy of cells co-transfected with RACK1-GFP and DFCP1-mCherry plasmids, treated with Torin1. (b) PLA to detect the proximity/interaction between endogenous RACK1 proteins and DFCP1 or Histone H3 (HH3). (c). RACK1 colocalized with LC3B. Fluorescence microscopy of cells transfected with RACK1-GFP and LC3B-BFP plasmids. (d) Fluorescence microscopy of RACK1-GFP, WIPI2-Halo and *ATG12* mRNA.

5.2.3 RACK1 associates with key Atg mRNAs

In cells treated with Torin1, RACK1 immunoprecipitated multiple mRNAs including *ATG3*, *ATG12*, *VPS34*, *p62* and *DFCP1*, while *GAPDH*, and *β-actin* mRNAs were not significantly associated with RACK1 (Figure.5-3a). However, RACK1 fail to precipitate several autophagy-related mRNAs in the absence of Torin1 treatment (Figure.5-3a). This indicates the interaction between Atg mRNAs and RACK1 is induced by autophagy inducer, and RACK1 emerges as a prime candidate for co-localizing with phagophores and recruiting these mRNAs to phagophores by selectively binding these mRNAs.

In addition, with mass spectrometry, RACK1(GNB2L1), DFCP1 protein, ribosomal proteins (RPL7, RPL18, RPS9), and the ER protein ATP2A2/SERCA2 were all immunoprecipitated by RACK1 antibody following Torin1 treatment (Figure.5-3b), indicating an interaction between RACK1 and DFCP1, as well as between RACK1 and ribosomal proteins under stress. Collectively, these findings confirm that RACK1 specifically and robustly associates with mRNAs encoding autophagy-related proteins during autophagy, further supporting its potential role in regulating the translation and localization of these mRNAs to phagophores.

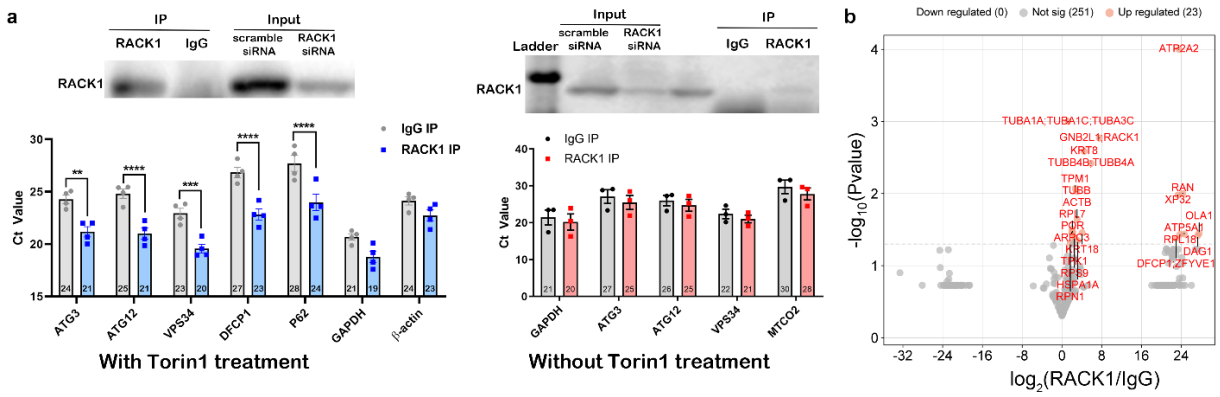

Figure.5-3 RACK1 associates with key Atg mRNAs.

(a) Western blot of RACK1 in immunoprecipitation using the RACK1 antibody and RT-qPCR of several mRNAs co-immunoprecipitated by the RACK1 antibody in cells treated with or without Torin1. Statistical significance was assessed using two-way ANOVA. Sample sizes are n=4 for the left panel and n=3 for the right panel. (b) Volcano plot of RACK1 IP data showing proteins immunoprecipitated by RACK1, with significance analyzed with independent t-test (n=3). Orange dots indicate proteins that were significantly precipitated by the RACK1 antibody. ****P<0.0001; ***P<0.001; **P<0.01; *P<0.05.

5.2.4 RACK1 regulates localization of Atg mRNAs to phagophores

Successful knockdown of RACK1 using siRNA was validated by Western blot and RT-qPCR (Figure.5-4a, b) and did not affect the cellular levels of several key Atg mRNAs (Figure.5-4c). This indicates that RACK1 knockdown does not alter the steady-state levels of Atg mRNAs, suggesting a post-transcriptional regulation mechanism. More biotinylated proteins were observed in the pulldowns from APEX2-DFCP1 comparing to input samples, regardless of RACK1 siRNA transfection, confirming successful proximity labeling and biotinylated protein pulldown under RACK1 knockdown conditions (Figure.5-4d).

RACK1 knockdown abrogated the recruitment of mRNAs essential for autophagy, including *ATG3*, *ATG12*, *VPS34*, *DFCP1* and *p62* into the vicinity of DFCP1 using proximity labeling-based pulldowns with APEX2-DFCP1 (Figure.5-4e). Similarly, the co-localization of *ATG3* or *ATG12* mRNAs with the phagophore marker WIPI1 was reduced upon RACK1 knockdown, as observed by FISH (Figure.5-4f, g). These results collectively demonstrate that RACK1 is essential for the recruitment of mRNA encoding proteins involved in autophagy to the phagophores.

Together, these multiple lines of evidence support a model in which mRNAs encoding proteins essential for autophagy, such as *ATG3* and *ATG12*, are recruited to forming autophagosomes in a process dependent on active translation and RACK1 (Bai et al., 2013; Lee et al., 2019; Thompson et al., 2016).

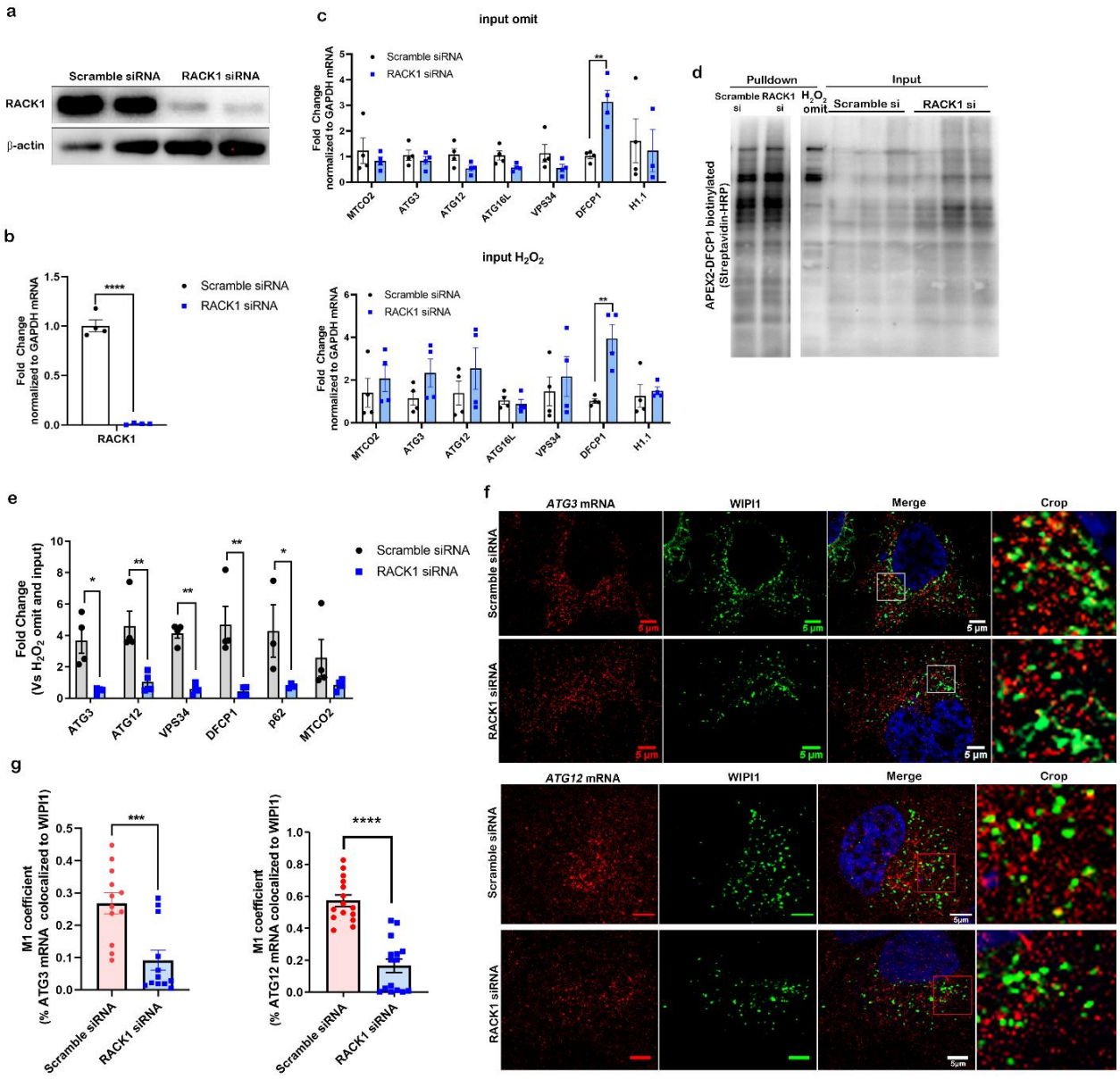
a
Scramble siRNA
RACK1 siRNA
RACK1
β-actin
b
Fold Change normalized to GAPDH mRNA
****
Scramble siRNA
RACK1 siRNA
RACK1
c
input omit
Scramble siRNA
RACK1 siRNA
Fold Change normalized to GAPDH mRNA
**
MTCO2
ATG3
ATG12
ATG16L
VPS34
DFCP1
H1.1
input H2O2
Scramble siRNA
RACK1 siRNA
Fold Change normalized to GAPDH mRNA
**
MTCO2
ATG3
ATG12
ATG16L
VPS34
DFCP1
H1.1
d
Pulldown
Input
Scramble si
RACK1 si
H2O2 omit
Scramble si
RACK1 si
APEX2-DFCP1 biotinylated (Streptavidin-HRP)
e
Fold Change (Vs H2O2 omit and input)
Scramble siRNA
RACK1 siRNA
*
**
**
**
*
ATG3
ATG12
VPS34
DFCP1
p62
MTCO2
f
ATG3 mRNA
WIPI1
Merge
Crop
Scramble siRNA
RACK1 siRNA
5 μm
ATG12 mRNA
WIPI1
Merge
Crop
Scramble siRNA
RACK1 siRNA
5μm
g
M1 coefficient (% ATG3 mRNA colocalized to WIPI1)
***
Scramble siRNA
RACK1 siRNA
M1 coefficient (% ATG12 mRNA colocalized to WIPI1)
****
Scramble siRNA
RACK1 siRNA

Figure.5-4 RACK1 regulates localization of core Atg mRNAs to phagophores.

(a, b) Knockdown of RACK1 mRNAs and proteins with RACK1 siRNAs. qPCR analysis of *RACK1* mRNAs and Western blot analysis of RACK1 protein following transfection with RACK1 siRNAs. n=4 and a t-test were used for statistical analysis. (c) RACK1 knockdown did not affect the cellular levels of autophagy-related mRNAs, RT-qPCR analysis of Atg mRNAs from cells transfected with RACK1 siRNA or scramble siRNA with or without H_2O_2 staining. n=4 and a two-way ANOVA analysis was used for statistical analysis. (d) Successful proximity labeling and pulldown by APEX2-DFCP1 under RACK1 knockdown conditions. Biotinylated proteins in input and pulldown from representative APEX2-DFCP1 proximity labeling experiments with or without RACK1 siRNAs. Protein samples from input and pulldown were displayed separately, but on the same PVDF membrane. (e) RACK1 knockdown abrogated the recruitment of several Atg mRNAs to DFCP1. RT-qPCR analysis of APEX2-DFCP1-labeled RNAs from cells transfected with RACK1 or scramble siRNAs, treated with Torin1 (250 nM, 4 h). A two-way ANOVA analysis was used for statistical analysis and n=4. (g) Fluorescence microscopy of *ATG3* mRNA or *ATG12* mRNA (FISH) and WIPI1-GFP in cells transfected with siRNAs targeting *RACK1* or scramble siRNAs and quantification of co-localization (M1 colocalization co-efficient) in the panel (f). More than 12 images of >40 cells were analyzed with a t-test. ****P<0.0001; ***P<0.001; **P<0.01; *P<0.05.

5.2.5 RACK1 regulates local translation of Atg mRNAs near phagophores

RACK1 associates with ribosomes and selectively regulates the translation of subpopulations of mRNAs (Coyle et al., 2009; Johnson et al., 2019; Kim et al., 2017). Since RACK1 has been shown to co-localize with forming autophagosomes, recruit Atg mRNAs to this site, and interact with multiple ribosomal proteins under stress conditions, it is plausible to hypothesize that RACK1 regulates translation of these Atg mRNAs in proximity to forming autophagosomes.

Consistent with the role of RACK1 in regulating translation by binding ribosomes (Gallo et al., 2018), knockdown of RACK1 detectably diminished levels of general translation in cells, as detected by polysome profiling (Figure.5-5a) and AHA nascent protein labelling (Figure.5-5b, top left input nascent proteins). However, RACK1 knockdown selectively had a more profound effect on translation in proximity to APEX2-DFCP1, even when this was normalized to account for its effect on global translation (input AHA-labelled proteins) and APEX2-DFCP1 proximity-based pulldowns (Figure.5-5b). Additionally, RACK1 knockdown reduced levels of *ATG3*, *DFCP1* and *VPS34* mRNAs in heavy polysome fractions in proximity to DFCP1 (Figure.5-5c). Cumulatively, this data demonstrates that RACK1 preferentially regulates local translation of mRNAs encoding proteins required for autophagy near forming autophagosomes.

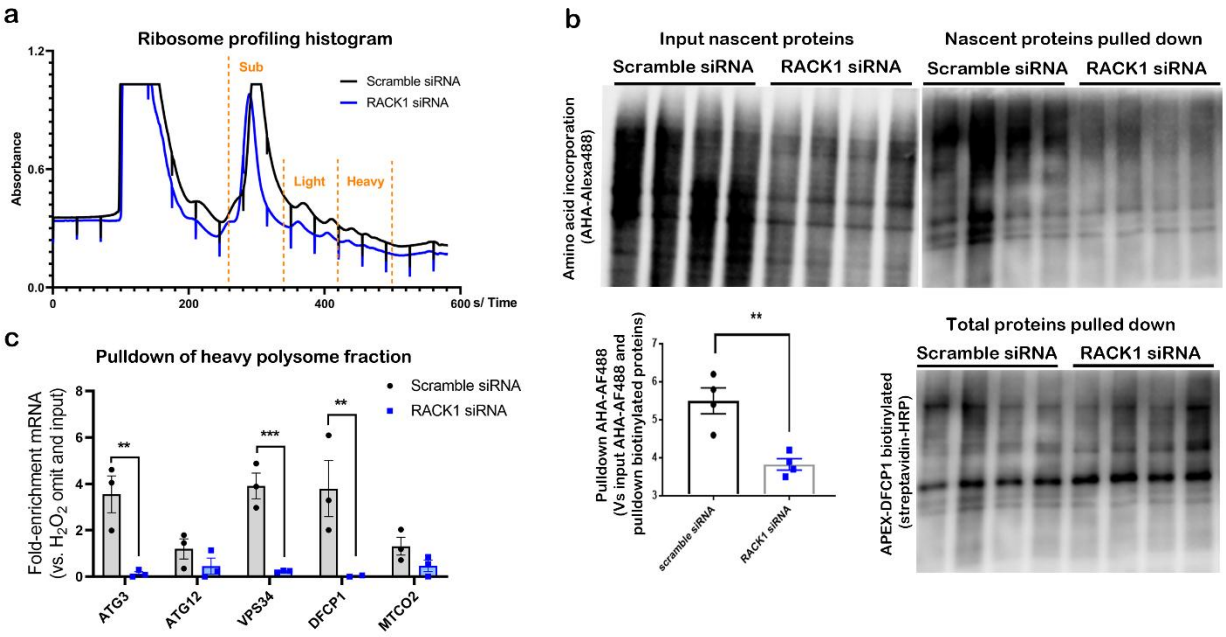

Figure.5-5 RACK1 regulates translation of several Atg proteins in proximity to phagophores.

(a) Representative A260 polysome fractionation plot from HeLa cells transfected with indicated siRNAs and treated with Torin1 (250 nM) for 4 h. (b) Quantification of nascent protein synthesis (AHA-Alexa488) in total cell lysate (input) and APEX2-DFCP1 proximity-labeled pulldown. Total biotinylated proteins pulled down after APEX2-DFCP1 labeling are detected with streptavidin-HRP (bottom panel). The graph quantifies nascent protein in proximity to APEX2-DFCP1, normalized to input nascent protein (t-test, n=4). (c) RT-qPCR quantification of mRNA in heavy polysome fractions from HeLa cells transfected with indicated siRNAs and treated with Torin1. A Two-way ANOVA analysis was used for statistical analysis (n=3).

5.2.6 RACK1 mediated localization of Atg mRNAs to phagophores for *in situ* translation is essential to sustained autophagy

If the recruitment of mRNAs encoding proteins essential for autophagy to the early phagophore for local translation is critical for sustained autophagy, then depleting RACK1 should decrease the rate of autophagy. Similar to cycloheximide treatment, RACK1 knockdown significantly decreased the protein level of p62/SQSTM, LC3A/B-II, NBR1, ATG5-ATG12, VPS34, and OPTN, all of which are required for autophagic degradation (Figure.5-6a-g). Although NDP52 protein levels appeared to decrease following RACK1 knockdown, this did not reach statistical significance (Figure.5-6h). RACK1 knockdown also significantly inhibited autophagosome and autolysosome formation, as measured using the LC3B-GFP-mCherry dural fluorescent system (Figure.5-6i-k), and again the reduction of autophagosomes and autophagolysosomes was not caused by a fluorescence intensity change of GFP (Figure.5-6l) and mCherry (Figure.5-6m).

RACK1 associates with an autophagosome initiation complex (Atg14L-Beclin 1-Vps34-Vps15) upon its phosphorylation by AMPK at Thr50 (Zhao et al., 2015) and the R36D/K38E mutant of RACK1 inhibits its binding to 40S ribosomes (Gallo et al., 2018). Thr50 and R36D/K38E mutants of RACK1 were generated and used to further dissect the mechanism by which RACK1 localizes mRNAs to phagophores. The whole plasmid sequencing of RACK1 plasmids carrying the mutants of Thr50 and R36D/K38E is displayed in Appendix E. APEX2-DFCP1 expressing cells were co-transfected with RACK1 siRNAs targeting the 3'UTR of RACK1 and Flag-RACK1 plasmids carrying these mutants or its wild-type form. As expected, reduced RACK1 protein levels and overexpression of Flag were observed in the protein lysates of these cells (Figure.5-6n). However, neither were observed in the protein lysates of cells transfected with

single scramble siRNAs or single RACK1 siRNAs targeting its 3'UTR (Figure.5-6n). Wild-type RACK1 rescued the recruitment of Atg mRNAs into proximity of DFCP1 (Figure.5-6o), whereas both RACK1 mutant abrogated the enrichment of Atg transcripts to DFCP1 (Figure.5-6o) and inhibited autophagosome formation (Figure.5-6p). These results suggest that disrupting RACK1's association with either ribosomes or phagophores impairs the recruitment of these Atg mRNAs to forming autophagosomes, thereby hindering autophagy.

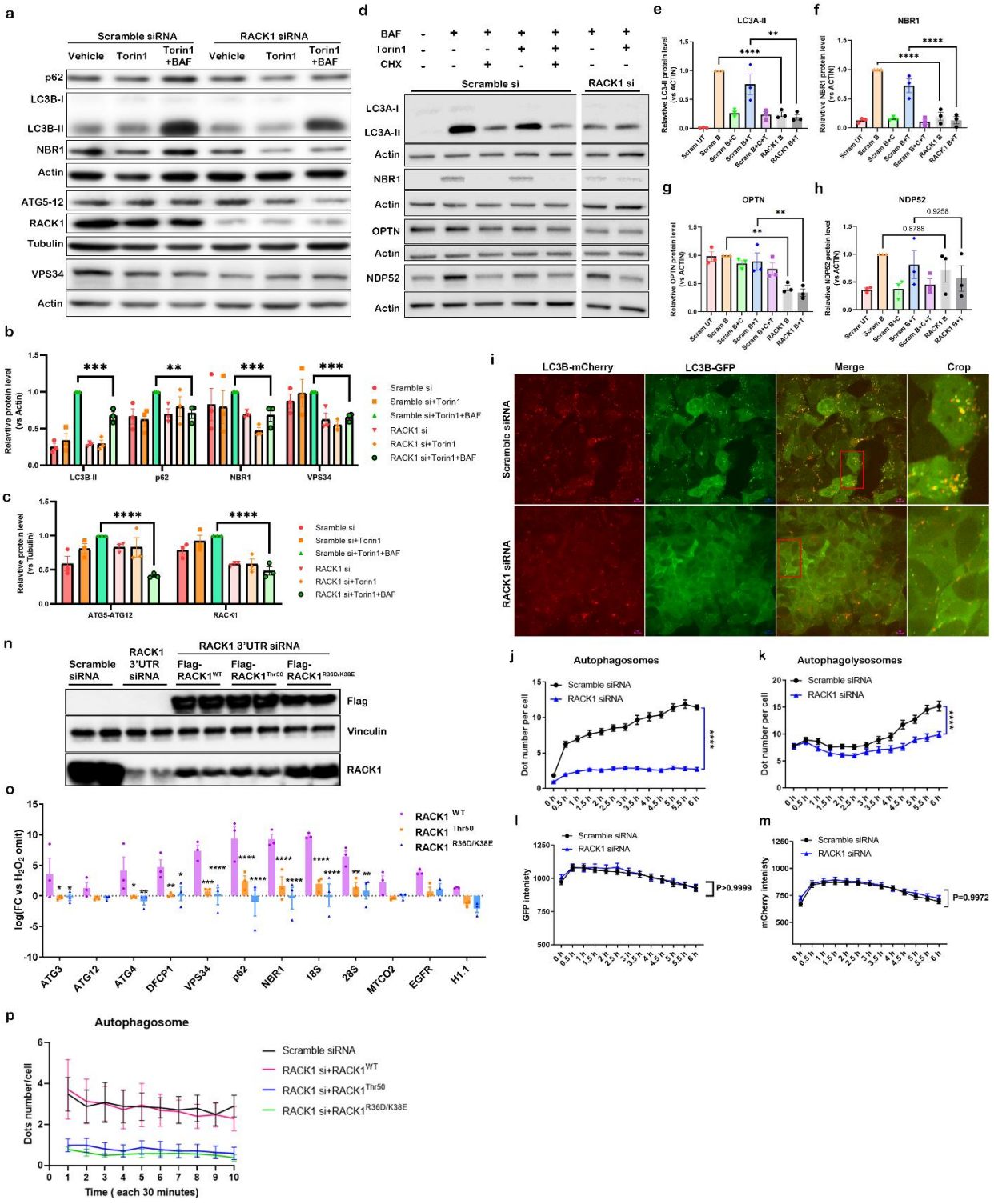
a
Scramble siRNA
RACK1 siRNA
Vehicle
Torin1
Torin1 +BAF
p62
LC3B-I
LC3B-II
NBR1
Actin
ATG5-12
RACK1
Tubulin
VPS34
d
BAF
Torin1
CHX
Scramble si
RACK1 si
LC3A-I
LC3A-II
NBR1
OPTN
NDP52
e
LC3A-II
Relative LC3-II protein level (vs ACTIN)
f
NBR1
Relative NBR1 protein level (vs ACTIN)
g
OPTN
Relative OPTN protein level (vs ACTIN)
h
NDP52
Relative NDP52 protein level (vs ACTIN)
0.9258
0.8788
Scram UT
Scram B
Scram B+C
Scram B+T
Scram B+C+T
RACK1 B
RACK1 B+T
b
Relative protein level (vs Actin)
LC3B-II
p62
NBR1
VPS34
Sramble si
Sramble si+Torin1
Sramble si+Torin1+BAF
RACK1 si
RACK1 si+Torin1
RACK1 si+Torin1+BAF
c
Relative protein level (vs Tubulin)
ATG5-ATG12
RACK1
i
LC3B-mCherry
LC3B-GFP
Merge
Crop
Scramble siRNA
RACK1 siRNA
n
Scramble siRNA
RACK1 3'UTR siRNA
RACK1 3'UTR siRNA
Flag-RACK1WT
Flag-RACK1Thr50
Flag-RACK1R36D/K38E
Flag
Vinculin
RACK1
j
Autophagosomes
Dot number per cell
k
Autophagolysosomes
l
GFP intensity
P>0.9999
m
mCherry intensity
P=0.9972
o
log(FC vs H2O2 omit)
RACK1 WT
RACK1 Thr50
RACK1 R36D/K38E
ATG3
ATG12
ATG4
DFCP1
VPS34
p62
NBR1
18S
28S
MTCO2
EGFR
H1.1
p
Autophagosome
Dots number/cell
Time (each 30 minutes)
Scramble siRNA
RACK1 si+RACK1WT
RACK1 si+RACK1Thr50
RACK1 si+RACK1R36D/K38E

Figure.5-6 RACK1 regulates translation of several Atg proteins in proximity to phagophores.

(a, d) WB analysis of Atg proteins in cells transfected with siRNA indicated siRNA and their quantification (b-c, e-h), B: BAF, T: Torin1, C: CHX. Displayed separated protein bands from different groups were run on the same PVDF membrane. (i) Microscopy of HEK293T cells expressing GFP-mCherry-LC3B and transfected with indicated siRNAs and quantification of autophagosome (j) and autophagolysosomes (k) in these cells. The number of dots per cell was counted (>500 cells per time point, two-way ANOVA analysis). (l-m) GFP and mCherry intensity of GFP-mCherry-LC3B cells transfected with indicated siRNAs under Torin1 treatment, and a two-way ANOVA analysis was applied. (n) WB showing RACK1 knockdown by siRNA targeting RACK1 3'UTR and overexpression of Flag-RACK1^{Thr50} or RACK1$^{R36D/K38E}$. (o) RACK1^{Thr50} and RACK1$^{R36D/K38E}$ mutants abrogated the recruitment of several Atg mRNAs to DFCP1. RT-qPCR of APEX2-DFCP1 biotinylated RNAs from APEX2-DFCP1 expressing cells co-transfected with RACK1 3'UTR siRNAs and plasmids (Flag-RACK1^{Thr50}, Flag-RACK1$^{R36D/K38E}$, or Flag-RACK1^{WT}) under Torin1 treatment (Two-way ANOVA analysis, n=3). (p) Quantification of autophagosomes in GFP-mCherry-LC3B expressing cells co-transfected with RACK1 3'UTR siRNA and plasmids (Flag-RACK1^{Thr50}, Flag-RACK1$^{R36D/K38E}$, or Flag-RACK1^{WT}) under Torin1 treatment for 5 h.

5.2.7 eIF5A regulates localization of Atg mRNAs to phagophores

While eIF5A proteins were observed to colocalize with DFCP1 or LC3B positive signals (Figure.5-7a), eIF5A antibodies fail to immunoprecipitate Atg mRNAs (Figure.5-7b), suggesting

that eIF5A does not directly bind to these Atg mRNAs. To further investigate the role of eIF5A in localizing Atg mRNAs to phagophores, APEX2-DFCP1 expressing cells transfected with siRNAs targeting either eIF5A or scramble were used for proximity biotinylation, followed by streptavidin bead pulldown. Knockdown of eIF5A protein and mRNAs were validated with WB (Figure.5-7b) and RT-qPCR (Figure.5-7c), respectively. eIF5A knockdown resulted in a significant reduction in the localization of several essential Atg mRNAs to DFCP1 (Figure.5-7e), while the overall cellular levels of these Atg mRNAs remained unchanged (Figure.5-7d). This indicates that eIF5A specifically regulates the recruitment of Atg mRNAs to phagophores without affecting their overall expression. Moreover, FISH staining further confirmed that the recruitment of *ATG12* mRNAs to DFCP1 was significantly inhibited following eIF5A knockdown (Figure.5-7f), reinforcing the importance of eIF5A in the spatial regulation of autophagy-related mRNAs.

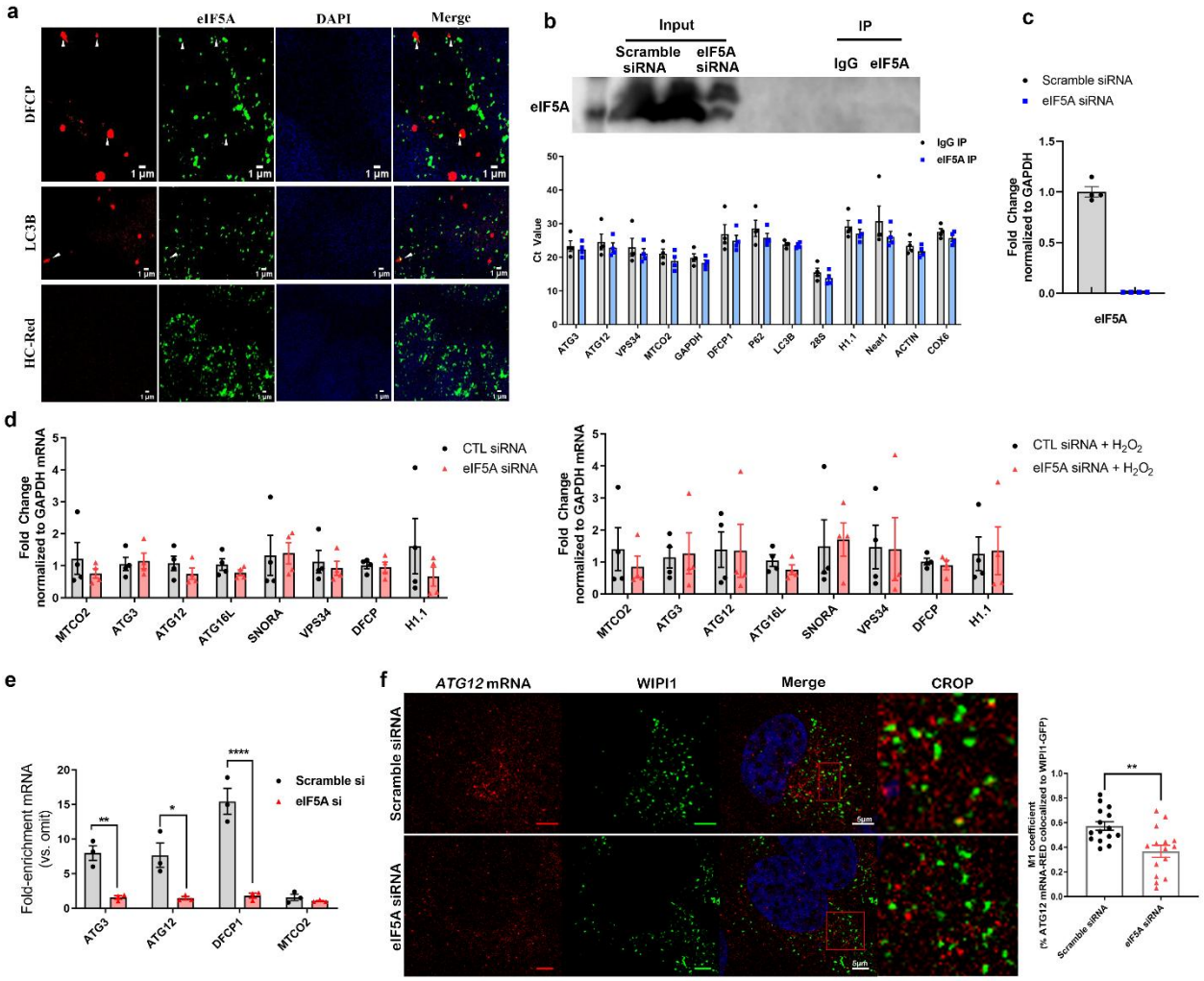
a
eIF5A
DAPI
Merge
DFCP
LC3B
HC-Red
1 μm
b
Input
IP
Scramble siRNA
eIF5A siRNA
IgG
eIF5A
eIF5A
IgG IP
eIF5A IP
Ct Value
ATG3
ATG12
VPS34
MTCO2
GAPDH
DFCP1
P62
LC3B
28S
H1.1
Neat1
ACTIN
COX6
c
Scramble siRNA
eIF5A siRNA
Fold Change normalized to GAPDH
eIF5A
d
CTL siRNA
eIF5A siRNA
Fold Change normalized to GAPDH mRNA
MTCO2
ATG3
ATG12
ATG16L
SNORA
VPS34
DFCP
H1.1
CTL siRNA + H2O2
eIF5A siRNA + H2O2
e
Fold-enrichment mRNA (vs. omit)
Scramble si
eIF5A si
ATG3
ATG12
DFCP1
MTCO2
f
ATG12 mRNA
WIPI1
Merge
CROP
Scramble siRNA
eIF5A siRNA
5μm
M1 coefficient (% ATG12 mRNA-RED colocalized to WIPI1-GFP)
Scramble siRNA
eIF5A siRNA

Figure.5-7 eIF5A regulates localization of Atg mRNAs to phagophores.

(a) Fluorescence microscopy of cells transfected with DFCP1 or LC3B-mCherry and blotted with primary antibody anti-eIF5A and treated with Torin1. (b) Western blot of eIF5A in immunoprecipitations using eIF5A antibody, and RT-qPCR analysis of several mRNAs co-immunoprecipitated by eIF5A antibody in cells treated with Torin1. Two-way ANOVA analysis, n=4. (c) qPCR of eIF5A knockdown by eIF5A siRNA transfection. (d) eIF5A knockdown did not affect the cellular levels of autophagy-related mRNAs, RT-qPCR analysis of Atg mRNAs from cells transfected with eIF5A siRNA or scramble siRNA with or without H_2O_2 staining. n=4 and a two-way ANOVA analysis was used for statistical analysis. (e) eIF5A knockdown abrogated the recruitment of several Atg mRNAs to DFCP1. RT-qPCR analysis of APEX2-DFCP1 biotinylated mRNAs from cells transfected with eIF5A or scramble siRNAs and treated with Torin1 (250 nM, 4 h). A two-way ANOVA was used statistical analysis (n=3). (f) Fluorescence microscopy of *ATG12* mRNAs (FISH) and WIPI1-GFP in cells transfected with siRNA targeting eIF5A or scramble siRNAs, and quantification of co-localization (M1 colocalization co-efficient) in these images. More than 12 images from more than 40 cells were analyzed and a t-test was applied. ****P<0.0001; ***P<0.001; **P<0.01; *P<0.05.

5.2.8 eIF5A regulates local translation of Atg mRNAs near phagophores

eIF5A knockdown reduced the protein levels of autophagosomes marker, LC3B and several autophagy-related receptors (NBR1, OPTN, NDP52) (Figure.5-8a). Consistent with this, eIF5A knockdown significantly reduced the synthesis of autophagosomes but not autophagolysosomes

with LC3-mCherry-GFP expressing cells (Figure.5-8b, c). Additionally, eIF5A knockdown reduced the percentage of nascent peptides labelled with AHA click-it chemistry reaction, that colocalized with DFCP1 (Figure.5-8d). eIF5A knockdown also led to a detectable reduction in cellular general translation levels, as detected by AHA-Alexa488 nascent protein labelling (Figure.5-8e, input panel) and polysome profiling (Figure.5-8g). However, eIF5A knockdown selectively had a more profound effect on translation in proximity to APEX2-DFCP1, even when normalized to account for its impact on global translation (input AHA-Alexa488-labelled proteins) and APEX2-DFCP1 pulldowns (Figure.5-8f). Furthermore, eIF5A knockdown reduced levels of *ATG3*, *DFCP1* and *VPS34* mRNAs in heavy polysome fractions in proximity to DFCP1 (Figure.5-8h). Cumulatively, these data demonstrate that eIF5A preferentially regulates the translation of mRNAs encoding proteins required for autophagy in proximity to phagophores. Our findings suggest that the localization of Atg mRNAs to phagophores is translation dependent and that eIF5A facilitates the recruitment of several Atg mRNAs to phagophores by influencing the ongoing translation of Atg mRNAs, rather than directly binding to them.

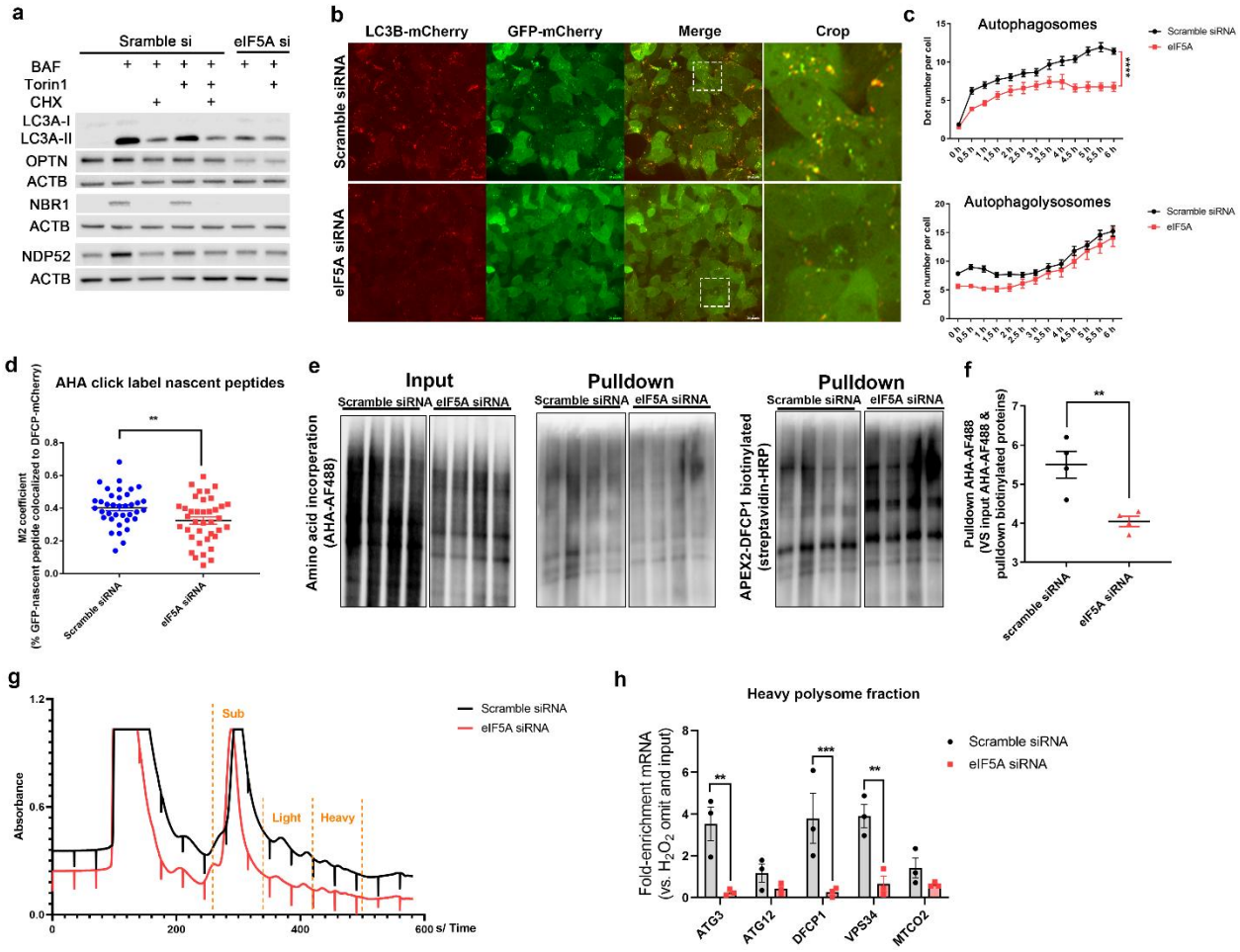
a
Sramble si
eIF5A si
BAF
Torin1
CHX
LC3A-I
LC3A-II
OPTN
ACTB
NBR1
ACTB
NDP52
ACTB
b
LC3B-mCherry
GFP-mCherry
Merge
Crop
Scramble siRNA
eIF5A siRNA
c
Autophagosomes
Autophagolysosomes
Dot number per cell
Scramble siRNA
eIF5A
d
AHA click label nascent peptides
M2 coefficient
(% GFP-nascent peptide colocalized to DFCP-mCherry)
Scramble siRNA
eIF5A siRNA
e
Input
Pulldown
Pulldown
Scramble siRNA
eIF5A siRNA
Amino acid incorperation
(AHA-AF488)
APEX2-DFCP1 biotinylated
(streptavidin-HRP)
f
Pulldown AHA-AF488
(VS input AHA-AF488 &
pulldown biotinylated proteins)
scramble siRNA
eIF5A siRNA
g
Absorbance
Sub
Light
Heavy
Scramble siRNA
eIF5A siRNA
s/ Time
h
Heavy polysome fraction
Fold-enrichment mRNA
(vs. H2O2 omit and input)
Scramble siRNA
eIF5A siRNA
ATG3
ATG12
DFCP1
VPS34
MTCO2

Figure.5-8 eIF5A regulates local translation of Atg mRNAs near phagophores.

(a) Western blot analysis of autophagy-related proteins in cells transfected with siRNAs targeting eIF5A or scramble siRNAs, along with their quantification. (b) Fluorescence microscopy of HEK293T cells expressing GFP-mCherry-LC3B and transfected with scramble siRNAs or eIF5A-targeting siRNAs. (c) quantification of autophagosome and autophagolysosomes formation in cells of panel (b). The number of dots per cell was counted (>500 cells per time point), and a two-way ANOVA was used for statistical analysis. (d) Manders' colocalization coefficient (MCC) quantification of Alexa488-tagged nascent proteins and mCherry-DFCP1 in cells transfected with scramble or eIF5A siRNAs. Unpaired t-test was used for significance and each dot represents one image. (e) Quantification of nascent protein synthesis (AHA-Alexa488) in total cell lysate (input) and APEX2-DFCP1 proximity-labeled pulldowns. Total biotinylated protein pulled down after APEX2-DFCP1 labeling are detected with streptavidin-HRP (right panel). (f) Graph quantifying nascent protein in proximity to APEX2-DFCP1, normalized to input nascent protein. A t-test was applied and n=4. (g) Representative A260 polysome fractionation plot from HeLa cells transfected with indicated siRNAs and treated with Torin1 (250 nM) for 4 h. (h) RT-qPCR quantification of mRNA in heavy polysome fractions from HeLa cells transfected with indicated siRNAs and treated with Torin1. A two-way ANOVA analysis was used for statistical analysis and n=3. ****P<0.0001; ***P<0.001; **P<0.01; *P<0.05.

5.3 Discussion

Harringtonine and puromycin blocked the recruitment of several essential Atg mRNAs to phagophores and autophagosomes, indicating that autophagy-related mRNAs require active

ongoing translation, and potentially a ribosome-associated factor for the recruitment of Atg mRNAs to or the retention at DFCP1 locales. This is consistent with increasing reports on co-translational mRNA targeting (Chouaib et al., 2020; Wang et al., 2016) or associated on-going translation with localized mRNAs (Cioni et al., 2019).

Our study reveals that RACK1 localizes in the vicinity of DFCP1 and LC3B and can successfully precipitate several Atg mRNAs during autophagy. Additionally, RACK1 facilitates the recruitment of several key Atg mRNAs to phagophores to be translated there through its association with ribosomes and autophagosome initiation complex (Atg14L-Beclin 1-Vps34-Vps15), thereby mediating the formation of autophagosomes and autophagolysosomes. In addition to RACK1, eIF5A also promotes the relocation of key Atg mRNAs to phagophores to be translated there through an unknown mechanism, rather than directly binding to them. This is supported by the observation that eIF5A colocalizes with DFCP1 or LC3B but fails to precipitate Atg mRNAs during autophagy. Meanwhile, eIF5A is essential for the recruitment of key Atg mRNAs to phagophores, the local translation of these Atg mRNAs near phagophores, and the synthesis of autophagosomes.

In conclusion, our study reveals that active translation of Atg mRNAs is essential for their recruitment to phagophores during autophagy. RACK1 facilitates this process through its interaction with ribosomes and autophagy complexes, while eIF5A, though not directly binding to these Atg mRNAs, also supports their localization and translation near phagophores. These findings enhance our understanding of the molecular mechanisms underlying autophagosome formation.

Chapter 6. Roles of RACK1 and eIF5A in Autophagy of Stress Granules and Mitochondria

6.1 Background

Stress granules (SCs) are dynamic, membrane-less structures that sequester untranslated mRNAs and regulatory proteins to protect cells from damage. RNA-binding protein Ras GTPase-activating protein SH3 domain-binding protein (G3BP) and TAR DNA-binding protein 43 (TDP-43) are key components of stress granules (Aulas et al., 2012; Yang et al., 2020). While TDP-43 is normally nuclear and involved in RNA processing, it translocates to the cytoplasm under stress, where, among other things, it contributes to stress granule formation. Stress granules form in response to various stressors and are classified into acute and chronic stress granules depending on the induced stressors. Transient stressors (e.g., hypoxia, oxidative stress, arsenite) induce acute stress granules, while prolonged stressors (e.g., genotoxic drugs, X-rays) lead to chronic stress granule aggregation (Arimoto et al., 2008). Both types contain common stress granule components, but chronic stress granules lack some acute stress granule components, including RACK1 (Arimoto et al., 2008). In acute stress granules, RACK1 is sequestered, promoting cell survival. However, in chronic stress granules, RACK1 remains diffused in the cytoplasm, where it activates stress-activated MAPK pathways, ultimately leading to cell apoptosis (Masi et al., 2022). Previous studies also revealed that hypusine-modified eIF5A promotes TDP-43 phosphorylation and aggregation during arsenite-induced stress, thereby playing a key role in the formation of stress granules (Li et al., 2010; Smeltzer et al., 2021).

Mitophagy is the selective degradation of damaged or dysfunctional mitochondria via autophagy. It is a vital process in maintaining cellular health and mitochondrial quality control. RACK1 has

been shown to promote mitophagy to enhance mitochondrial function (Zhao et al., 2024). RACK1 also enhances mitochondrial function by reducing ROS accumulation, boosting mitochondrial membrane potential, and inhibiting cytochrome C release, thereby reducing mitochondria-mediated cell apoptosis (Zhao et al., 2024). Hypusine-modified eIF5A is involved in mitochondrial quality control via autophagy/mitophagy, but the molecular mechanisms remain unclear (Hofer et al., 2021; Schroeder et al., 2021).

Our previous study demonstrated that RACK1 and eIF5A play a crucial role in recruiting core Atg mRNAs to forming autophagosomes for *in situ* translation, supplying key Atg proteins necessary for sustained autophagy. While autophagy is responsible for degrading damaged mitochondria and SCs, the specific contributions of RACK1 and eIF5A in this process have not been fully explored.

6.2 Results

6.2.1 CHX and knockdown of RACK1 or eIF5A prevent stress granule degradation

Cells expressing G3BP2-eGFP were treated with sodium arsenite for 0.5 h to induce stress granules. CHX treatment was found to significantly inhibit the induction of stress granules by sodium arsenite (Figure.6-1a). Furthermore, CHX treatment significantly prevented the elimination of stress granules, as evidenced by a higher number of stress granules in CHX-treated cells compared to the control group after 2 hours of recovery from sodium arsenite treatment (Figure.6-1a). After 2 hours of recovery following a 30-minute sodium arsenite

exposure, 25% of CHX-treated cells still contained stress granules (Figure. 6-1b). These findings indicate that translation is essential for both the formation and degradation of stress granules.

To investigate the role of RACK1 and eIF5A in the elimination of stress granules, cells expressing G3BP2-eGFP were transfected with siRNAs targeting scramble, RACK1, or eIF5A for 72 h. On the day of collection, cells were treated with sodium arsenite for 0.5 h to induce stress granules, followed by replacement of the medium with full condition medium for an additional 2 hours to assess stress granule elimination. We found that knockdown of eIF5A, but not RACK1, inhibited the formation of stress granules (Figure.6-1c). This can be explained by the fact that eIF5A is a component of the stalled translation initiation complex that accumulates at stress granules, and the hypusine-modified eIF5A is essential for stress granule assembly by promoting stress- or arsenite-induced polysome disassembly (Li et al., 2010). Additionally, the knockdown of either eIF5A or RACK1 inhibited the elimination of stress granules, resulting in substantial accumulation of stress granules during the recovery phase following sodium arsenite treatment (Figure.6-1d). These findings suggest that both RACK1 and eIF5A are essential to the degradation of stress granules.

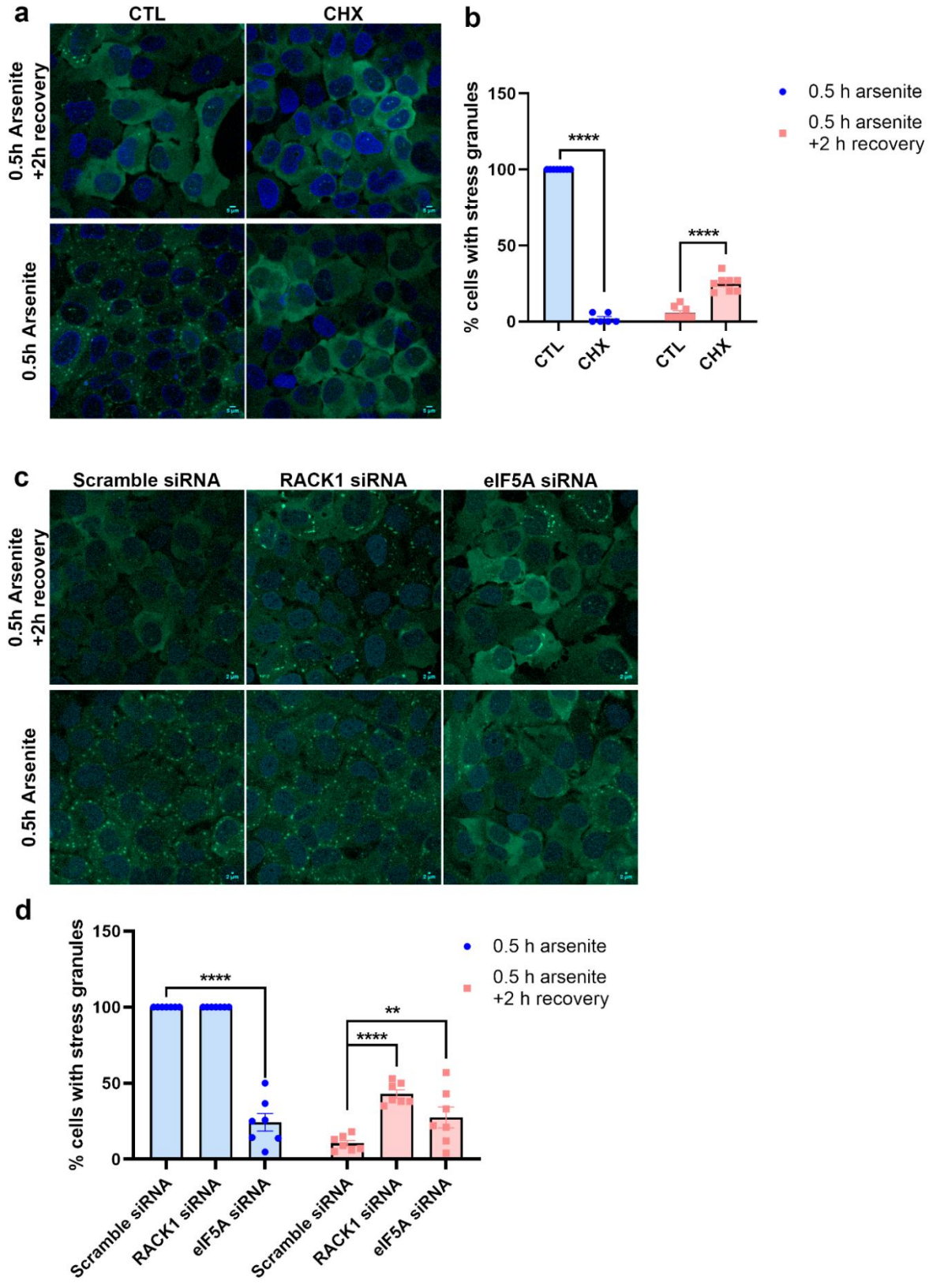
a
CTL
CHX
0.5h Arsenite +2h recovery
0.5h Arsenite
b
% cells with stress granules
150
100
50
0
****
****
CTL
CHX
CTL
CHX
0.5 h arsenite
0.5 h arsenite +2 h recovery
c
Scramble siRNA
RACK1 siRNA
eIF5A siRNA
0.5h Arsenite +2h recovery
0.5h Arsenite
d
% cells with stress granules
150
100
50
0
****
**
****
Scramble siRNA
RACK1 siRNA
eIF5A siRNA
Scramble siRNA
RACK1 siRNA
eIF5A siRNA
0.5 h arsenite
0.5 h arsenite +2 h recovery

Figure.6-1 CHX and knockdown of RACK1 or eIF5A inhibit stress granule clearance. (a) Representative images of stress granules in cells treated with control or CHX after 30 min sodium arsenite, or two hours after removal of sodium arsenite. (b) quantification of percentage of cells with stress granules in cells used in panel (a) ($n \geq 6$ figures, each figure contains ≥20 cells, mean ± SEM). (c) Representative images of stress granules in cells transfected with scramble, RACK1, or eIF5A siRNAs and 30 min of sodium arsenite treatment, or two hours after removal of sodium arsenite. (d) quantification of percentage of cells with stress granules in cells used in panel (c) ($n \geq 7$, each figure contains ≥20 cells, mean ± SEM). A two-way ANOVA analysis was used for statistical analysis **** $P<0.0001$; ** $P<0.01$.

6.2.2 CHX and knockdown of RACK1 or eIF5A affect mitochondrial respiratory function

Mitochondrial respiratory function including basal respiration capacity, ATP-linked respiration, proton leak, maximal respiration capacity, spare capacity, and non-mitochondrial respiration, was quantified with OCR (Rose et al., 2014). Basal respiration capacity was measured with OCR without any inhibitor treatment. Different inhibitors that specifically target components of the electron transport chain were used to derive multiple parameters of non-basal mitochondrial respiration. Oligomycin inhibits ATP synthase, causing the reduction of ATP synthesis-linked respiration in OCR plots. The remaining mitochondrial OCR after oligomycin treatment is considered as proton leak. Uncoupler FCCP disrupts the proton gradient between the matrix and inner membrane space and mitochondrial membrane potential, causing uninhibited electron flow through the electron transport chain and maximal oxygen consumption by complex IV. The spare

capacity is defined as the difference between maximal and basal OCR. Antimycin A and rotenone inhibit complexes III and I, respectively, therefore abolishing all mitochondrial-associated respiration. The residual OCR after the addition of Antimycin A and rotenone is non-mitochondrial respiration (Underwood et al., 2020). The OCR curve shows the characteristic responses of mitochondrial respiratory function to mitochondrial inhibitors (Rose et al., 2014) (Figure.6-2a).

The maximal respiration capacity was significantly reduced upon CHX administration or knockdown of RACK1 or eIF5A. However, spare respiratory capacity was reduced by only eIF5A knockdown, but not by RACK1 knockdown or CHX treatment (Figure.6-2b, c). We also observed that in cells pretreated with Torin1 for 2 hours, both maximal and spare respiration capacities were significantly reduced by CHX administration or knockdown of RACK1 or eIF5A (Figure.6-2d, e). Furthermore, in cells pretreated with Torin1 and BAF for 2 hours, spare respiration capacity was reduced only by eIF5A knockdown, and maximal respiration capacity was significantly decreased by CHX administration or eIF5A knockdown (Figure.6-2f, g). Notably, RACK1 knockdown had no effect on mitochondrial respiratory function in cells treated with Torin + BAF (Figure.6-2f, g). CHX was found to inhibit the function of basal respiration capacity, maximal respiration capacity, and ATP production in cells treated without Torin or with Torin ± BAF (Figure.6-2c, e, f).

Collectively, these findings suggest that both RACK1 and eIF5A are essential for maintaining mitochondrial respiratory function, with the role of RACK1 being mainly mediated by Torin1-induced autophagic turnover. The effects of CHX on inhibiting basal respiration capacity, maximal respiration capacity, and spare capacity of mitochondria could be attributed to its role in

blocking mitochondrial energy transfer at Site I of the respiratory chain (Jomain-Baum et al., 1973).

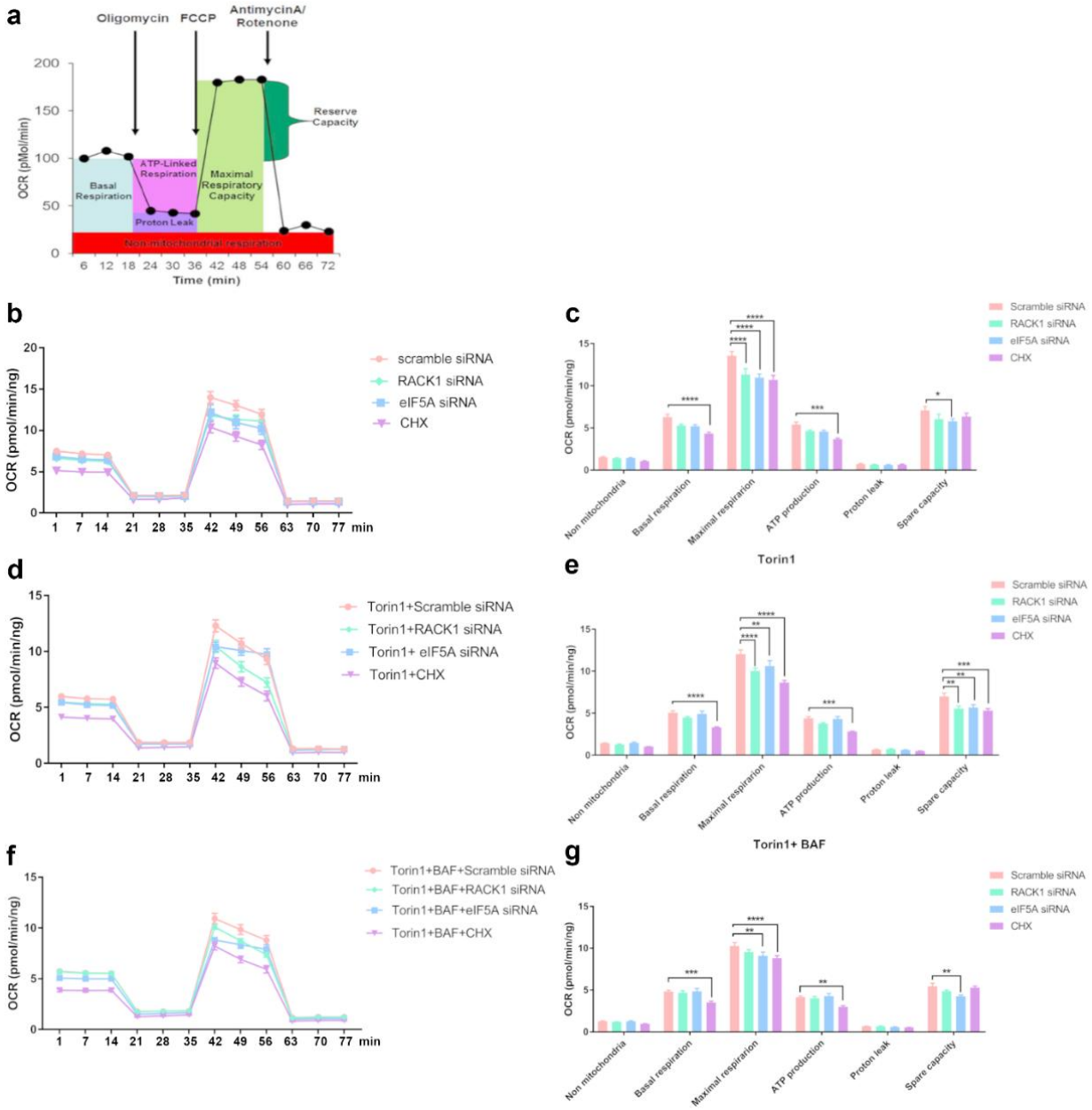

Figure.6-2 CHX, RACK1 siRNAs and eIF5A siRNAs affect mitochondrial respiratory function.

(a) Seahorse analysis profiles of OCR in cells from (Rose et al., 2014), in open access form. (b) OCR profile of cells transfected with specific siRNAs targeting scramble, RACK1, or eIF5A or treated with CHX. (c) Quantification of OCR from different aspects of mitochondrial respiration in cells used in panel (b). (d) OCR profiles of cells transfected with specific siRNAs or treated with CHX, in combination with Torin1 treatment. (e) Quantification of OCR from different aspects of mitochondrial respiration in cells shown in panel (d). (f) OCR profile of cells transfected with siRNAs or treated with CHX, together with Torin1+BAF treatment. (g) Quantification of OCR from different aspects of mitochondrial respiration in cells shown in panel (f), ($n \geq 4$, each replicate contains 6 technical replicates, mean ± SEM). A two-way ANOVA analysis was used for statistical analysis **** P<0.0001; *** P<0.001 ** P<0.01, * P<0.05.

6.2.3 CHX and knockdown RACK1 or eIF5A inhibit mitophagy

FCCP is a mitochondrial uncoupler that disrupts the mitochondrial membrane potential by transporting protons across the inner mitochondrial membrane, leading to mitochondrial fragmentation and the initiation of autophagy. According to several publications that the 2 h of FCCP (10uM) treatment will promote mitophagy, although this effect may vary depending on cell type. The mitochondrial fragmentation was characterized by a decrease in perimeter and area, along with an increase in the number of mitochondria, which is the active cleavage of individual mitochondria (Coronado et al., 2018).

In our study, wild-type HeLa cells transfected with scrambled siRNAs were treated with Torin1 for 2 hours to induce autophagy, followed by FCCP treatment for 0.5, 2.5, and 4.5 hours. The mean area and mean perimeter of Tomm20-labelled mitochondria significantly decreased with longer FCCP treatment durations, an effect that was prevented by the knockdown of RACK1, eIF5A, and the translation inhibitor CHX (Figure.6-3a, b). Notably, the number of mitochondria decreased following FCCP treatment, with eIF5A knockdown having a more pronounced effect on reducing mitochondrial count, while CHX treatment increased mitochondrial numbers (Figure.6-3a, b). In contrast, RACK1 knockdown had no impact on mitochondrial numbers (Figure.6-3a, b). This indicates that CHX increased the size, perimeter, and number of mitochondria under FCCP+Torin1 treatment, likely due to CHX-mediated inhibition of mitophagy and induction of mitochondrial hyperfusion, as reported in a previous study (Abdullah et al., 2022). The role of RACK1 and eIF5A knockdown in increasing the mean perimeter and area of mitochondria, along with eIF5A knockdown reducing the number of mitochondria under FCCP+Torin1 treatment, suggests that RACK1 and eIF5A may promote mitochondrial fragmentation during FCCP+Torin1-induced mitophagy. Collectively, these results strongly suggest that translation, RACK1, and eIF5A play important roles in mitophagy.

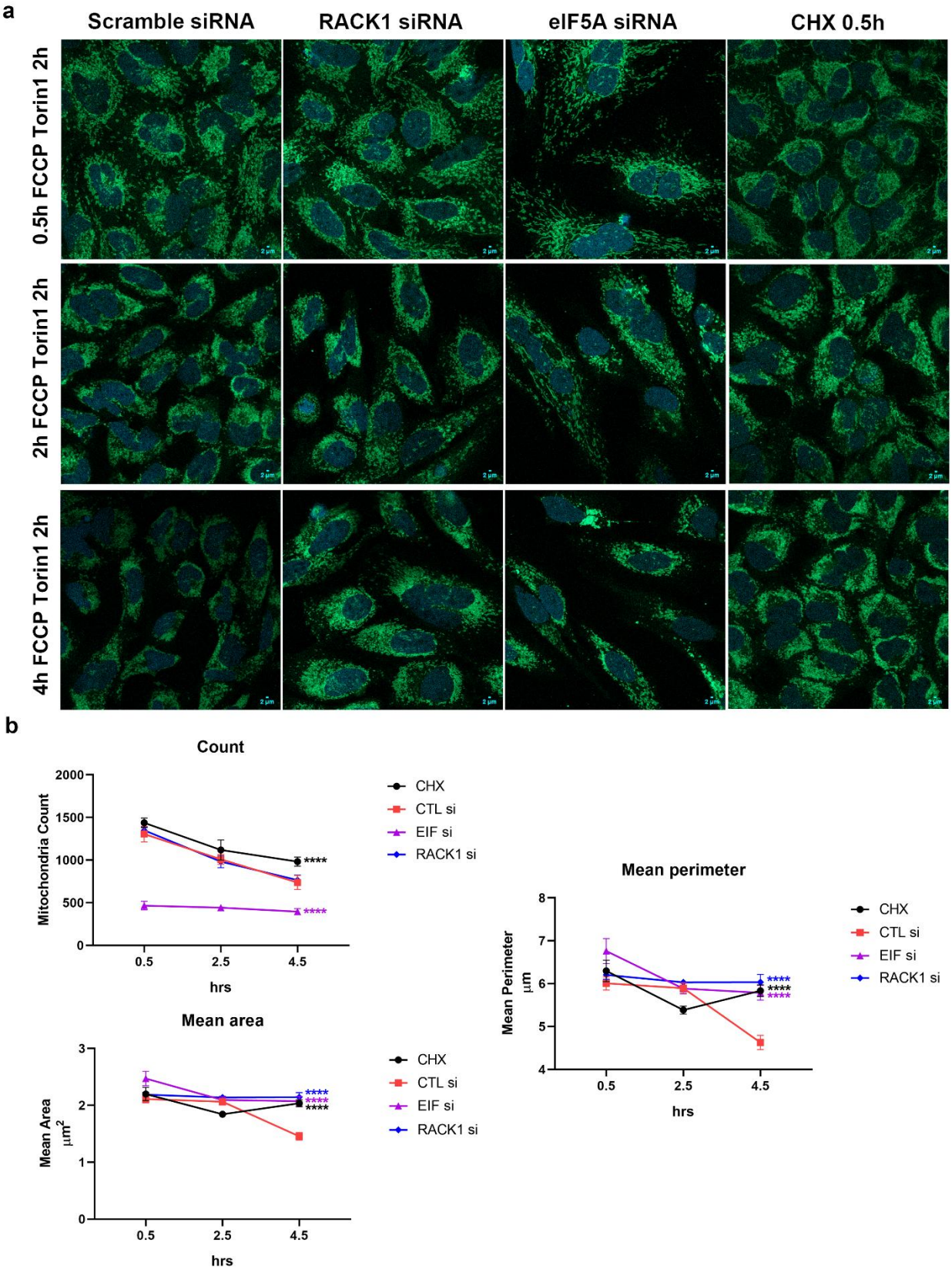
a
Scramble siRNA
RACK1 siRNA
eIF5A siRNA
CHX 0.5h
0.5h FCCP Torin1 2h
2h FCCP Torin1 2h
4h FCCP Torin1 2h
b
Count
Mitochondria Count
2000
1500
1000
500
0
0.5
2.5
4.5
hrs
****
****
CHX
CTL si
EIF si
RACK1 si
Mean area
Mean Area µm2
3
2
1
0
0.5
2.5
4.5
hrs
****
****
****
CHX
CTL si
EIF si
RACK1 si
Mean perimeter
Mean Perimeter µm
8
7
6
5
4
0.5
2.5
4.5
hrs
****
****
****
CHX
CTL si
EIF si
RACK1 si

Figure.6-3 Mitophagy is affected by CHX and knockdown of RACK1 or eIF5A.

(a) WT Hela cells were transfected with siRNAs for 72 h. On the collection day, cells were treated with FCCP (20 uM) for 0.5 h, 2.5 h, and 4.5 h together with 2 h Torin1 treatment, before being fixed for Tomm20 labeling and Alexa488-conjugated secondary antibody. (b) Quantification of mitochondria count, mean area, and mean perimeter in cells transfected with indicated siRNAs or treated with CHX (n =5 Figures, mean ± SEM). A two-way ANOVA was used for statistical analysis, with all significance values compared to the CTL siRNA group. **** P<0.0001; *** P<0.001 ** P<0.01, * P<0.05.

6.3 Discussion

Since stress granules have been demonstrated to be mainly eliminated by autophagy (Yang et al., 2023a). The CHX, translation inhibitor, inhibited the clearance of stress granules, indicating translation was necessary in autophagy-mediated degradation of stress granules. This is consistent with our previous results showing that translation is required for sustained autophagy and by extension, autophagy of stress granules. In addition, knockdown of RACK1 and eIF5A both prevent the elimination of stress granules, this suggests RACK1 and eIF5A promote the degradation of stress granules, potentially via their effects on local translation of mRNAs near autophagosomes. Therefore, this also suggests that RACK1 and eIF5A promoted clearance of stress granules is likely mediated by promoting local translation in autophagy.

It is well known that damaged mitochondria are mainly degraded by autophagy, named mitophagy. If autophagy is inhibited, damaged or non-functional mitochondria will accumulate, thus causing the downregulation of mitochondria-mediated function. Using the Seahorse assay, we found that under Torin1-induced stress, the knockdown of RACK1 and eIF5A, as well as

CHX treatment, inhibited mitochondrial functions, particularly maximal and spare respiration. This suggests that both eIF5A and RACK1 are also crucial for maintaining mitochondrial function. Notably, the role of RACK1 in mitochondrial respiratory function was primarily mediated by Torin1-induced autophagic turnover, emphasizing the critical role of autophagy in maintaining mitochondrial integrity. This also strongly suggest that RACK1-mediated local translation of mRNAs near autophagosomes is essential for proper mitochondrial function, although we cannot yet conclude definitively. The knockdown of RACK1 and eIF5A, as well as CHX treatment, both increased the mean perimeter and area of mitochondria under FCCP+Torin1 treatment, suggesting that these factors likely promote mitochondrial fragmentation under FCCP+Torin1-induced mitophagy. This further highlights the importance of translation, RACK1, and eIF5A in clearance of mitochondria via autophagy.

Considering the roles of RACK1 and eIF5A in the localization and local translation of Atg mRNAs, as evidenced by our data from the earlier chapters, the findings presented thus far strongly suggest that RACK1 and eIF5A are crucial for maintaining mitochondrial function under stress by promoting the clearance of damaged mitochondria and are important for the clearance of stress granules. However, despite these strong indications, we cannot yet draw definitive conclusions about the full extent of their roles in these processes.

Chapter 7. General Discussion and Conclusion

During autophagy, cells respond rapidly to nutritional stress for survival. General protein translation is inhibited under autophagy, caused by mTOR inhibition, which dephosphorylates 4E-BPs, and dephosphorylated 4E-BPs binds eIF4E to interrupt its association with eIF4G to from the eIF4F complex, thus inhibiting cap-dependent translation (Ma and Blenis, 2009). Consistently, the synthesis of several key Atg proteins and the formation of autophagosomes and autophagolysosomes are both inhibited under sustained autophagy, indicating translation of key autophagy proteins is essential to support the autophagy, especially when general translation is inhibited during sustained autophagy. In this case, the rapid formation of autophagosomes is a more efficient mechanism, and the local translation of Atg mRNAs likely promotes a rapid supply of Atg proteins.

With the APEX2-proximity labeling, molecules within a 20 nm radius of APEX2 can be biotinylated and pulled down for quantification (Hwang and Espenshade, 2016). This method provides high spatial and temporal specificity of identification of molecules nearby APEX2-protein of interest, despite that the fusion of APEX2 to a protein of interest may alter the protein's native function or localization. Therefore, the specificity of APEX2-LC3B/DFCP1 construct used in our project are both validated with the colocalization between DFCP1/LC3B proteins and the APEX2-biotinylated signals. Additionally, the endogenous SQSTM/p62 proteins, which interact with LC3 and associate with growing phagophores, colocalized to biotinylated signals of APEX2-DFCP1, indicating the function or localization of DFCP1 is not changed in APEX2-DFCP1.

The evidence presented here that were generated using FISH and APEX2-based proximity-labeling, indicates that many mRNAs encoding proteins required for autophagy are enriched in proximity to forming autophagosomes compared to other mRNAs including those encoding histones, mitochondrial proteins and β-Actin. Microscopic analyses revealed that not every punctate structure with DFCP1, WIPI2 or WIPI1 co-localizes with these mRNAs, or sites of local translation. This could have several explanations. Some of these puncta may be proteins associated with ER or other membranes that are not currently involved in forming autophagosomes. Alternatively, recruitment of mRNAs and local translation could occur only at specific time points during autophagosome formation. Additionally, RNA-seq of APEX2 proximity-based pulldowns further validates that these core Atg mRNAs are specifically recruited to regions near DFCP1 and LC3B under stress, rather than randomly, comparing to the enrichment of these Atg mRNAs in pulldowns of cytoplasmic APEX2-Perilipin2, APEX2-Cytoplasmic-V5, and nuclear APEX2-NPM1. The recruitment of these key Atg mRNAs to phagophores was blocked by FIP200 knockout or LC3B lipidation mutants. Since FIP200 is an essential component of ULK1 complex, involved in the initiation of autophagosome formation, and the lipidated LC3 (LC3-II) is recruited to growing phagophores to contribute to their elongation and final closure to form autophagosomes. Therefore, this strongly indicates that these key Atg transcripts are specifically recruited to phagophores to participate in the canonical autophagy process. The local translation of these Atg mRNAs near phagophores were identified with APEX2 proximity labeling along with ribosome profiling or with SILAC labeling. The enrichment of several core Atg mRNAs in heavy polysomes near DFCP1, along with nascent Atg proteins biotinylated by APEX2-DFCP1, strongly suggests that these Atg mRNAs are actively being translated in proximity to phagophores during autophagy.

EM studies have suggested that ribosomes are absent from the ER membranes which are directly incorporated into forming autophagosomes. Others have noted that in the vicinity of forming autophagosomes ribosomes are apparent, or the presence of ER populated with ribosomes parallel to the phagophore (Dunkle and Cate, 2010; Eskelinen et al., 2011; Yla-Anttila et al., 2009). This suggests the possibility of translationally competent ribosomes in proximity to forming autophagosomes that could furnish a rapid, local supply of key proteins involved in autophagosome biogenesis. Notably, the autophagy-related mRNAs and sites of translation frequently appear to be immediately adjacent to or partially overlapping with markers of forming autophagosomes. This is consistent with their being adjacent to omegaosomes or phagophores and not directly on the ribosome-free membranes forming these.

Others have shown that ribosomes can be degraded by autophagy in both yeast and mammalian cells (An and Harper, 2020; An et al., 2020; Bassham and MacIntosh, 2017; Kraft et al., 2008; Lopez et al., 2023). These studies used extended treatments with mTOR inhibitors or starvation (24-72 h) to observe ribophagy. Even after 24-72 h of mTOR inhibition, a comprehensive analysis demonstrated only a 3-4% reduction in levels of ribosomes due to ribophagy (An et al., 2020). Ribophagy was undetectable prior to 10 h in all studies to our knowledge (An et al., 2020; Wyant et al., 2018). In contrast, our experiments analyzed cells after 2-4 h of mTOR inhibitor treatment when ribophagy is undetectable. Studies on ribophagy, to our knowledge, have not examined whether ribosomes degraded by autophagy are bound to mRNAs. The ribosomes degraded by autophagy are poly-ubiquitinated however, and are hypothesized to be damaged, inappropriately assembled, or non-functional (Frankel et al., 2017). In contrast, our data using fractionation of heavy polysomes, Click-iT and SILAC labeling of nascent translation suggests that mRNAs encoding proteins involved in autophagy are selectively translated in proximity to

forming autophagosomes. Ribophagy has been reported to be a selective process dependent on NUFIP1 (Wyant et al., 2018), although recent data disputes this and suggests ribophagy is a non-selective bystander process (An et al., 2020). Our data demonstrates the selective enrichment of specific mRNAs in proximity to phagophores, and that the translation in proximity to phagophores is independent of NUFIP1. Collectively, our evidence therefore suggests that ribophagy and local translation of mRNAs near forming autophagosomes are two independent processes differentiated by their timing, selectivity for specific mRNAs and actively translating ribosomes. It remains probable that a small proportion of the ribosomes detected in proximity to phagophores could be prone to ribophagy. Our work suggests that ribosomes involved in translating mRNAs in proximity to forming autophagosomes escape engulfment and degradation. Mechanisms which position these ribosomes on proximal membranes or the exterior surface of phagophores could enable these ribosomes to better escape degradation.

Data presented here also demonstrates that localization of autophagy-related mRNAs to forming autophagosomes is dependent on RACK1. Previous reports showed that RACK1 promotes autophagy (Erbil et al., 2016) and serves as a scaffold for VPS34-PI3K complex and Atg14 to regulate phagophore initiation (Zhao et al., 2015). This places RACK1 at the forming autophagosome and suggests it can regulate autophagy. RACK1 can also bind to 40S ribosomes and regulate translation. RACK1 does not appear to be a constitutive member of the 40S ribosome and it regulates translation of selective sets of mRNAs (Kim et al., 2017), including shorter mRNAs and those undergoing m^7g Cap-independent translation (Rollins et al., 2021; Thompson et al., 2016). In neurons, RACK1 has been documented to regulate mRNA localization and local mRNA translation by associating with proteins bound to the mRNAs (Kershner and Welshhans, 2017; Romano et al., 2022). Our data suggests that mRNA

localization to forming autophagosomes and local translation there is dependent on RACK1. Localization of mRNA into proximity of forming autophagosomes was also dependent on binding of ribosomes to mRNA, as it was reduced by puromycin treatment. eIF5A, as an RBP, does not directly bind Atg mRNAs but mediates their recruitment to phagophores for local translation, likely through its binding to ribosomes. mRNA recruitment to forming autophagosomes, or the retention of mRNA there may require RACK1-associated ribosomes. This may be another among increasing examples of mRNA localization which requires ongoing translation (Chouaib et al., 2020) beyond the example of co-translational targeting of mRNAs encoding transmembrane and secreted proteins to the rough ER.

mRNAs required for autophagy continue to be translated when global translation is decreased during stress. Continued translation of mRNA encoding the core autophagy machinery may enable a rapid increase in autophagosome formation during stress. How mRNAs required for autophagy continue to be translated to induce autophagy when global translation is decreased during stress is not entirely clear. Our study revealed that this process required involvement of RACK1 and eIF5A, though role of additional factors helping to promote localization and translation of mRNAs encoding proteins involved in autophagy cannot be ruled out. Several post-transcriptional mechanisms control translation of these mRNAs, for example involving microRNAs, and the RNA-binding protein HuR (Pullmann et al., 2007). eIF5A regulates translation of ATG3 and p62, but this was dependent on a polyproline sequence not found in many of the mRNAs detected in proximity to phagophores (Lubas et al., 2018). A sequence or structure could recruit mRNAs to the phagophore.

One candidate protein that may work with RACK1 to control local translation of mRNAs is EIF3D. When mTOR is inhibited EIF4E-dependent translation is greatly diminished. EIF3D can bind to the 5' cap of mRNA and the 40S ribosomal subunit to initiate translation of a selective set of mRNAs independent of EIF4E (Lee et al., 2015). EIF3D has been identified to allow and induce translation when EIF4E-dependent translation was blocked by mTOR inhibition (Shin et al., 2023). Notably, a recent paper suggested that RACK1 may help control EIF3D-dependent translation (Silvestri et al., 2025). This suggests that RACK1 and EIF3D may help localize and regulate the translation of mRNAs at forming autophagosomes.

The role of RACK1, eIF5A, and continuous translation were proven to be necessary in autophagy-mediated degradation of stress granules and damaged mitochondria. Additionally, RACK1's involvement in mitochondrial respiratory function was found primarily mediated by Torin1-induced autophagic turnover, strongly suggesting a role of RACK1 and eIF5A-mediated local Atg mRNA translation in the clearance of damaged mitochondria and stress granules. However, we cannot yet draw definitive conclusions about the full extent of their roles in these processes.

Co-translational recruitment of mRNAs by nascent proteins could also explain the enrichment of mRNAs encoding proteins involved in autophagy in proximity to phagophores. mRNAs were detected in heavy polysomes in proximity to phagophores, which means as one ribosome initiates translation, others may be midway through the coding sequence or nearing the stop codon. Nascent proteins begin to fold as they emerge from the ribosome, and these could bind mature proteins which localize to phagophores, recruiting polysome-associated mRNAs with

them. Similar processes have been observed now at multiple sites including mitochondria (Arceo et al., 2022) endosomes (Chouaib et al., 2020) and nuclear pores (Lautier et al., 2021).

Cumulatively, our evidence suggests that mRNAs encoding proteins required for autophagy preferentially localize in proximity to forming autophagosomes and are translated there in a ribosome, RACK1-, and eIF5A-dependent manner. Large proportion of mRNAs in cells localize to the sites where their encoded proteins are necessary (Lecuyer et al., 2007). This is hypothesized to conserve cellular energy and provide a rapid local supply of the required proteins. Local translation during autophagosome formation may empower cells in the midst of stress responses to rapidly form autophagosomes in cells while conserving energy. Additionally, local translation of these key Atg mRNAs is essential for maintaining autophagy levels and the degradation of SCs and dysfunctional mitochondria.

In the future, the potential role of EIF3D in localizing and regulating the translation of Atg mRNAs at forming autophagosomes could be explored. The localization of Atg mRNAs and their local translation in proximity to forming autophagosomes could be further validated using Suntag techniques, which can image the local, ongoing translation of Atg mRNAs in proximity to phagophores (Tanenbaum et al., 2014). In addition, the specific sequence or structural features within ATG mRNAs that mediate their localization to phagophores remain to be identified. Furthermore, how eIF5A cooperates with RACK1 in recruiting ATG mRNAs to phagophores could be investigated by examining the colocalization of eIF5A with ATG mRNAs and phagophores, particularly under conditions where RACK1 is mutated at Thr50 or R36D/K38E. The underlying mechanism of how RACK1 and eIF5A recruit Atg mRNAs to phagophores and the potential association with EIF3D should also be further investigated.

APPENDICES

1. Appendix A

Enriched Atg mRNAs in the APEX2-DFCP1, APEX2-NPM1, and APEX2-Perilipin RNA-seq data can be found in Figure.1f sheet of attached source data from paper *Translation in Proximity to Forming Autophagosomes During Sustained Autophagy* by Yunping Xue et al., which was submitted for second-round revision to *Nature Communications*.

https://mts-ncomms.nature.com/ncomms_files/2025/01/08/00422168/02/422168_2_data_set_10152721_spsfhn.xlsx

2. Appendix B

RNA-seq data of RNAs proximity labelled by APEX2-DFCP1

The pathways analysis of RNAs with Log2FC>0.2 and average count of H_2O_2 >600 from APEX2-DFCP1 RNA-seq data can be found in GO analysis of APEX2-DFCP1 sheet of attached source data from paper *Translation in Proximity to Forming Autophagosomes During Sustained Autophagy* by Yunping Xue et al., which was submitted for second-round revision to *Nature Communications*.

https://mts-ncomms.nature.com/ncomms_files/2025/01/08/00422168/02/422168_2_data_set_10152721_spsfhn.xlsx

3. Appendix C

293A C4 FIP200-/-

WT GUIDE 1

Atgttataaatactgagcgtgcacattgccttcaatatatgaagcaaataaaccttacttttgaacactgagttcccaatgtgatgtaaagatgtt

gcattcttgtgtgaaaggactcttgaatacctaccgtcccagcactgtaggtacacactcttcgatctgcagccatgcattctcctccattgacc

accagcacctggtgttgaatagcaatcttgtatttgctttgaatggcatgcttaaggtctgccacacttcaaaaaatgaaataaaataaatcagtt

gtttatatttgcccaatgactttattttccaagtagtactatgtaaaaacaccttagaggttaatgaatttcactctaaaaccttccccaaaaacagt

aataaaaatataagcttcctatttaatgaacaggattccataacaactggctgatcttaggtaaataacagcaaaagaatatgctcaaactggtt

atcaggtctattaaaatcctcaggctacataatttttgttaaaatctcca

Alelle 1: 2bp deletion GUIDE 1

Atgttataaatactgagcgtgcacattgccttcaatatatgaagcaaataaaccttacttttgaacactgagttcccaatgtgatgtaaagatgtt

gcattcttgtgtgaaaggactcttgaatacctaccgtcccagca~~ct~~gtaggtacacactctt**c**gatctgcagccatgcattctcctccattgacc

accagcacctggtgttgaatagcaatcttgtatttgctttgaatggcatgcttaaggtctgccacacttcaaaaaatgaaataaaataaatcagtt

gtttatatttgcccaatgactttattttccaagtagtactatgtaaaaacaccttagaggttaatgaatttcactctaaaaccttccccaaaaacagt

aataaaaatataagcttcctatttaatgaacaggattccataacaactggctgatcttaggtaaataacagcaaaagaatatgctcaaactggtt

atcaggtctattaaaatcctcaggctacataatttttgttaaaatctcca

Alelle 2: 14bp deletion + 1bp insertion=13bp INDEL GUIDE 1

Atgttataaatactgagcgtgcacattgccttcaatatatgaagcaaataaaccttacttttgaacactgagttcccaatgtgatgtaaagatgtt

gcattcttgtgtgaaaggactcttgaatacctaccgtcccagcac**C**~~tgtaggtacacact~~cttcgatctgcagc**c**atgcattctcctccattgac

caccagcacctggtgttgaatagcaatcttgtatttgctttgaatggcatgcttaaggtctgccacacttcaaaaaatgaaataaaataaatcagt

tgtttatatttgcccaatgactttattttccaagtagtactatgtaaaaacaccttagaggttaatgaatttcactctaaaaccttccccaaaaacagt

aataaaaatataagcttcctatttaatgaacaggattccataacaactggctgatcttaggtaaataacagcaaaagaatatgctcaaactggtt

atcaggtctattaaaatcctcaggctacataatttttgttaaaatctcca

4. Appendix D

Raw mass spectrometry data of SILAC labeling can be found in Figure.3i sheet of attached source data from paper *Translation in Proximity to Forming Autophagosomes During Sustained Autophagy* by Yunping Xue et al., which was submitted for second-round revision to *Nature Communications*.

https://mts-ncomms.nature.com/ncomms_files/2025/01/08/00422168/02/422168_2_data_set_10152721_spsfhn.xlsx

5. Appendix E

The whole plasmid sequencing of RACK1^{WT}, RACK1^{Thr50} and RACK1$^{R36D/K38E}$ mutants.

RACK1^{WT}

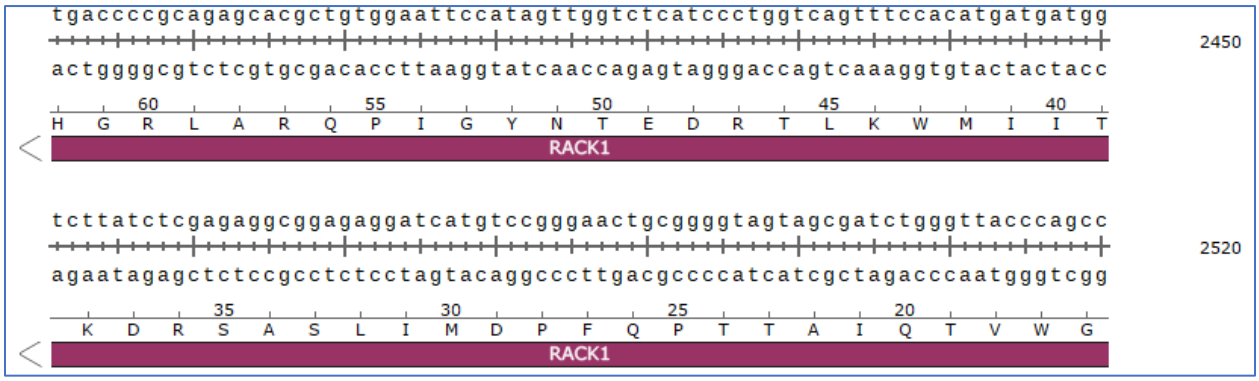

RACK1^{Thr50}

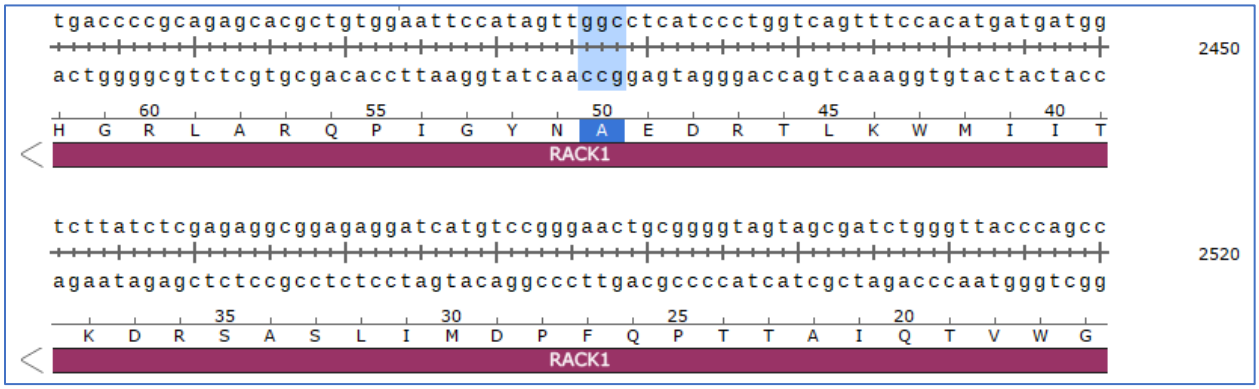

RACK1$^{R36D/K38E}$

6. Appendix F

SPRINGER NATURE LICENSE
TERMS AND CONDITIONS

Mar 03, 2025

This Agreement between Yunping Xue ("You") and Springer Nature ("Springer Nature") consists of your license details and the terms and conditions provided by Springer Nature and Copyright Clearance Center.

License Number	5981640018161
License date	Mar 03, 2025
Licensed Content Publisher	Springer Nature
Licensed Content Publication	Nature Reviews Endocrinology
Licensed Content Title	Autophagy in metabolic disease and ageing
Licensed Content Author	Munehiro Kitada et al
Licensed Content Date	Sep 10, 2021
Type of Use	Thesis/Dissertation
Requestor type	academic/university or research institute
Format	electronic
Portion	figures/tables/illustrations

BIBLIOGRAPHY

Abdullah, M.O., Zeng, R.X., Margerum, C.L., Papadopoli, D., Monnin, C., Punter, K.B., Chu, C., Al-Rofaidi, M., Al-Tannak, N.F., Berardi, D.*, et al.* (2022). Mitochondrial hyperfusion via metabolic sensing of regulatory amino acids. Cell Rep *40*, 111198.

Abu Bakar, Z.H., Bellier, J.P., Wan Ngah, W.Z., Yanagisawa, D., Mukaisho, K.I., and Tooyama, I. (2023). Optimization of 3D Immunofluorescence Analysis and Visualization Using IMARIS and MeshLab. Cells *12*.

Adams, D.R., Ron, D., and Kiely, P.A. (2011). RACK1, A multifaceted scaffolding protein: Structure and function. Cell Commun Signal *9*, 22.

Alers, S., Loffler, A.S., Wesselborg, S., and Stork, B. (2012). Role of AMPK-mTOR-Ulk1/2 in the regulation of autophagy: cross talk, shortcuts, and feedbacks. Mol Cell Biol *32*, 2-11.

An, H., and Harper, J.W. (2018). Systematic analysis of ribophagy in human cells reveals bystander flux during selective autophagy. Nat Cell Biol *20*, 135-143.

An, H., and Harper, J.W. (2020). Ribosome Abundance Control Via the Ubiquitin-Proteasome System and Autophagy. J Mol Biol *432*, 170-184.

An, H., Ordureau, A., Korner, M., Paulo, J.A., and Harper, J.W. (2020). Systematic quantitative analysis of ribosome inventory during nutrient stress. Nature *583*, 303-309.

Angenstein, F., Evans, A.M., Settlage, R.E., Moran, S.T., Ling, S.C., Klintsova, A.Y., Shabanowitz, J., Hunt, D.F., and Greenough, W.T. (2002). A receptor for activated C kinase is part of messenger ribonucleoprotein complexes associated with polyA-mRNAs in neurons. J Neurosci *22*, 8827-8837.

Arceo, X.G., Koslover, E.F., Zid, B.M., and Brown, A.I. (2022). Mitochondrial mRNA localization is governed by translation kinetics and spatial transport. PLoS Comput Biol *18*, e1010413.

Arimoto, K., Fukuda, H., Imajoh-Ohmi, S., Saito, H., and Takekawa, M. (2008). Formation of stress granules inhibits apoptosis by suppressing stress-responsive MAPK pathways. Nat Cell Biol *10*, 1324-1332.

Ast, T., Cohen, G., and Schuldiner, M. (2013). A network of cytosolic factors targets SRP-independent proteins to the endoplasmic reticulum. Cell *152*, 1134-1145.

Aulas, A., Stabile, S., and Vande Velde, C. (2012). Endogenous TDP-43, but not FUS, contributes to stress granule assembly via G3BP. Mol Neurodegener *7*, 54.

Aviner, R. (2020). The science of puromycin: From studies of ribosome function to applications in biotechnology. Comput Struct Biotechnol J *18*, 1074-1083.

Axe, E.L., Walker, S.A., Manifava, M., Chandra, P., Roderick, H.L., Habermann, A., Griffiths, G., and Ktistakis, N.T. (2008). Autophagosome formation from membrane compartments enriched in phosphatidylinositol 3-phosphate and dynamically connected to the endoplasmic reticulum. J Cell Biol *182*, 685-701.

Bai, Y., Zhou, K., and Doudna, J.A. (2013). Hepatitis C virus 3'UTR regulates viral translation through direct interactions with the host translation machinery. Nucleic Acids Res *41*, 7861-7874.

Bassell, G.J., and Warren, S.T. (2008). Fragile X syndrome: loss of local mRNA regulation alters synaptic development and function. Neuron *60*, 201-214.

Bassham, D.C., and MacIntosh, G.C. (2017). Degradation of cytosolic ribosomes by autophagy-related pathways. Plant Sci *262*, 169-174.

Bastide, A., Yewdell, J.W., and David, A. (2018). The RiboPuromycylation Method (RPM): an Immunofluorescence Technique to Map Translation Sites at the Sub-cellular Level. Bio Protoc *8*.

Belozerov, V.E., Ratkovic, S., McNeill, H., Hilliker, A.J., and McDermott, J.C. (2014). In vivo interaction proteomics reveal a novel p38 mitogen-activated protein kinase/Rack1 pathway regulating proteostasis in Drosophila muscle. Mol Cell Biol *34*, 474-484.

Bento, C.F., Renna, M., Ghislat, G., Puri, C., Ashkenazi, A., Vicinanza, M., Menzies, F.M., and Rubinsztein, D.C. (2016). Mammalian Autophagy: How Does It Work? Annu Rev Biochem *85*, 685-713.

Bernales, S., McDonald, K.L., and Walter, P. (2006). Autophagy counterbalances endoplasmic reticulum expansion during the unfolded protein response. PLoS Biol *4*, e423.

Besse, F., and Ephrussi, A. (2008). Translational control of localized mRNAs: restricting protein synthesis in space and time. Nat Rev Mol Cell Biol *9*, 971-980.

Biazik, J., Yla-Anttila, P., Vihinen, H., Jokitalo, E., and Eskelinen, E.L. (2015). Ultrastructural relationship of the phagophore with surrounding organelles. Autophagy *11*, 439-451.

Biswas, J., Nunez, L., Das, S., Yoon, Y.J., Eliscovich, C., and Singer, R.H. (2019). Zipcode Binding Protein 1 (ZBP1; IGF2BP1): A Model for Sequence-Specific RNA Regulation. Cold Spring Harb Symp Quant Biol *84*, 1-10.

Bjorkoy, G., Lamark, T., Brech, A., Outzen, H., Perander, M., Overvatn, A., Stenmark, H., and Johansen, T. (2005). p62/SQSTM1 forms protein aggregates degraded by autophagy and has a protective effect on huntingtin-induced cell death. J Cell Biol *171*, 603-614.

Buchan, J.R., and Parker, R. (2009). Eukaryotic stress granules: the ins and outs of translation. Mol Cell *36*, 932-941.

Buskila, A.A., Kannaiah, S., and Amster-Choder, O. (2014). RNA localization in bacteria. RNA Biol *11*, 1051-1060.

Buxbaum, A.R., Haimovich, G., and Singer, R.H. (2015). In the right place at the right time: visualizing and understanding mRNA localization. Nat Rev Mol Cell Biol *16*, 95-109.

Calvo, S.E., Pagliarini, D.J., and Mootha, V.K. (2009). Upstream open reading frames cause widespread reduction of protein expression and are polymorphic among humans. Proc Natl Acad Sci U S A *106*, 7507-7512.

Castellana, M., Hsin-Jung Li, S., and Wingreen, N.S. (2016). Spatial organization of bacterial transcription and translation. Proc Natl Acad Sci U S A *113*, 9286-9291.

Ceci, M., Welshhans, K., Ciotti, M.T., Brandi, R., Parisi, C., Paoletti, F., Pistillo, L., Bassell, G.J., and Cattaneo, A. (2012). RACK1 is a ribosome scaffold protein for beta-actin mRNA/ZBP1 complex. PLoS One *7*, e35034.

Chang, C., Jensen, L.E., and Hurley, J.H. (2021). Autophagosome biogenesis comes out of the black box. Nat Cell Biol *23*, 450-456.

Chappell, S.A., LeQuesne, J.P., Paulin, F.E., deSchoolmeester, M.L., Stoneley, M., Soutar, R.L., Ralston, S.H., Helfrich, M.H., and Willis, A.E. (2000). A mutation in the c-myc-IRES leads to enhanced internal ribosome entry in multiple myeloma: a novel mechanism of oncogene de-regulation. Oncogene *19*, 4437-4440.

Chasse, H., Boulben, S., Costache, V., Cormier, P., and Morales, J. (2017). Analysis of translation using polysome profiling. Nucleic Acids Res *45*, e15.

Chaudhry, A., Shi, R., and Luciani, D.S. (2020). A pipeline for multidimensional confocal analysis of mitochondrial morphology, function, and dynamics in pancreatic beta-cells. Am J Physiol Endocrinol Metab *318*, E87-E101.

Chen, E., Sharma, M.R., Shi, X., Agrawal, R.K., and Joseph, S. (2014). Fragile X mental retardation protein regulates translation by binding directly to the ribosome. Mol Cell *54*, 407-417.

Chen, Y.J., Knupp, J., Wang, E., Arvan, P., and Tsai, B. (2024). SIGMAR1/Sigma-1 receptor: a key regulator in stabilizing and translating LC3B mRNA for autophagosome formation. Autophagy *20*, 2843-2845.

Chitiprolu, M., Jagow, C., Tremblay, V., Bondy-Chorney, E., Paris, G., Savard, A., Palidwor, G., Barry, F.A., Zinman, L., Keith, J.*, et al.* (2018). A complex of C9ORF72 and p62 uses arginine methylation to eliminate stress granules by autophagy. Nat Commun *9*, 2794.

Chouaib, R., Safieddine, A., Pichon, X., Imbert, A., Kwon, O.S., Samacoits, A., Traboulsi, A.M., Robert, M.C., Tsanov, N., Coleno, E.*, et al.* (2020). A Dual Protein-mRNA Localization Screen Reveals Compartmentalized Translation and Widespread Co-translational RNA Targeting. Dev Cell *54*, 773-791 e775.

Christ, M.G., Huesmann, H., Nagel, H., Kern, A., and Behl, C. (2019). Sigma-1 Receptor Activation Induces Autophagy and Increases Proteostasis Capacity In Vitro and In Vivo. Cells *8*.

Cioni, J.M., Lin, J.Q., Holtermann, A.V., Koppers, M., Jakobs, M.A.H., Azizi, A., Turner-Bridger, B., Shigeoka, T., Franze, K., Harris, W.A.*, et al.* (2019). Late Endosomes Act as mRNA Translation Platforms and Sustain Mitochondria in Axons. Cell *176*, 56-72 e15.

Clohessy, J.G., Reschke, M., and Pandolfi, P.P. (2012). Found in translation of mTOR signaling. Cell Res *22*, 1315-1318.

Cookson, M.R. (2012). Parkinsonism due to mutations in PINK1, parkin, and DJ-1 and oxidative stress and mitochondrial pathways. Cold Spring Harb Perspect Med *2*, a009415.

Coronado, M., Fajardo, G., Nguyen, K., Zhao, M., Kooiker, K., Jung, G., Hu, D.Q., Reddy, S., Sandoval, E., Stotland, A.*, et al.* (2018). Physiological Mitochondrial Fragmentation Is a Normal Cardiac Adaptation to Increased Energy Demand. Circ Res *122*, 282-295.

Coyle, S.M., Gilbert, W.V., and Doudna, J.A. (2009). Direct link between RACK1 function and localization at the ribosome in vivo. Mol Cell Biol *29*, 1626-1634.

Das, R., and Chakrabarti, O. (2020). Mitochondrial hyperfusion: a friend or a foe. Biochem Soc Trans *48*, 631-644.

Deffieu, M., Bhatia-Kissova, I., Salin, B., Galinier, A., Manon, S., and Camougrand, N. (2009). Glutathione participates in the regulation of mitophagy in yeast. J Biol Chem *284*, 14828-14837.

Dermit, M., Dodel, M., Lee, F.C.Y., Azman, M.S., Schwenzer, H., Jones, J.L., Blagden, S.P., Ule, J., and Mardakheh, F.K. (2020). Subcellular mRNA Localization Regulates Ribosome Biogenesis in Migrating Cells. Dev Cell *55*, 298-313 e210.

Dever, T.E., Gutierrez, E., and Shin, B.S. (2014). The hypusine-containing translation factor eIF5A. Crit Rev Biochem Mol Biol *49*, 413-425.

Dikic, I., and Elazar, Z. (2018). Mechanism and medical implications of mammalian autophagy. Nat Rev Mol Cell Biol *19*, 349-364.

Dobin, A., Davis, C.A., Schlesinger, F., Drenkow, J., Zaleski, C., Jha, S., Batut, P., Chaisson, M., and Gingeras, T.R. (2013). STAR: ultrafast universal RNA-seq aligner. Bioinformatics *29*, 15-21.

Dobrikov, M.I., Dobrikova, E.Y., and Gromeier, M. (2018). Ribosomal RACK1:Protein Kinase C betaII Phosphorylates Eukaryotic Initiation Factor 4G1 at S1093 To Modulate Cap-Dependent and -Independent Translation Initiation. Mol Cell Biol *38*.

Dreser, A., Vollrath, J.T., Sechi, A., Johann, S., Roos, A., Yamoah, A., Katona, I., Bohlega, S., Wiemuth, D., Tian, Y.*, et al.* (2017). The ALS-linked E102Q mutation in Sigma receptor-1 leads

to ER stress-mediated defects in protein homeostasis and dysregulation of RNA-binding proteins. Cell Death Differ *24*, 1655-1671.

Driever, W., and Nusslein-Volhard, C. (1988). The bicoid protein determines position in the Drosophila embryo in a concentration-dependent manner. Cell *54*, 95-104.

Dunkle, J.A., and Cate, J.H. (2010). Ribosome structure and dynamics during translocation and termination. Annu Rev Biophys *39*, 227-244.

Durgan, J., and Florey, O. (2022). Many roads lead to CASM: Diverse stimuli of noncanonical autophagy share a unifying molecular mechanism. Sci Adv *8*, eabo1274.

Eiyama, A., and Okamoto, K. (2015). PINK1/Parkin-mediated mitophagy in mammalian cells. Curr Opin Cell Biol *33*, 95-101.

Ephrussi, A., Dickinson, L.K., and Lehmann, R. (1991). Oskar organizes the germ plasm and directs localization of the posterior determinant nanos. Cell *66*, 37-50.

Erbil, S., Oral, O., Mitou, G., Kig, C., Durmaz-Timucin, E., Guven-Maiorov, E., Gulacti, F., Gokce, G., Dengjel, J., Sezerman, O.U.*, et al.* (2016). RACK1 Is an Interaction Partner of ATG5 and a Novel Regulator of Autophagy. J Biol Chem *291*, 16753-16765.

Erdi, B., Nagy, P., Zvara, A., Varga, A., Pircs, K., Menesi, D., Puskas, L.G., and Juhasz, G. (2012). Loss of the starvation-induced gene Rack1 leads to glycogen deficiency and impaired autophagic responses in Drosophila. Autophagy *8*, 1124-1135.

Eskelinen, E.L., Reggiori, F., Baba, M., Kovacs, A.L., and Seglen, P.O. (2011). Seeing is believing: the impact of electron microscopy on autophagy research. Autophagy *7*, 935-956.

Ewels, P.A., Peltzer, A., Fillinger, S., Patel, H., Alneberg, J., Wilm, A., Garcia, M.U., Di Tommaso, P., and Nahnsen, S. (2020). The nf-core framework for community-curated bioinformatics pipelines. Nat Biotechnol *38*, 276-278.

Fazal, F.M., Han, S., Parker, K.R., Kaewsapsak, P., Xu, J., Boettiger, A.N., Chang, H.Y., and Ting, A.Y. (2019). Atlas of Subcellular RNA Localization Revealed by APEX-Seq. Cell *178*, 473-490 e426.

Fonseca, B., Graber, T., Hoang, H., González, A., Soukas, A., Hernández, G., Alain, T., Weisman, R., Meyer, C., and Robaglia, C. (2016). TOR and translation control in evolution. Evolution of the protein synthesis machinery and its regulation, 327-412.

Frankel, L.B., Lubas, M., and Lund, A.H. (2017). Emerging connections between RNA and autophagy. Autophagy *13*, 3-23.

Fresno, M., Jimenez, A., and Vazquez, D. (1977). Inhibition of translation in eukaryotic systems by harringtonine. Eur J Biochem *72*, 323-330.

Gallo, S., Ricciardi, S., Manfrini, N., Pesce, E., Oliveto, S., Calamita, P., Mancino, M., Maffioli, E., Moro, M., Crosti, M.*, et al.* (2018). RACK1 Specifically Regulates Translation through Its Binding to Ribosomes. Mol Cell Biol *38*.

Gao, G., Sheng, Y., Yang, H., Chua, B.T., and Xu, L. (2019). DFCP1 associates with lipid droplets. Cell Biol Int *43*, 1492-1504.

Gao, S., and Hu, J. (2021). Mitochondrial Fusion: The Machineries In and Out. Trends Cell Biol *31*, 62-74.

Gardner, J.O., Leidal, A.M., Nguyen, T.A., and Debnath, J. (2023). LC3-dependent EV loading and secretion (LDELS) promotes TFRC (transferrin receptor) secretion via extracellular vesicles. Autophagy *19*, 1551-1561.

Gaubitz, C., Prouteau, M., Kusmider, B., and Loewith, R. (2016). TORC2 Structure and Function. Trends Biochem Sci *41*, 532-545.

Gavis, E.R., and Lehmann, R. (1992). Localization of nanos RNA controls embryonic polarity. Cell *71*, 301-313.

Gu, X., Ma, Y., Liu, Y., and Wan, Q. (2021). Measurement of mitochondrial respiration in adherent cells by Seahorse XF96 Cell Mito Stress Test. STAR Protoc *2*, 100245.

Guo, F., Liu, X., Cai, H., and Le, W. (2018). Autophagy in neurodegenerative diseases: pathogenesis and therapy. Brain Pathol *28*, 3-13.

Guo, H., Chitiprolu, M., Roncevic, L., Javalet, C., Hemming, F.J., Trung, M.T., Meng, L., Latreille, E., Tanese de Souza, C., McCulloch, D.*, et al.* (2017). Atg5 Disassociates the V(1)V(0)-ATPase to Promote Exosome Production and Tumor Metastasis Independent of Canonical Macroautophagy. Dev Cell *43*, 716-730 e717.

Gwinn, D.M., Shackelford, D.B., Egan, D.F., Mihaylova, M.M., Mery, A., Vasquez, D.S., Turk, B.E., and Shaw, R.J. (2008). AMPK phosphorylation of raptor mediates a metabolic checkpoint. Mol Cell *30*, 214-226.

Halstead, J.M., Lionnet, T., Wilbertz, J.H., Wippich, F., Ephrussi, A., Singer, R.H., and Chao, J.A. (2015). Translation. An RNA biosensor for imaging the first round of translation from single cells to living animals. Science *347*, 1367-1671.

Hampel, H., Hardy, J., Blennow, K., Chen, C., Perry, G., Kim, S.H., Villemagne, V.L., Aisen, P., Vendruscolo, M., Iwatsubo, T.*, et al.* (2021). The Amyloid-beta Pathway in Alzheimer's Disease. Mol Psychiatry *26*, 5481-5503.

Hara, T., and Mizushima, N. (2009). Role of ULK-FIP200 complex in mammalian autophagy: FIP200, a counterpart of yeast Atg17? Autophagy *5*, 85-87.

Hemel, I., Engelen, B.P.H., Luber, N., and Gerards, M. (2021). A hitchhiker's guide to mitochondrial quantification. Mitochondrion *59*, 216-224.

Hofer, S.J., Liang, Y., Zimmermann, A., Schroeder, S., Dengjel, J., Kroemer, G., Eisenberg, T., Sigrist, S.J., and Madeo, F. (2021). Spermidine-induced hypusination preserves mitochondrial and cognitive function during aging. Autophagy *17*, 2037-2039.

Hung, V., Zou, P., Rhee, H.W., Udeshi, N.D., Cracan, V., Svinkina, T., Carr, S.A., Mootha, V.K., and Ting, A.Y. (2014). Proteomic mapping of the human mitochondrial intermembrane space in live cells via ratiometric APEX tagging. Mol Cell *55*, 332-341.

Hurley, J.H., and Young, L.N. (2017). Mechanisms of Autophagy Initiation. Annu Rev Biochem *86*, 225-244.

Huttelmaier, S., Zenklusen, D., Lederer, M., Dictenberg, J., Lorenz, M., Meng, X., Bassell, G.J., Condeelis, J., and Singer, R.H. (2005). Spatial regulation of beta-actin translation by Src-dependent phosphorylation of ZBP1. Nature *438*, 512-515.

Hwang, J., and Espenshade, P.J. (2016). Proximity-dependent biotin labelling in yeast using the engineered ascorbate peroxidase APEX2. Biochem J *473*, 2463-2469.

Ingolia, N.T., Ghaemmaghami, S., Newman, J.R., and Weissman, J.S. (2009). Genome-wide analysis in vivo of translation with nucleotide resolution using ribosome profiling. Science *324*, 218-223.

Ingolia, N.T., Lareau, L.F., and Weissman, J.S. (2011). Ribosome profiling of mouse embryonic stem cells reveals the complexity and dynamics of mammalian proteomes. Cell *147*, 789-802.

Ismail, V.A., Naismith, T., and Kast, D.J. (2023). The NTPase activity of the double FYVE domain-containing protein 1 regulates lipid droplet metabolism. J Biol Chem *299*, 102830.

Itakura, E., and Mizushima, N. (2011). p62 Targeting to the autophagosome formation site requires self-oligomerization but not LC3 binding. J Cell Biol *192*, 17-27.

Jagannathan, S., Reid, D.W., Cox, A.H., and Nicchitta, C.V. (2014). De novo translation initiation on membrane-bound ribosomes as a mechanism for localization of cytosolic protein mRNAs to the endoplasmic reticulum. RNA *20*, 1489-1498.

Jain, V., Singh, M.P., and Amaravadi, R.K. (2023). Recent advances in targeting autophagy in cancer. Trends Pharmacol Sci *44*, 290-302.

Jan, C.H., Williams, C.C., and Weissman, J.S. (2015). LOCAL TRANSLATION. Response to Comment on "Principles of ER cotranslational translocation revealed by proximity-specific ribosome profiling". Science *348*, 1217.

Jansen, R.P. (2001). mRNA localization: message on the move. Nat Rev Mol Cell Biol *2*, 247-256.

Jeffery, W.R., Tomlinson, C.R., and Brodeur, R.D. (1983). Localization of actin messenger RNA during early ascidian development. Dev Biol *99*, 408-417.

Jin, S.M., and Youle, R.J. (2012). PINK1- and Parkin-mediated mitophagy at a glance. J Cell Sci *125*, 795-799.

Johansen, T., and Lamark, T. (2011). Selective autophagy mediated by autophagic adapter proteins. Autophagy *7*, 279-296.

Johnson, A.G., Lapointe, C.P., Wang, J., Corsepius, N.C., Choi, J., Fuchs, G., and Puglisi, J.D. (2019). RACK1 on and off the ribosome. RNA *25*, 881-895.

Jomain-Baum, M., Garber, A.J., Farber, E., and Hanson, R.W. (1973). The effect of cycloheximide on the interaction between mitochondrial respiration and gluconeogenesis in guinea pig and rat liver. J Biol Chem *248*, 1536-1543.

Jung, M.Y., Lorenz, L., and Richter, J.D. (2006). Translational control by neuroguidin, a eukaryotic initiation factor 4E and CPEB binding protein. Mol Cell Biol *26*, 4277-4287.

Kabeya, Y., Mizushima, N., Ueno, T., Yamamoto, A., Kirisako, T., Noda, T., Kominami, E., Ohsumi, Y., and Yoshimori, T. (2000). LC3, a mammalian homologue of yeast Apg8p, is localized in autophagosome membranes after processing. EMBO J *19*, 5720-5728.

Kaewsapsak, P., Shechner, D.M., Mallard, W., Rinn, J.L., and Ting, A.Y. (2017). Live-cell mapping of organelle-associated RNAs via proximity biotinylation combined with protein-RNA crosslinking. Elife *6*.

Karanasios, E., Walker, S.A., Okkenhaug, H., Manifava, M., Hummel, E., Zimmermann, H., Ahmed, Q., Domart, M.C., Collinson, L., and Ktistakis, N.T. (2016). Autophagy initiation by ULK complex assembly on ER tubulovesicular regions marked by ATG9 vesicles. Nat Commun *7*, 12420.

Kedersha, N., Chen, S., Gilks, N., Li, W., Miller, I.J., Stahl, J., and Anderson, P. (2002). Evidence that ternary complex (eIF2-GTP-tRNA(i)(Met))-deficient preinitiation complexes are core constituents of mammalian stress granules. Mol Biol Cell *13*, 195-210.

Kershner, L., and Welshhans, K. (2017). RACK1 is necessary for the formation of point contacts and regulates axon growth. Dev Neurobiol *77*, 1038-1056.

Kim, H.D., Kong, E., Kim, Y., Chang, J.S., and Kim, J. (2017). RACK1 depletion in the ribosome induces selective translation for non-canonical autophagy. Cell Death Dis *8*, e2800.

Kim, J., Kundu, M., Viollet, B., and Guan, K.L. (2011). AMPK and mTOR regulate autophagy through direct phosphorylation of Ulk1. Nat Cell Biol *13*, 132-141.

Kim, J., Yang, G., Kim, Y., Kim, J., and Ha, J. (2016). AMPK activators: mechanisms of action and physiological activities. Exp Mol Med *48*, e224.

Kim, Y.C., and Guan, K.L. (2015). mTOR: a pharmacologic target for autophagy regulation. J Clin Invest *125*, 25-32.

Kishi-Itakura, C., Koyama-Honda, I., Itakura, E., and Mizushima, N. (2014). Ultrastructural analysis of autophagosome organization using mammalian autophagy-deficient cells. J Cell Sci *127*, 4089-4102.

Kitada, M., and Koya, D. (2021). Autophagy in metabolic disease and ageing. Nat Rev Endocrinol *17*, 647-661.

Klann, K., Tascher, G., and Munch, C. (2020). Functional Translatome Proteomics Reveal Converging and Dose-Dependent Regulation by mTORC1 and eIF2alpha. Mol Cell *77*, 913-925 e914.

Klionsky, D.J. (2007). Autophagy: from phenomenology to molecular understanding in less than a decade. Nat Rev Mol Cell Biol *8*, 931-937.

Klionsky, D.J., Abdel-Aziz, A.K., Abdelfatah, S., Abdellatif, M., Abdoli, A., Abel, S., Abeliovich, H., Abildgaard, M.H., Abudu, Y.P., Acevedo-Arozena, A.*, et al.* (2021). Guidelines for the use and interpretation of assays for monitoring autophagy (4th edition)(1). Autophagy *17*, 1-382.

Klionsky, D.J., Baehrecke, E.H., Brumell, J.H., Chu, C.T., Codogno, P., Cuervo, A.M., Debnath, J., Deretic, V., Elazar, Z., Eskelinen, E.L.*, et al.* (2011). A comprehensive glossary of autophagy-related molecules and processes (2nd edition). Autophagy *7*, 1273-1294.

Knupp, J., Chen, Y.J., Wang, E., Arvan, P., and Tsai, B. (2024). Sigma-1 receptor recruits LC3 mRNA to ER-associated omegasomes to promote localized LC3 translation enabling functional autophagy. Cell Rep *43*, 114619.

Koppers, M., Cagnetta, R., Shigeoka, T., Wunderlich, L.C., Vallejo-Ramirez, P., Qiaojin Lin, J., Zhao, S., Jakobs, M.A., Dwivedy, A., Minett, M.S.*, et al.* (2019). Receptor-specific interactome as a hub for rapid cue-induced selective translation in axons. Elife *8*.

Kraft, C., Deplazes, A., Sohrmann, M., and Peter, M. (2008). Mature ribosomes are selectively degraded upon starvation by an autophagy pathway requiring the Ubp3p/Bre5p ubiquitin protease. Nat Cell Biol *10*, 602-610.

Kuballa, P., Huett, A., Rioux, J.D., Daly, M.J., and Xavier, R.J. (2008). Impaired autophagy of an intracellular pathogen induced by a Crohn's disease associated ATG16L1 variant. PLoS One *3*, e3391.

Kumar, S., Javed, R., Mudd, M., Pallikkuth, S., Lidke, K.A., Jain, A., Tangavelou, K., Gudmundsson, S.R., Ye, C., Rusten, T.E.*, et al.* (2021). Mammalian hybrid pre-autophagosomal structure HyPAS generates autophagosomes. Cell *184*, 5950-5969 e5922.

Lacerda, R., Menezes, J., and Romao, L. (2017). More than just scanning: the importance of cap-independent mRNA translation initiation for cellular stress response and cancer. Cell Mol Life Sci *74*, 1659-1680.

Lai, C.H., Ko, K.T., Fan, P.J., Yu, T.A., Chang, C.F., Draczkowski, P., and Hsu, S.D. (2024). Structural insight into the ZFAND1-p97 interaction involved in stress granule clearance. J Biol Chem *300*, 107230.

Lam, S.S., Martell, J.D., Kamer, K.J., Deerinck, T.J., Ellisman, M.H., Mootha, V.K., and Ting, A.Y. (2015). Directed evolution of APEX2 for electron microscopy and proximity labeling. Nat Methods *12*, 51-54.

Lamb, C.A., Yoshimori, T., and Tooze, S.A. (2013). The autophagosome: origins unknown, biogenesis complex. Nat Rev Mol Cell Biol *14*, 759-774.

Lamper, A.M., Fleming, R.H., Ladd, K.M., and Lee, A.S.Y. (2020). A phosphorylation-regulated eIF3d translation switch mediates cellular adaptation to metabolic stress. Science *370*, 853-856.

Latallo, M.J., Wang, S., Dong, D., Nelson, B., Livingston, N.M., Wu, R., Zhao, N., Stasevich, T.J., Bassik, M.C., Sun, S.*, et al.* (2023). Single-molecule imaging reveals distinct elongation and frameshifting dynamics between frames of expanded RNA repeats in C9ORF72-ALS/FTD. Nat Commun *14*, 5581.

Lautier, O., Penzo, A., Rouviere, J.O., Chevreux, G., Collet, L., Loiodice, I., Taddei, A., Devaux, F., Collart, M.A., and Palancade, B. (2021). Co-translational assembly and localized translation of nucleoporins in nuclear pore complex biogenesis. Mol Cell *81*, 2417-2427 e2415.

Lecuyer, E., Yoshida, H., Parthasarathy, N., Alm, C., Babak, T., Cerovina, T., Hughes, T.R., Tomancak, P., and Krause, H.M. (2007). Global analysis of mRNA localization reveals a prominent role in organizing cellular architecture and function. Cell *131*, 174-187.

Lee, A.S., Kranzusch, P.J., and Cate, J.H. (2015). eIF3 targets cell-proliferation messenger RNAs for translational activation or repression. Nature *522*, 111-114.

Lee, J.S., Tabata, K., Twu, W.I., Rahman, M.S., Kim, H.S., Yu, J.B., Jee, M.H., Bartenschlager, R., and Jang, S.K. (2019). RACK1 mediates rewiring of intracellular networks induced by hepatitis C virus infection. PLoS Pathog *15*, e1008021.

Lee, P.T., Lievens, J.C., Wang, S.M., Chuang, J.Y., Khalil, B., Wu, H.E., Chang, W.C., Maurice, T., and Su, T.P. (2020). Sigma-1 receptor chaperones rescue nucleocytoplasmic transport deficit seen in cellular and Drosophila ALS/FTD models. Nat Commun *11*, 5580.

Leighton, J., and Schatz, G. (1995). An ABC transporter in the mitochondrial inner membrane is required for normal growth of yeast. EMBO J *14*, 188-195.

Lerner, R.S., and Nicchitta, C.V. (2006). mRNA translation is compartmentalized to the endoplasmic reticulum following physiological inhibition of cap-dependent translation. RNA *12*, 775-789.

Li, C.H., Ohn, T., Ivanov, P., Tisdale, S., and Anderson, P. (2010). eIF5A promotes translation elongation, polysome disassembly and stress granule assembly. PLoS One *5*, e9942.

Li, D., and Roberts, R. (2001). WD-repeat proteins: structure characteristics, biological function, and their involvement in human diseases. Cell Mol Life Sci *58*, 2085-2097.

Li, J., Yang, D., Li, Z., Zhao, M., Wang, D., Sun, Z., Wen, P., Dai, Y., Gou, F., Ji, Y.*, et al.* (2023). PINK1/Parkin-mediated mitophagy in neurodegenerative diseases. Ageing Res Rev *84*, 101817.

Li, Y.R., King, O.D., Shorter, J., and Gitler, A.D. (2013). Stress granules as crucibles of ALS pathogenesis. J Cell Biol *201*, 361-372.

Lin, A.C., and Holt, C.E. (2007). Local translation and directional steering in axons. EMBO J *26*, 3729-3736.

Long, L., Deng, Y., Yao, F., Guan, D., Feng, Y., Jiang, H., Li, X., Hu, P., Lu, X., Wang, H.*, et al.* (2014). Recruitment of phosphatase PP2A by RACK1 adaptor protein deactivates transcription factor IRF3 and limits type I interferon signaling. Immunity *40*, 515-529.

Lopez, A.R., Jorgensen, M.H., Havelund, J.F., Arendrup, F.S., Kolapalli, S.P., Nielsen, T.M., Pais, E., Beese, C.J., Abdul-Al, A., Vind, A.C.*, et al.* (2023). Autophagy-mediated control of ribosome homeostasis in oncogene-induced senescence. Cell Rep *42*, 113381.

Lubas, M., Harder, L.M., Kumsta, C., Tiessen, I., Hansen, M., Andersen, J.S., Lund, A.H., and Frankel, L.B. (2018). eIF5A is required for autophagy by mediating ATG3 translation. EMBO Rep *19*.

Ma, S., Liu, J.Y., and Zhang, J.T. (2023). eIF3d: A driver of noncanonical cap-dependent translation of specific mRNAs and a trigger of biological/pathological processes. J Biol Chem *299*, 104658.

Ma, X.M., and Blenis, J. (2009). Molecular mechanisms of mTOR-mediated translational control. Nat Rev Mol Cell Biol *10*, 307-318.

Majzoub, K., Hafirassou, M.L., Meignin, C., Goto, A., Marzi, S., Fedorova, A., Verdier, Y., Vinh, J., Hoffmann, J.A., Martin, F.*, et al.* (2014). RACK1 controls IRES-mediated translation of viruses. Cell *159*, 1086-1095.

Mandal, A., Mandal, S., and Park, M.H. (2016). Global quantitative proteomics reveal up-regulation of endoplasmic reticulum stress response proteins upon depletion of eIF5A in HeLa cells. Sci Rep *6*, 25795.

Marcelo, A., Koppenol, R., de Almeida, L.P., Matos, C.A., and Nobrega, C. (2021). Stress granules, RNA-binding proteins and polyglutamine diseases: too much aggregation? Cell Death Dis *12*, 592.

Masi, M., Attanzio, A., Racchi, M., Wolozin, B., Borella, S., Biundo, F., and Buoso, E. (2022). Proteostasis Deregulation in Neurodegeneration and Its Link with Stress Granules: Focus on the Scaffold and Ribosomal Protein RACK1. Cells *11*.

Mateju, D., Franzmann, T.M., Patel, A., Kopach, A., Boczek, E.E., Maharana, S., Lee, H.O., Carra, S., Hyman, A.A., and Alberti, S. (2017). An aberrant phase transition of stress granules triggered by misfolded protein and prevented by chaperone function. EMBO J *36*, 1669-1687.

Mauvezin, C., Nagy, P., Juhasz, G., and Neufeld, T.P. (2015). Autophagosome-lysosome fusion is independent of V-ATPase-mediated acidification. Nat Commun *6*, 7007.

Mauvezin, C., and Neufeld, T.P. (2015). Bafilomycin A1 disrupts autophagic flux by inhibiting both V-ATPase-dependent acidification and Ca-P60A/SERCA-dependent autophagosome-lysosome fusion. Autophagy *11*, 1437-1438.

Melia, T.J., Lystad, A.H., and Simonsen, A. (2020). Autophagosome biogenesis: From membrane growth to closure. J Cell Biol *219*.

Menikdiwela, K.R., Ramalingam, L., Rasha, F., Wang, S., Dufour, J.M., Kalupahana, N.S., Sunahara, K.K.S., Martins, J.O., and Moustaid-Moussa, N. (2020). Autophagy in metabolic syndrome: breaking the wheel by targeting the renin-angiotensin system. Cell Death Dis *11*, 87.

Mihaylova, M.M., and Shaw, R.J. (2011). The AMPK signalling pathway coordinates cell growth, autophagy and metabolism. Nat Cell Biol *13*, 1016-1023.

Miller, B.R., Wei, T., Fields, C.J., Sheng, P., and Xie, M. (2018). Near-infrared fluorescent northern blot. RNA *24*, 1871-1877.

Mizushima, N., and Yoshimori, T. (2007). How to interpret LC3 immunoblotting. Autophagy *3*, 542-545.

Mizushima, N., Yoshimori, T., and Levine, B. (2010). Methods in mammalian autophagy research. Cell *140*, 313-326.

Moor, A.E., Golan, M., Massasa, E.E., Lemze, D., Weizman, T., Shenhav, R., Baydatch, S., Mizrahi, O., Winkler, R., Golani, O.*, et al.* (2017). Global mRNA polarization regulates translation efficiency in the intestinal epithelium. Science *357*, 1299-1303.

Moulton, V.R., Suarez-Fueyo, A., Meidan, E., Li, H., Mizui, M., and Tsokos, G.C. (2017). Pathogenesis of Human Systemic Lupus Erythematosus: A Cellular Perspective. Trends Mol Med *23*, 615-635.

Nanao, T., Koike, M., Yamaguchi, J., Sasaki, M., and Uchiyama, Y. (2015). Cellular localization and tissue distribution of endogenous DFCP1 protein. Biomed Res *36*, 121-133.

Neer, E.J., Schmidt, C.J., Nambudripad, R., and Smith, T.F. (1994). The ancient regulatory-protein family of WD-repeat proteins. Nature *371*, 297-300.

Niessing, D., Jansen, R.P., Pohlmann, T., and Feldbrugge, M. (2018). mRNA transport in fungal top models. Wiley Interdiscip Rev RNA *9*.

Nilsson, J., Sengupta, J., Frank, J., and Nissen, P. (2004). Regulation of eukaryotic translation by the RACK1 protein: a platform for signalling molecules on the ribosome. EMBO Rep *5*, 1137-1141.

Noda, T., Fujita, N., and Yoshimori, T. (2009). The late stages of autophagy: how does the end begin? Cell Death Differ *16*, 984-990.

Obrig, T.G., Culp, W.J., McKeehan, W.L., and Hardesty, B. (1971). The mechanism by which cycloheximide and related glutarimide antibiotics inhibit peptide synthesis on reticulocyte ribosomes. J Biol Chem *246*, 174-181.

Ohsumi, Y. (2001). Molecular dissection of autophagy: two ubiquitin-like systems. Nat Rev Mol Cell Biol *2*, 211-216.

Oksvold, M., Huitfeldt, H., Stang, E., and Madshus, I. (2002). Localizing the EGF receptor. Nat Cell Biol *4*, E22; author reply E22-23.

Oku, M., and Sakai, Y. (2018). Three Distinct Types of Microautophagy Based on Membrane Dynamics and Molecular Machineries. Bioessays *40*, e1800008.

Osawa, T., Kotani, T., Kawaoka, T., Hirata, E., Suzuki, K., Nakatogawa, H., Ohsumi, Y., and Noda, N.N. (2019). Atg2 mediates direct lipid transfer between membranes for autophagosome formation. Nat Struct Mol Biol *26*, 281-288.

Oudart, M., Avila-Gutierrez, K., Moch, C., Dossi, E., Milior, G., Boulay, A.C., Gaudey, M., Moulard, J., Lombard, B., Loew, D*., et al.* (2023). The ribosome-associated protein RACK1 represses Kir4.1 translation in astrocytes and influences neuronal activity. Cell Rep *42*, 112456.

Pan, P., and van Breukelen, F. (2011). Preference of IRES-mediated initiation of translation during hibernation in golden-mantled ground squirrels, Spermophilus lateralis. Am J Physiol Regul Integr Comp Physiol *301*, R370-377.

Pankiv, S., Clausen, T.H., Lamark, T., Brech, A., Bruun, J.A., Outzen, H., Overvatn, A., Bjorkoy, G., and Johansen, T. (2007). p62/SQSTM1 binds directly to Atg8/LC3 to facilitate degradation of ubiquitinated protein aggregates by autophagy. J Biol Chem *282*, 24131-24145.

Patro, R., Duggal, G., Love, M.I., Irizarry, R.A., and Kingsford, C. (2017). Salmon provides fast and bias-aware quantification of transcript expression. Nat Methods *14*, 417-419.

Pelletier, A.R., Chung, Y.E., Ning, Z., Wong, N., Figeys, D., and Lavallee-Adam, M. (2020). MealTime-MS: A Machine Learning-Guided Real-Time Mass Spectrometry Analysis for Protein Identification and Efficient Dynamic Exclusion. J Am Soc Mass Spectrom *31*, 1459-1472.

Poehlsgaard, J., and Douthwaite, S. (2005). The bacterial ribosome as a target for antibiotics. Nat Rev Microbiol *3*, 870-881.

Proud, C.G. (2019). Phosphorylation and Signal Transduction Pathways in Translational Control. Cold Spring Harb Perspect Biol *11*.

Pullmann, R., Jr., Kim, H.H., Abdelmohsen, K., Lal, A., Martindale, J.L., Yang, X., and Gorospe, M. (2007). Analysis of turnover and translation regulatory RNA-binding protein expression through binding to cognate mRNAs. Mol Cell Biol *27*, 6265-6278.

Pyhtila, B., Zheng, T., Lager, P.J., Keene, J.D., Reedy, M.C., and Nicchitta, C.V. (2008). Signal sequence- and translation-independent mRNA localization to the endoplasmic reticulum. RNA *14*, 445-453.

Rambold, A.S., Kostelecky, B., Elia, N., and Lippincott-Schwartz, J. (2011). Tubular network formation protects mitochondria from autophagosomal degradation during nutrient starvation. Proc Natl Acad Sci U S A *108*, 10190-10195.

Reid, D.W., and Nicchitta, C.V. (2015). Diversity and selectivity in mRNA translation on the endoplasmic reticulum. Nat Rev Mol Cell Biol *16*, 221-231.

Richter, J.D., and Sonenberg, N. (2005). Regulation of cap-dependent translation by eIF4E inhibitory proteins. Nature *433*, 477-480.

Rogov, V., Dotsch, V., Johansen, T., and Kirkin, V. (2014). Interactions between autophagy receptors and ubiquitin-like proteins form the molecular basis for selective autophagy. Mol Cell *53*, 167-178.

Rollins, M.G., Shasmal, M., Meade, N., Astar, H., Shen, P.S., and Walsh, D. (2021). Negative charge in the RACK1 loop broadens the translational capacity of the human ribosome. Cell Rep *36*, 109663.

Romano, N., Di Giacomo, B., Nobile, V., Borreca, A., Willems, D., Tilesi, F., Catalani, E., Agrawal, M., Welshhans, K., Ricciardi, S.*, et al.* (2022). Ribosomal RACK1 Regulates the Dendritic Arborization by Repressing FMRP Activity. Int J Mol Sci *23*.

Romero-Fernandez, W., Carvajal-Tapia, C., Prusky, A., Katdare, K., Wang, E., Shostak, A., Ventura-Antunes, L., Harmsen, H., Lippmann, E., Borroto-Escuela, D.*, et al.* (2023). Detection, Visualization and Quantification of Protein Complexes in Human Alzheimer's Disease Brains using Proximity Ligation Assay. Res Sq.

Ron, D., Jiang, Z., Yao, L., Vagts, A., Diamond, I., and Gordon, A. (1999). Coordinated movement of RACK1 with activated betaIIPKC. J Biol Chem *274*, 27039-27046.

Rose, S., Frye, R.E., Slattery, J., Wynne, R., Tippett, M., Pavliv, O., Melnyk, S., and James, S.J. (2014). Oxidative stress induces mitochondrial dysfunction in a subset of autism lymphoblastoid cell lines in a well-matched case control cohort. PLoS One *9*, e85436.

Rosenfeld, A.B., and Racaniello, V.R. (2005). Hepatitis C virus internal ribosome entry site-dependent translation in Saccharomyces cerevisiae is independent of polypyrimidine tract-binding protein, poly(rC)-binding protein 2, and La protein. J Virol *79*, 10126-10137.

Roux, P.P., and Topisirovic, I. (2018). Signaling Pathways Involved in the Regulation of mRNA Translation. Mol Cell Biol *38*.

Ryan, L., and Rubinsztein, D.C. (2024). The autophagy of stress granules. FEBS Lett *598*, 59-72.

Safieddine, A., Coleno, E., Salloum, S., Imbert, A., Traboulsi, A.M., Kwon, O.S., Lionneton, F., Georget, V., Robert, M.C., Gostan, T.*, et al.* (2021). A choreography of centrosomal mRNAs reveals a conserved localization mechanism involving active polysome transport. Nat Commun *12*, 1352.

Saini, P., Eyler, D.E., Green, R., and Dever, T.E. (2009). Hypusine-containing protein eIF5A promotes translation elongation. Nature *459*, 118-121.

Saxton, R.A., and Sabatini, D.M. (2017). mTOR Signaling in Growth, Metabolism, and Disease. Cell *168*, 960-976.

Schneider-Poetsch, T., Ju, J., Eyler, D.E., Dang, Y., Bhat, S., Merrick, W.C., Green, R., Shen, B., and Liu, J.O. (2010). Inhibition of eukaryotic translation elongation by cycloheximide and lactimidomycin. Nat Chem Biol *6*, 209-217.

Schroeder, S., Hofer, S.J., Zimmermann, A., Pechlaner, R., Dammbrueck, C., Pendl, T., Marcello, G.M., Pogatschnigg, V., Bergmann, M., Muller, M.*, et al.* (2021). Dietary spermidine improves cognitive function. Cell Rep *35*, 108985.

Schuller, A.P., Wu, C.C., Dever, T.E., Buskirk, A.R., and Green, R. (2017). eIF5A Functions Globally in Translation Elongation and Termination. Mol Cell *66*, 194-205 e195.

Sengupta, J., Nilsson, J., Gursky, R., Spahn, C.M., Nissen, P., and Frank, J. (2004). Identification of the versatile scaffold protein RACK1 on the eukaryotic ribosome by cryo-EM. Nat Struct Mol Biol *11*, 957-962.

Sharma, G., Pallesen, J., Das, S., Grassucci, R., Langlois, R., Hampton, C.M., Kelly, D.F., des Georges, A., and Frank, J. (2013). Affinity grid-based cryo-EM of PKC binding to RACK1 on the ribosome. J Struct Biol *181*, 190-194.

Shefa, U., Jeong, N.Y., Song, I.O., Chung, H.J., Kim, D., Jung, J., and Huh, Y. (2019). Mitophagy links oxidative stress conditions and neurodegenerative diseases. Neural Regen Res *14*, 749-756.

Shin, S., Han, M.J., Jedrychowski, M.P., Zhang, Z., Shokat, K.M., Plas, D.R., Dephoure, N., and Yoon, S.O. (2023). mTOR inhibition reprograms cellular proteostasis by regulating eIF3D-mediated selective mRNA translation and promotes cell phenotype switching. Cell Rep *42*, 112868.

Silvestri, F., Montuoro, R., Catalani, E., Tilesi, F., Willems, D., Romano, N., Ricciardi, S., Cervia, D., and Ceci, M. (2025). eIF3d specialized translation requires a RACK1-driven eIF3d binding to 43S PIC in proliferating SH-SY5Y neuroblastoma cells. Cell Signal *125*, 111494.

Smeltzer, S., Quadri, Z., Miller, A., Zamudio, F., Hunter, J., Stewart, N.J.F., Saji, S., Lee, D.C., Chaput, D., and Selenica, M.B. (2021). Hypusination of Eif5a regulates cytoplasmic TDP-43 aggregation and accumulation in a stress-induced cellular model. Biochim Biophys Acta Mol Basis Dis *1867*, 165939.

Spriggs, K.A., Bushell, M., Mitchell, S.A., and Willis, A.E. (2005). Internal ribosome entry segment-mediated translation during apoptosis: the role of IRES-trans-acting factors. Cell Death Differ *12*, 585-591.

Stirnimann, C.U., Petsalaki, E., Russell, R.B., and Muller, C.W. (2010). WD40 proteins propel cellular networks. Trends Biochem Sci *35*, 565-574.

Sun, S., Hou, H., Ma, G., Ma, Q., Li, N., Zhang, L., Dong, C., Cao, M., Tam, K.Y., Ying, Z.*, et al.* (2022). The interaction between E3 ubiquitin ligase Parkin and mitophagy receptor PHB2 links inner mitochondrial membrane ubiquitination to efficient mitophagy. J Biol Chem *298*, 102704.

Tanenbaum, M.E., Gilbert, L.A., Qi, L.S., Weissman, J.S., and Vale, R.D. (2014). A protein-tagging system for signal amplification in gene expression and fluorescence imaging. Cell *159*, 635-646.

Tanida, I., Yamaji, T., Ueno, T., Ishiura, S., Kominami, E., and Hanada, K. (2008). Consideration about negative controls for LC3 and expression vectors for four colored fluorescent protein-LC3 negative controls. Autophagy *4*, 131-134.

Tekirdag, K., and Cuervo, A.M. (2018). Chaperone-mediated autophagy and endosomal microautophagy: Joint by a chaperone. J Biol Chem *293*, 5414-5424.

Thompson, M.K., Rojas-Duran, M.F., Gangaramani, P., and Gilbert, W.V. (2016). The ribosomal protein Asc1/RACK1 is required for efficient translation of short mRNAs. Elife *5*.

Thoreen, C.C., Kang, S.A., Chang, J.W., Liu, Q., Zhang, J., Gao, Y., Reichling, L.J., Sim, T., Sabatini, D.M., and Gray, N.S. (2009). An ATP-competitive mammalian target of rapamycin inhibitor reveals rapamycin-resistant functions of mTORC1. J Biol Chem *284*, 8023-8032.

Tilokani, L., Nagashima, S., Paupe, V., and Prudent, J. (2018). Mitochondrial dynamics: overview of molecular mechanisms. Essays Biochem *62*, 341-360.

Tsukada, M., and Ohsumi, Y. (1993). Isolation and characterization of autophagy-defective mutants of Saccharomyces cerevisiae. FEBS Lett *333*, 169-174.

Turakhiya, A., Meyer, S.R., Marincola, G., Bohm, S., Vanselow, J.T., Schlosser, A., Hofmann, K., and Buchberger, A. (2018). ZFAND1 Recruits p97 and the 26S Proteasome to Promote the Clearance of Arsenite-Induced Stress Granules. Mol Cell *70*, 906-919 e907.

Uemura, T., Yamamoto, M., Kametaka, A., Sou, Y.S., Yabashi, A., Yamada, A., Annoh, H., Kametaka, S., Komatsu, M., and Waguri, S. (2014). A cluster of thin tubular structures mediates transformation of the endoplasmic reticulum to autophagic isolation membrane. Mol Cell Biol *34*, 1695-1706.

Unsworth, H., Raguz, S., Edwards, H.J., Higgins, C.F., and Yague, E. (2010). mRNA escape from stress granule sequestration is dictated by localization to the endoplasmic reticulum. FASEB J *24*, 3370-3380.

Vargas, J.N.S., Hamasaki, M., Kawabata, T., Youle, R.J., and Yoshimori, T. (2023). The mechanisms and roles of selective autophagy in mammals. Nat Rev Mol Cell Biol *24*, 167-185.

Vattem, K.M., and Wek, R.C. (2004). Reinitiation involving upstream ORFs regulates ATF4 mRNA translation in mammalian cells. Proc Natl Acad Sci U S A *101*, 11269-11274.

Voigt, F., Zhang, H., Cui, X.A., Triebold, D., Liu, A.X., Eglinger, J., Lee, E.S., Chao, J.A., and Palazzo, A.F. (2017). Single-Molecule Quantification of Translation-Dependent Association of mRNAs with the Endoplasmic Reticulum. Cell Rep *21*, 3740-3753.

Vollrath, J.T., Sechi, A., Dreser, A., Katona, I., Wiemuth, D., Vervoorts, J., Dohmen, M., Chandrasekar, A., Prause, J., Brauers, E.*, et al.* (2014). Loss of function of the ALS protein SigR1 leads to ER pathology associated with defective autophagy and lipid raft disturbances. Cell Death Dis *5*, e1290.

Walter, P., and Johnson, A.E. (1994). Signal sequence recognition and protein targeting to the endoplasmic reticulum membrane. Annu Rev Cell Biol *10*, 87-119.

Wang, C., Han, B., Zhou, R., and Zhuang, X. (2016). Real-Time Imaging of Translation on Single mRNA Transcripts in Live Cells. Cell *165*, 990-1001.

Wang, J., Zhang, J., Lee, Y.M., Ng, S., Shi, Y., Hua, Z.C., Lin, Q., and Shen, H.M. (2017). Nonradioactive quantification of autophagic protein degradation with L-azidohomoalanine labeling. Nat Protoc *12*, 279-288.

Wang, S., Long, H., Hou, L., Feng, B., Ma, Z., Wu, Y., Zeng, Y., Cai, J., Zhang, D.W., and Zhao, G. (2023). The mitophagy pathway and its implications in human diseases. Signal Transduct Target Ther *8*, 304.

Watanabe-Asano, T., Kuma, A., and Mizushima, N. (2014). Cycloheximide inhibits starvation-induced autophagy through mTORC1 activation. Biochem Biophys Res Commun *445*, 334-339.

Wek, R.C. (2018). Role of eIF2alpha Kinases in Translational Control and Adaptation to Cellular Stress. Cold Spring Harb Perspect Biol *10*.

Westermann, B. (2010). Mitochondrial fusion and fission in cell life and death. Nat Rev Mol Cell Biol *11*, 872-884.

Westrate, L.M., Sayfie, A.D., Burgenske, D.M., and MacKeigan, J.P. (2014). Persistent mitochondrial hyperfusion promotes G2/M accumulation and caspase-dependent cell death. PLoS One *9*, e91911.

White, E. (2015). The role for autophagy in cancer. J Clin Invest *125*, 42-46.

Wildenberg, M.E., Koelink, P.J., Diederen, K., Te Velde, A.A., Wolfkamp, S.C., Nuij, V.J., Peppelenbosch, M.P., Nobis, M., Sansom, O.J., Anderson, K.I.*, et al.* (2017). The ATG16L1 risk

allele associated with Crohn's disease results in a Rac1-dependent defect in dendritic cell migration that is corrected by thiopurines. Mucosal Immunol *10*, 352-360.

Wong, H.H., Watt, A.J., and Sjostrom, P.J. (2024). Synapse-specific burst coding sustained by local axonal translation. Neuron *112*, 264-276 e266.

Wyant, G.A., Abu-Remaileh, M., Frenkel, E.M., Laqtom, N.N., Dharamdasani, V., Lewis, C.A., Chan, S.H., Heinze, I., Ori, A., and Sabatini, D.M. (2018). NUFIP1 is a ribosome receptor for starvation-induced ribophagy. Science *360*, 751-758.

Xia, C., Fan, J., Emanuel, G., Hao, J., and Zhuang, X. (2019). Spatial transcriptome profiling by MERFISH reveals subcellular RNA compartmentalization and cell cycle-dependent gene expression. Proc Natl Acad Sci U S A *116*, 19490-19499.

Xie, J., Wang, X., and Proud, C.G. (2018). Who does TORC2 talk to? Biochem J *475*, 1721-1738.

Xie, X., Li, F., Wang, Y., Wang, Y., Lin, Z., Cheng, X., Liu, J., Chen, C., and Pan, L. (2015a). Molecular basis of ubiquitin recognition by the autophagy receptor CALCOCO2. Autophagy *11*, 1775-1789.

Xie, Y., Kang, R., Sun, X., Zhong, M., Huang, J., Klionsky, D.J., and Tang, D. (2015b). Posttranslational modification of autophagy-related proteins in macroautophagy. Autophagy *11*, 28-45.

Xu, A., and Chen, K.Y. (2001). Hypusine is required for a sequence-specific interaction of eukaryotic initiation factor 5A with postsystematic evolution of ligands by exponential enrichment RNA. J Biol Chem *276*, 2555-2561.

Xu, A., Jao, D.L., and Chen, K.Y. (2004). Identification of mRNA that binds to eukaryotic initiation factor 5A by affinity co-purification and differential display. Biochem J *384*, 585-590.

Yamamoto, H., Zhang, S., and Mizushima, N. (2023). Autophagy genes in biology and disease. Nat Rev Genet *24*, 382-400.

Yamamoto, S., Kuramoto, K., Wang, N., Situ, X., Priyadarshini, M., Zhang, W., Cordoba-Chacon, J., Layden, B.T., and He, C. (2018). Autophagy Differentially Regulates Insulin Production and Insulin Sensitivity. Cell Rep *23*, 3286-3299.

Yang, C., Wang, Z., Kang, Y., Yi, Q., Wang, T., Bai, Y., and Liu, Y. (2023a). Stress granule homeostasis is modulated by TRIM21-mediated ubiquitination of G3BP1 and autophagy-dependent elimination of stress granules. Autophagy *19*, 1934-1951.

Yang, P., Mathieu, C., Kolaitis, R.M., Zhang, P., Messing, J., Yurtsever, U., Yang, Z., Wu, J., Li, Y., Pan, Q.*, et al.* (2020). G3BP1 Is a Tunable Switch that Triggers Phase Separation to Assemble Stress Granules. Cell *181*, 325-345 e328.

Yang, Y., Gatica, D., Liu, X., Wu, R., Kang, R., Tang, D., and Klionsky, D.J. (2023b). Upstream open reading frames mediate autophagy-related protein translation. Autophagy *19*, 457-473.

Yang, Z., Goronzy, J.J., and Weyand, C.M. (2015). Autophagy in autoimmune disease. J Mol Med (Berl) *93*, 707-717.

Yang, Z., and Klionsky, D.J. (2010). Mammalian autophagy: core molecular machinery and signaling regulation. Curr Opin Cell Biol *22*, 124-131.

Yla-Anttila, P., Vihinen, H., Jokitalo, E., and Eskelinen, E.L. (2009). 3D tomography reveals connections between the phagophore and endoplasmic reticulum. Autophagy *5*, 1180-1185.

Youle, R.J., and Narendra, D.P. (2011). Mechanisms of mitophagy. Nat Rev Mol Cell Biol *12*, 9-14.

Yu, L., Chen, Y., and Tooze, S.A. (2018). Autophagy pathway: Cellular and molecular mechanisms. Autophagy *14*, 207-215.

Zhang, H., Alsaleh, G., Feltham, J., Sun, Y., Napolitano, G., Riffelmacher, T., Charles, P., Frau, L., Hublitz, P., Yu, Z., *et al.* (2019). Polyamines Control eIF5A Hypusination, TFEB Translation, and Autophagy to Reverse B Cell Senescence. Mol Cell *76*, 110-125 e119.

Zhang, J., Wang, J., Ng, S., Lin, Q., and Shen, H.M. (2014). Development of a novel method for quantification of autophagic protein degradation by AHA labeling. Autophagy *10*, 901-912.

Zhang, S., Yazaki, E., Sakamoto, H., Yamamoto, H., and Mizushima, N. (2022). Evolutionary diversification of the autophagy-related ubiquitin-like conjugation systems. Autophagy *18*, 2969-2984.

Zhao, L., Chen, Y., Li, H., Ding, X., and Li, J. (2024). Deciphering the neuroprotective mechanisms of RACK1 in cerebral ischemia-reperfusion injury: Pioneering insights into mitochondrial autophagy and the PINK1/Parkin axis. CNS Neurosci Ther *30*, e14836.

Zhao, Y., Wang, Q., Qiu, G., Zhou, S., Jing, Z., Wang, J., Wang, W., Cao, J., Han, K., Cheng, Q., *et al.* (2015). RACK1 Promotes Autophagy by Enhancing the Atg14L-Beclin 1-Vps34-Vps15 Complex Formation upon Phosphorylation by AMPK. Cell Rep *13*, 1407-1417.

Zhu, C.L., Yao, R.Q., Li, L.X., Li, P., Xie, J., Wang, J.F., and Deng, X.M. (2021). Mechanism of Mitophagy and Its Role in Sepsis Induced Organ Dysfunction: A Review. Front Cell Dev Biol *9*, 664896.